

Dissertation zur Erlangung des Doktorgrades
der Fakultät für Chemie und Pharmazie
der Ludwig-Maximilians-Universität München

Periodic Mesoporous Organosilicas with Functional Chromophores



Von

Yan Li

Dezhou, Shandong, China

2012

Erklärung

Diese Dissertation wurde im Sinne von § 7 der Promotionsordnung vom 28. November 2011 von Herrn Prof. Dr. Thomas Bein betreut.

Eidesstattliche Versicherung

Diese Dissertation wurde eigenständig und ohne unerlaubte Hilfe erarbeitet.

München, 28.06.2012

.....

(Unterschrift der Autorin)

Dissertation eingereicht am 28.06.2012

1. Gutachter: Prof. Dr. Thomas Bein
2. Gutachter: Prof. Dr. Achim Hartschuh

Mündliche Prüfung am 19.07.2012

Acknowledgement

This PhD thesis could not be achieved without the help and support of many people who are gratefully acknowledged here.

My deepest gratitude goes first and foremost to Prof. Thomas Bein, my supervisor, for his constant encouragement and enlightening guidance throughout the years of my PhD studies. Without his profound knowledge, invaluable ideas and suggestions, I could not have completed all the research in my thesis. His kindness, patience and generous support through every stage of my foreign Ph.D. life in Germany are greatly appreciated.

I want to thank Prof. Achim Hartschuh for his time and kindness to be the second reviewer of my thesis.

I shall express my thanks to Prof. Dr. Dirk Trauner in organic chemistry department for the efficient and fruitful collaborations. His remarkable expertise provided the possibility to diversify the systems studied in this thesis.

My thanks are then extended to Florian Löbermann from Prof. Trauner's group for his great help with the organic synthesis. With his intellectual ideas and his patience of exploring the appropriate synthetic approach, we could go through the challenges in each synthetic step.

I am also very grateful to other collaborators who contributed their time and expertise to this thesis: Prof. Dr. Paul Knochel and Dr. Marcel Kienle from the organic chemistry division for supplying organic molecules, which ensured a smooth start of this thesis;

Acknowledgement

Dr. Shinji Inagaki and Yasutomo Goto from Toyota Central R&D Laboratories for sharing with us their experience in synthesizing PMO materials; Prof. Laurie Peter from University of Bath for providing his expertise to detect and explore the opto-electroactivities of our PMO films; Priv. Doz. Dr. Bert Nickel and Christian Westermeier from the physics department for their effort to investigate the charge mobility of our PMO film materials; Prof. Alexander Holleitner and Nadine Erhard from the Walter Schottky Institute for their kindness of probing the properties of PMO/AAM composites.

What's more, I would like to thank each member of the Bein's group who create a good working environment and show their kindness, help and support during this very important period of my life.

My sincere and special thanks are given to Dr. Andreas Keilbach who has been helping and teaching me a lot as a patient mentor in the scientific field and also as a nice friend in my daily life.

My great appreciation also goes to Dr. Markus Döblinger and Dr. Jörg Schuster for their experience and time on detailed analysis of the nanostructures, as well as other members in the subgroup of "nanostructures and nanowires", Dr. Ralf Köhn, Kun Hou and Fabian Hanusch, for their opinions and advice on my research project.

Many thanks to Florian Auras for his great effort and help with the opto-electrochemical experiments and data analysis; Benjamin Mandlmeier, Askhat Jumabekov and Norma Minar from the photovoltaic subgroup for their suggestions and kind help with the device fabrication.

Acknowledgement

I would like to thank Dr. Steffen Schmidt who kindly arranged some TEM and SEM sessions for my samples, and Tina Reuther who is always patient to do sorption measurements and who organizes the chemicals and lab-utilities so well.

I would also like to sincerely thank Mrs. Regina Huber for her continuous and thoughtful help with all the paperwork for me over the years.

Many thanks go to the present and previous members of the Bein group for all the warm hugs, nice conversations and funny jokes between us, Karin Möller, Dina Fattakhova-Rohlfing, Maria Lohse, Alexandra Schmidt, Christian Argyo, Ilina Kondofersky, Hans Feckl, Stefan Niedermayer, Alesja Ivanova, Florian Hinterholzinger, Bastian Rühle, Mirjam Dogru, Dana Medina, Elisabeth Botz, Halina Dunn, Stefan Wuttke, Johann Szeifert, Axel Schlossbauer, Monika Plabst, Camilla Scherb, Shaofeng Shao, Hongji Wang, Vesna Müller and Mihaela Nedelcu. Thank you all for the help and company during my time in the lab. My special thanks go to Yujing Liu and Hsin-Yi Chiu who are always willing to provide their suggestions and encouragement whenever I needed it.

I should also thank my flatmate Fei Wang and my neighbor Haiyan Sun who offered a lot of delicious food and happy moments in my foreign life.

My great and deep thanks go to my beloved parents for their boundless love and unconditional support over all these past years. Thanks to them for sharing with me my worries, frustrations, and hopefully my ultimate happiness in eventually finishing this thesis.

Acknowledgement

Last but not least, I'd like to thank the China Scholarship Council (CSC) for financially supporting me to conduct the Ph.D. study at the University of Munich and to live a life in Germany.

Abstract

Periodic mesoporous organosilicas (PMOs) are attractive materials because of their ordered pore systems as well as the great diversity of intrinsically functionalized pore walls, which could lead to potential applications of PMOs in areas such as catalysis, gas storage, drug delivery, sensing, and optics. Different organic molecules (R') can be integrated within the frameworks of PMOs by condensation of the bis- or poly-(trialkoxysilyl) precursors $R'[Si(OR)]_n$ ($n \geq 2$) in the presence of surfactant templates. It is often challenging to synthesize PMOs from organosilane precursors with bulky organic units, as such precursors can have low solubility and high hydrolysis rates which lead to disordered precipitates under common synthetic conditions. In this project, a modified evaporation-induced self-assembly (EISA) process was developed to produce oriented PMO materials either in the tubular channels of anodic alumina membranes (AAM) or on the surface of a flat substrate. Four different functional chromophores were successfully integrated into the PMO pore walls followed by the investigation of their optical properties.

At first, a biphenyl-bridged PMO (Bp-PMO) material was successfully synthesized within the AAM host systems. 4,4'-bis(triethoxysilyl)biphenyl (BTEBP) was used as organosilane precursor in combination with cetyltrimethylammonium bromide (CTAB) or triblock co-polymer Pluronic F127 as structure directing agent (SDA). Depending on the SDA, three different mesophases were observed, *i.e.*, a structural mixture of a 2D-hexagonal columnar and a lamellar phase, a hexagonal circular phase as well as a body centered cubic (*Im-3m*) mesophase. The obtained circular and cubic structured Bp-PMOs confined within AAM channels were found to be stable against calcination

temperatures of up to 250 °C. The composite materials also showed good stability in the electron beam of the electron microscope. Furthermore, all the hierarchically structured Bp-PMO/AAM materials showed fluorescence in the ultra-violet light region due to the existence of biphenyl organic units in the stable organosilica frameworks.

In the second part, within the channel-host of AAM, 1,3,5-tris(4-triethoxysilylstyryl)benzene (a three-armed oligo(phenylenevinylene) molecule, denoted as 3a-OPV) was used as organosilica source and the triblock co-polymers Pluronic F127 or F108 were chosen to assist the assembly of 3a-OPV precursors into PMOs. After the EISA process, the sample formed with the Pluronic F127 as template had a 2D-hexagonal circular structure, while the one with the block co-polymer F108 as template showed a body centered cubic (*Im-3m*) structure. As the phenylenevinylene chromophores exist within the obtained PMO pore walls, the resulting mesostructured 3a-OPV-PMO/AAM composites were observed to be fluorescent in the visible light region. The energy shift of the fluorescence emission of the PMOs with respect to the precursor molecules indicates strong electronic interactions of the chromophores in the confined organosilica networks.

In the third part, a newly designed poly-triethoxysilyl molecule containing an octa-substituted zinc-phthalocyanine macrocycle was synthesized as organosilane precursor. Then with Pluronic F108 as structure directing agent and tetraethoxysilane (TEOS) as co-precursor, highly ordered phthalocyanine-containing organosilica (denoted as Pc-Si-PMO) films were formed on flat substrates using the spin-coating method. Subsequent removal of the template was achieved through supercritical CO₂ extraction. The resulting extracted Pc-Si-PMO film material features a highly ordered orthorhombic porous structure with pore diameter of 17 nm and surface area of

379 m² g⁻¹. It was confirmed by energy dispersive X-ray spectroscopy (EDXS), electron energy loss spectroscopy (EELS) and nuclear magnetic resonance (NMR) spectroscopy that the phthalocyanine molecules are preserved after being incorporated in the PMO pore-walls. Furthermore, the optoelectronic activities of the Pc-Si-PMO films were investigated with the inclusion of electron-accepting species such as the fullerene derivative PCBM, showing indeed the anticipated light-induced charge generation capability and hole-conducting behavior.

In the fourth part, another novel ethoxysilyl precursor with a tetra-substituted porphyrin bridging-unit was designed and the corresponding PMO film material (Por-PMO) was successfully synthesized. Triblock co-polymer Pluronic F127 was used as structure directing agent to direct the assembly of the porphyrin-bridged precursors into an ordered mesostructure. The template F127 was removed from the mesopores through solvent extraction. The resulting orthorhombic structured mesoporous film has a surface area of 364 m² g⁻¹ and a pore size of 15 nm. The investigation on the optoelectronic activity of the film in an electrolyte indicates that the obtained porphyrin-bridged PMO material also has light-induced charge generation capability and that it features a p-type semiconducting character.

To summarize, highly ordered PMOs with four different chromophores, ranging from two aromatic rings to large aromatic macrocycles, were synthesized and their light-absorbing, light-emitting as well as charge-generation and transport abilities were investigated. These studies indicate that PMOs are promising candidates for energy and electron transfer systems, and are expected to lead a way towards designing and synthesizing novel periodically ordered interpenetrating networks of electron donors and acceptors.

TABLE OF CONTENTS

1. Introduction	1
1.1. Periodic Mesoporous Organosilica Materials	2
1.2. Synthesis of PMOs by evaporation-induced self-assembly (EISA)	7
1.2.1. <i>PMO Films on Flat Substrates</i>	10
1.2.2. <i>PMOs Confined in Anodic Alumina Membranes</i>	14
1.3. Photoactive Properties of PMOs with Functional Chromophores	17
1.4. Chapter References	20
2. Characterization	29
2.1. X-ray Scattering.....	29
2.2. Electron Microscopy.....	34
2.2.1. <i>Scanning Electron Microscopy (SEM)</i>	35
2.2.2. <i>Transmission Electron Microscopy</i>	37
2.2.3. <i>Elemental analysis (EDX, EELS)</i>	39
2.3. Nitrogen Sorption Measurements	40
2.4. Nuclear Magnetic Resonance Spectroscopy.....	43
2.5. Ultraviolet - visible Spectrophotometer	44
2.6. Fluorescence Spectroscopy.....	45
2.7. External Quantum Efficiency	47
2.8. Chapter References.....	47
3. Hierarchically Structured Biphenylene-Bridged Periodic Mesoporous Organosilica	51
3.1. Introduction	51
3.2. Experimental Section.....	54
3.2.1. <i>Synthesis of siloxane precursor</i>	54
3.2.2. <i>Preparation of bipenylene-bridged PMO in AAM channels</i>	55
3.2.3. <i>Characterization</i>	56
3.3. Results and Discussion	57
3.3.1. <i>CTAB-columnar-lamellar Bp-PMO</i>	57
3.3.2. <i>F127-circular Bp-PMO</i>	59
3.3.3. <i>F127-cubic Bp-PMO</i>	65
3.3.4. <i>Fluorescent properties</i>	69
3.4. Conclusions	70
3.5. References	71
4. Formation of Hexagonal and Cubic Fluorescent Periodic Mesoporous Organosilicas in the Channels of Anodic Alumina Membranes	79

Table of Contents

4.1. Introduction	79
4.2. Experimental Section.....	82
4.2.1. Preparation of 1,3,5-tris(styryl)benzene-bridged PMO in AAM channels ..	82
4.2.2. Characterization.....	84
4.3. Results and Discussion	85
4.3.1. F127-circular 3a-OPV-PMO	85
4.3.2. F108-cubic 3a-OPV-PMO.....	89
4.3.3. Fluorescence emission of 3a-OPV-PMO/AAM composites	92
4.4. Conclusions	94
4.5. References	95
5. A Periodic Mesoporous Organosilica with Phthalocyanine Macrocycles Exhibiting Optoelectronic Properties	99
5.1. Introduction	99
5.2. Experimental Section.....	102
5.2.1. Preparation of phthalocyanine-bridged PMO films.....	102
5.2.2. Structure Characterization.....	103
5.2.3. Photoelectrochemical Characterization.....	104
5.3. Results and Discussion	107
5.3.1. Mesostructured phthalocyanine-bridged PMO films	107
5.3.2. Framework constitution of the phthalocyanine-bridged PMO films.....	113
5.3.3. UV-Vis absorption properties.....	114
5.3.4. Optoelectronic behavior.....	116
5.4. Conclusion	122
5.5. References	123
6. Optoelectronically Active Periodic Mesoporous Organosilica Films Containing Porphyrin Chromophores.....	131
6.1. Introduction	131
6.2. Experimental Section.....	133
6.2.1. Preparation of porphyrin-based PMO films	133
6.2.2. Structural Characterization.....	134
6.2.3. Photoelectrochemical Characterization.....	136
6.3. Results and discussion	138
6.3.1. Mesostructured porphyrin-bridged PMO films.....	138
6.3.2. UV-Vis absorption properties.....	143
6.3.3. Optoelectronic properties.....	145
6.4. Conclusion	149
6.5. References	150
7. Conclusions and Outlook	157
8. Appendix	161

Table of Contents

9. Curriculum Vitae.....	173
10. Publications and Presentations	175
Publications	175
Presentations	175

1. Introduction

A mesoporous material is a material containing pores with diameters between 2 and 50 nm according to the IUPAC definition.¹ Typical mesoporous materials include mesoporous silica,²⁻⁶ alumina⁷⁻⁹ and other mesoporous oxides of titanium, niobium, tin, etc..¹⁰⁻¹⁸ Among them, periodic mesoporous silica materials have attracted considerable attention for designing nanoscale architectures by applying bottom-up strategies since their discovery in 1992 by the researchers of the Mobil Oil company.^{5, 19} These reported periodic inorganic mesoporous silica materials, known as M41S phases, are formed by a sol-gel process²⁰ in the presence of structure-directing agents (SDAs), *i.e.*, self-assembled aggregates of surfactants. The most well-known representatives of this class of materials include the silica solids MCM-41 (hexagonal arrangement of the mesopores), MCM-48 (cubic arrangement of the mesopores) and MCM-50 (lamellar structure), in all of which MCM stands for “Mobile Composition of Matter”.²¹

Following the discovery of ordered mesostructured silica, there have been many studies and reports on synthesizing novel compositions based on mesoporous silica for applications in areas such as catalysis, gas storage, drug delivery, sensing, and optics.²²⁻²⁶ The key point of these studies is to combine the advantages of inorganic mesoporous silicas such as tunable pore sizes, high specific surface areas, and ordered pore systems with the great diversity of organic chemistry, which could lead to the development of mesoporous organic-inorganic hybrid materials.²⁷⁻²⁸ The organic modification of the porous materials allows one to tailor the properties of the inorganic silica to specific needs. A special group of the organically modified mesoporous silica

materials is represented by periodic mesoporous organosilicas (PMOs), which were discovered in 1999 by three groups independently.²⁹⁻³¹

1.1. Periodic Mesoporous Organosilica Materials

A specific class of mesoporous organic-inorganic hybrid materials is known as periodic mesoporous organosilica (PMO).³² In 1999, three groups independently reported the first examples of PMO synthesized with organically bridged bis(trialkoxysilyl) precursors as building blocks.²⁹⁻³¹ Ozin's group reported an organic-inorganic hybrid material containing ethene groups which were directly integrated into the silica framework. They used 1,2-(bistriethoxysilyl)ethene as precursor and CTAB (cetyltrimethylammonium bromide) as structure directing agent and were able to solvent-extract the surfactant molecules to create a stable and periodic mesoporous ethene-silica with high surface area and ethene groups which are readily accessible for chemical reaction.³¹

Inagaki and coworkers used 1,2-bis(trimethoxysilyl)ethane to produce such a periodic mesoporous organosilica material with hexagonal symmetry and pore diameter of 3.1 nm templated by surfactant C₁₈TMACl (octadecyltrimethylammonium chloride).³⁰

At nearly the same time, Stein and coworkers also synthesized porous organosilica frameworks in which silicon atoms are bridged by ethane or ethene groups similarly by making use of the cetyltrimethylammonium (CTA⁺) surfactant and trialkoxysilyl precursors such as bis(triethoxysilyl)ethane or bis(triethoxysilyl)ethene.²⁹

1. Introduction

Commonly, PMOs (periodic mesoporous organosilicas) are materials which can be synthesized from bis- or poly-(trialkoxysilyl) precursors $R[Si(OR')]_n$ ($n \geq 2$) in the presence of structure directing agents (*e.g.*, surfactants such as tetraalkylammonium halides or nonionic copolymers), as shown in Figure 1.1 (in this Figure $n=2$). In PMOs, each individual organic group is covalently bonded to two or more silicon atoms. These organic bridges are uniformly distributed within the porous framework, which can enhance the activity of these functional groups and makes PMO materials attractive in application fields such as catalysis^{22, 33} and adsorbent³⁴⁻³⁵ systems.

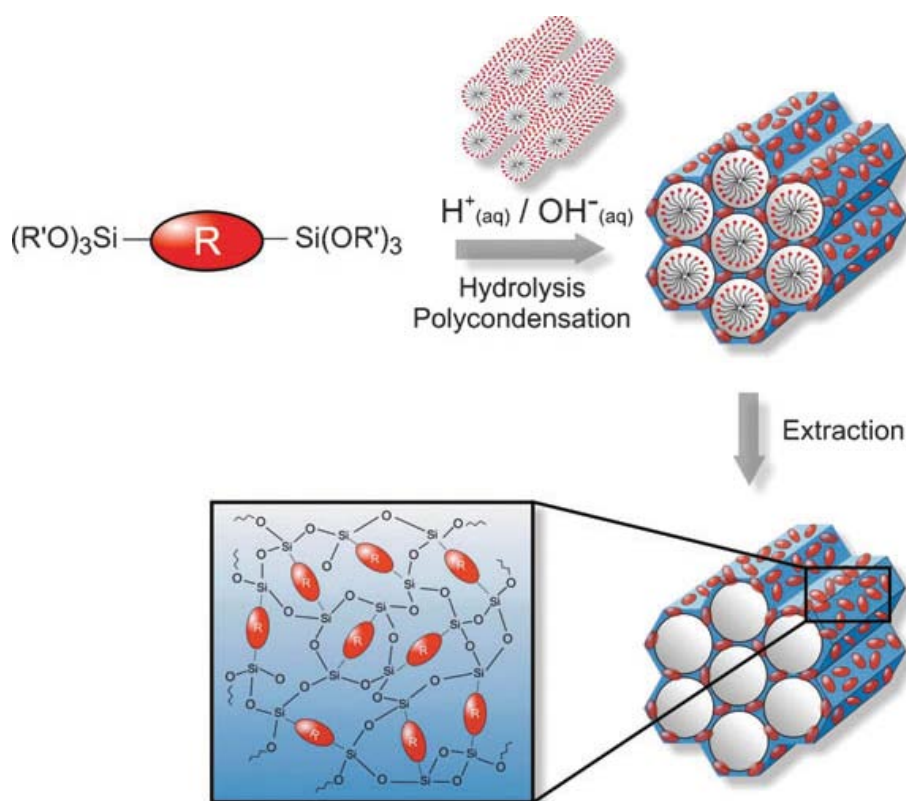


Figure 1.1: General synthetic pathway to PMOs that are formed from bis-silylated organic bridging units R . (Figure adapted from ref. 21.)

Since the initial reports of periodic mesoporous organosilicas, there have been many studies on incorporating various organic moieties within PMO frameworks. To date, numerous organic groups have been successfully incorporated in the framework of PMOs.^{21, 27, 36-40} Figure 1.2 shows some of the silane precursors used for their preparation, from which it is obvious that researchers have relied mostly on short, rigid organic linkers or aromatic linkers, as flexible organic linkers over two carbons in length could easily result in disordered materials.²¹ During recent years, great efforts have been made towards developing novel PMOs with photoactive or electroactive functions within their frameworks.^{24-25, 41-43} In that way, these materials could be potentially employed in optical or electrical systems, broadening the application fields of PMO materials.

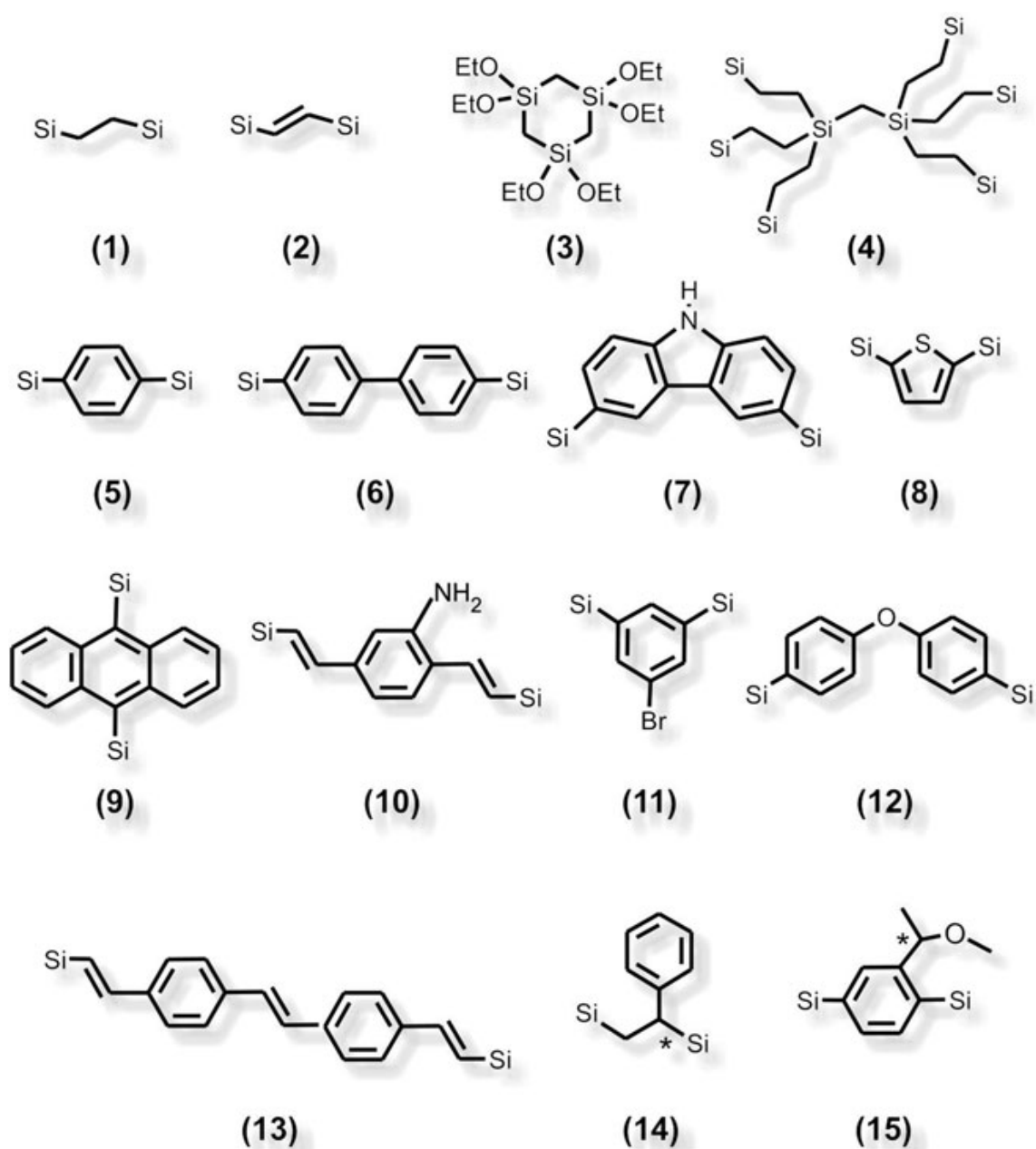


Figure 1.2: A selection of organosilica precursor molecules used for the preparation of PMOs. Si = Si(OR)₃, R= Me, Et or ⁱPr. (Figure adapted from ref. 21.)

A noteworthy aspect regarding the obtained PMOs is that some compounds do not only show a periodicity at the mesoscale but also exhibit a crystal-like arrangement of organic bridges within the framework (Figure 1.3). This phenomenon was first described in 2002 by Inagaki *et al.* for a benzene-bridged PMO.⁴⁴ Here, following the

1. Introduction

convention of Fröba and coworkers,²¹ the term ‘crystal-like’ instead of ‘crystalline’ is used because (i) the organic bridges do not have to possess strict translational symmetry, they can be slightly tilted with respect to each other, and (ii) the silica part of the pore walls does not possess long-range order. Apparently, precursors that are rather rigid, linear or symmetric and do not carry too long or bulky substituents more easily arrange into this crystal-like networks.

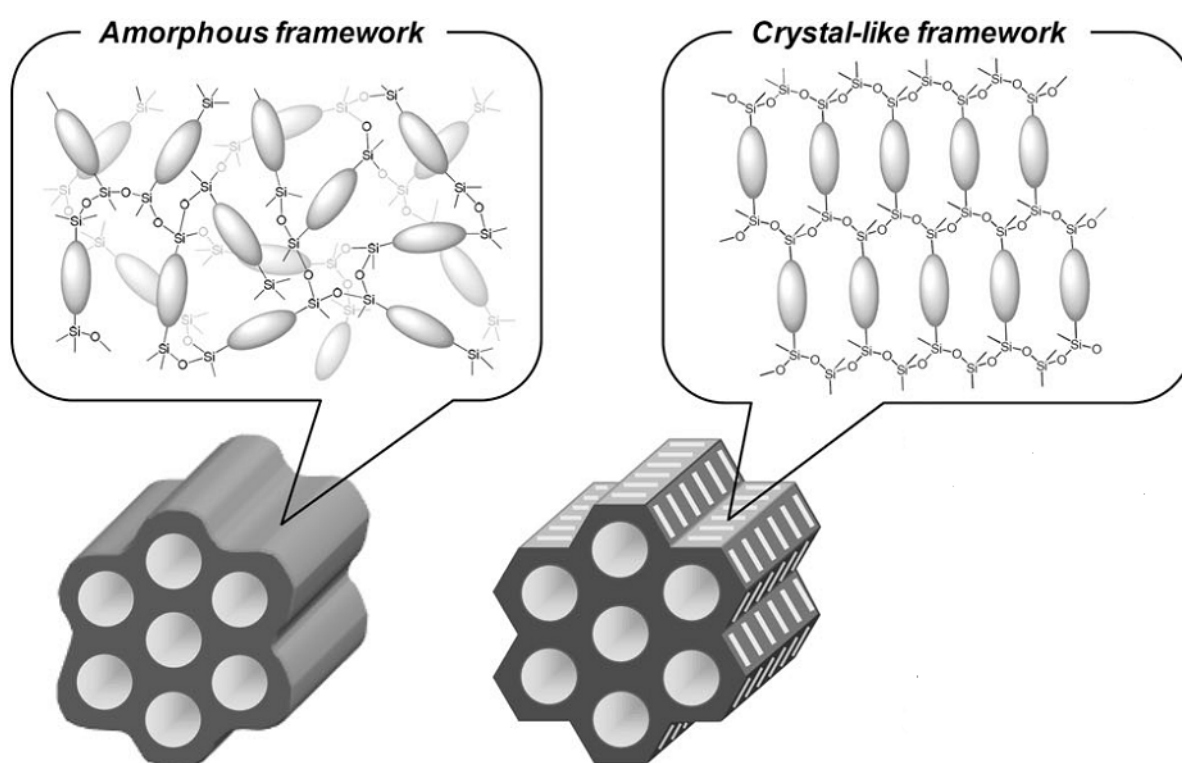


Figure 1.3: Schematic illustration of amorphous and crystal-like frameworks of PMO. (Figure adapted from ref. 32.)

1.2. Synthesis of PMOs by evaporation-induced self-assembly (EISA)

The first reported periodic mesoporous organosilica materials were synthesized in the form of powders by a precipitation mechanism.²⁹⁻³¹ As PMO materials have promising properties towards applications in fields such as nanoscale catalysts, gas sensors, and optical devices, preparing PMOs as films on surfaces or at interfaces could be more beneficial compared to powder synthesis.

In order to produce mesostructured thin films, an evaporation-induced self-assembly (EISA) process is often employed.⁴⁵ In this EISA approach, the self-assembly of silica precursor molecules is directed by a structure-directing agent (SDA) which serves as a scaffold for the polycondensation of the precursor molecules. The structure-directing agents are normally supramolecular structures formed by the aggregation of amphiphilic molecules such as surfactants which contain both hydrophilic and hydrophobic groups. Once the amphiphilic surfactants are dissolved in solvents, they are able to form micellar aggregates when their concentrations are above their critical micelle concentrations (CMC).

The packing behavior of the surfactant template can be designed by adjusting the packing parameter g

$$g = V/a_0l,$$

where V is the total volume of the hydrophobic part of the surfactant, a_0 is the effective area at the aqueous-micellar surface and l is the length of the hydrophobic hydrocarbon

chains. The value of g can be influenced by the addition of a cosurfactant, the polarity of the solvent as well as the presence of other ionic or nonionic species.

Taking the formation of mesoporous inorganic networks as example, the details of various steps involved in the EISA process are illustrated in Figure 1.4.⁴⁶ These steps do not necessarily take place precisely in the given order and sometimes may overlap along the process of thin film formation.

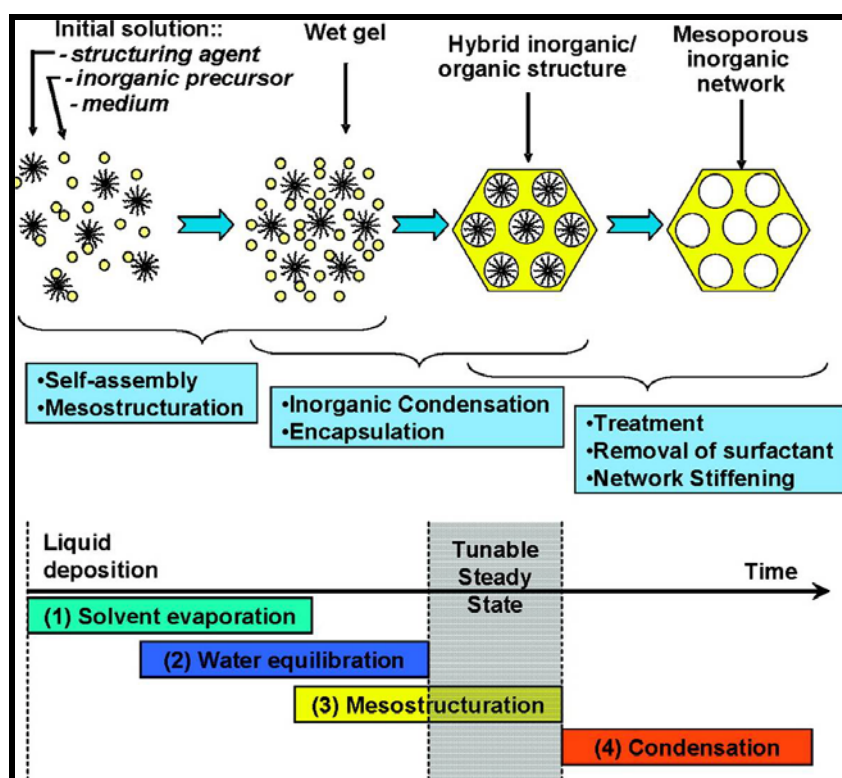


Figure 1.4: Scheme illustrating the various steps involved in the EISA process during thin film formation by liquid deposition techniques. (Figure adapted from ref. 46.)

Correspondingly, for the synthesis of PMO thin films, the EISA approach typically employs a homogeneous solution containing the organosilica source dissolved in

volatile solvent (*e.g.* ethanol) and water, catalytic amounts of HCl, as well as surfactant with a concentration below its CMC. During the EISA process, the solvent evaporation causes an increase in the concentration of non-volatile species in the deposited solution and triggers both self-assembly and crosslinking of organosilica precursor molecules. More precisely, as soon as the initial solution is deposited on the substrate, evaporation of volatile components (*e.g.* EtOH, H₂O and HCl) takes place at the air/film interface. Once the surfactant concentration reaches its CMC, micelles start to form by aggregation of the hydrophobic parts of the surfactant. With the attraction between the organosilica source and the hydrophilic headgroups of the surfactant, assembly of the precursor molecules around the micelles is achieved. Finally, after polycondensation of the silane precursors a mesostructured organosilica film is obtained.

Since the starting point for the film formation is the initial solution, in order to achieve a certain structure and a desired rate of the polycondensation of precursors, the chemical properties of the solution need to be adjusted, including its chemical composition and aging time. The final resulting periodic mesoporous organosilica materials can possess different mesophases depending on spherical, elongated, rod- or sheet-like micellar structures formed in the deposited solution (Figure 1.5).⁴⁷⁻⁴⁸

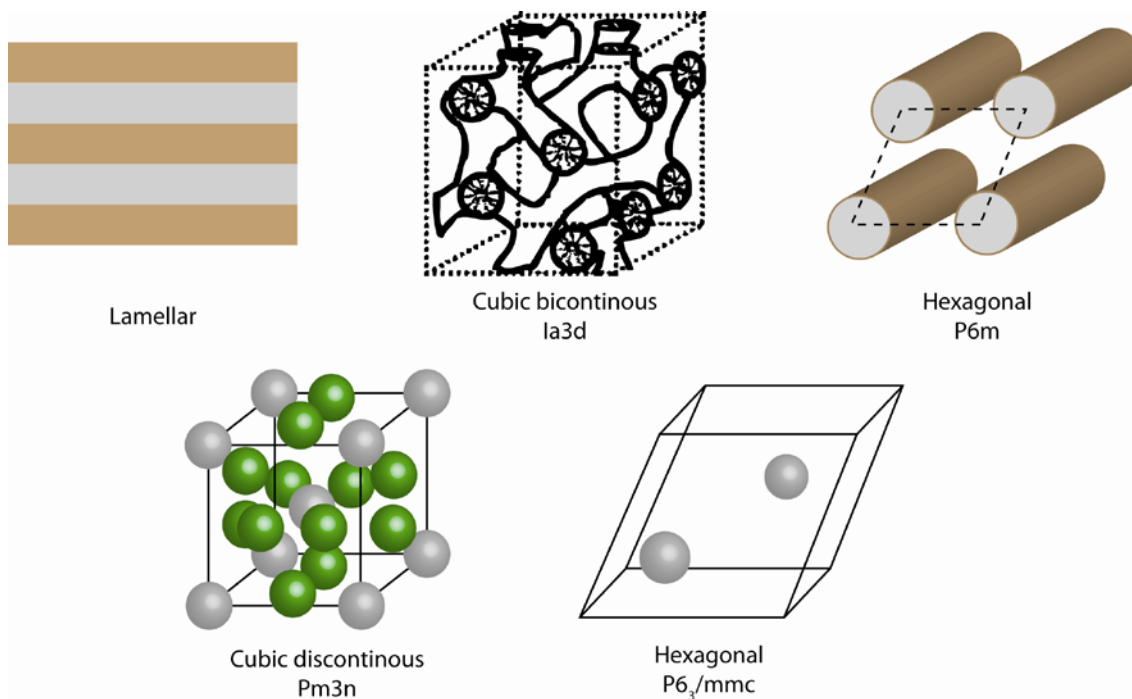


Figure 1.5: Schematic illustration of different lamellar, hexagonal, and cubic structures formed with sheet-like, cylindrical, or spherical micelle aggregate structures. Different colored aggregates in the sketch of the cubic $Pm3n$ structure are used to clarify the structure. The grey micelles are arranged in a cubic body-centered manner, two green micelles are positioned on each plane of the cube. (Figure adapted from ref. 47.)

1.2.1. PMO Films on Flat Substrates

A variety of applications can benefit from the development of organosilica in thin film morphologies. For example, many sensing applications where one needs to coat an electronic device, chemically selective membranes or organic photovoltaic devices rely on thin film morphologies.^{21, 40}

Most commonly, thin films are prepared through an EISA process by dip- or spin-coating techniques (Figure 1.6). In dip-coating, a substrate is dipped into a solution

containing precursor(s), SDA and catalysts and then extracted at a constant speed. Due to the solution-substrate wettability, a film is formed on the substrate, whose thickness depends on the pulling speed and the viscosity of the solution. In spin-coating, few drops of the precursor solution are cast at the center of a flat substrate and then spun at a constant speed to be spread on the substrate due to the centrifugal force, leading to the formation of a homogeneous film.

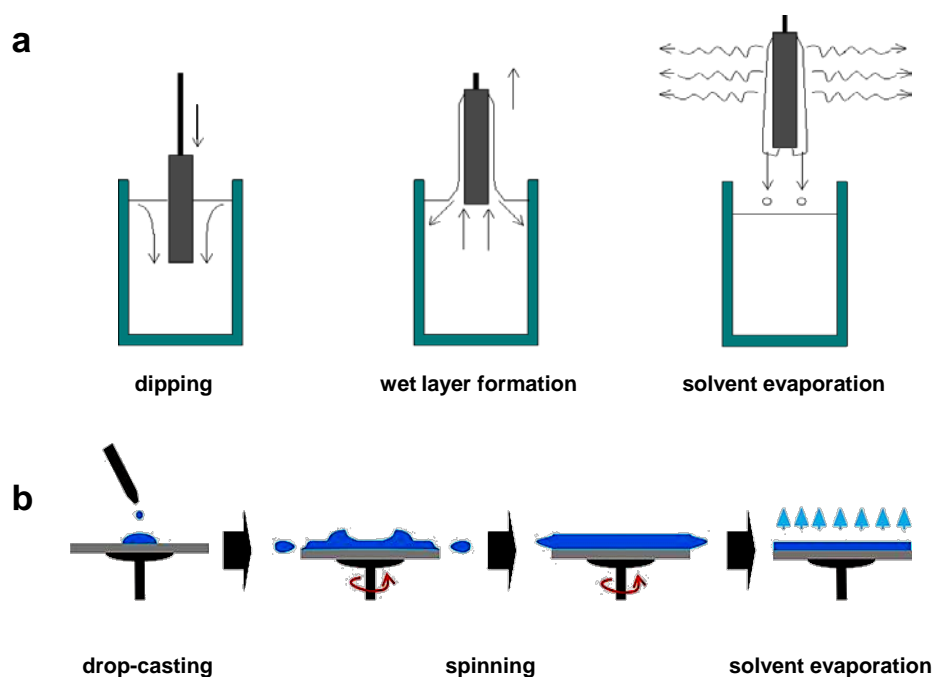


Figure 1.6: Stages of dip-coating (a) and spin-coating (b) processes. (Figure adapted from ref. 49 and ref. 50.)

The synthesis of PMO thin films was first realized in C. J. Brinker's group by applying both spin-coating and dip-coating methods. These PMO thin films which contain ethane, ethene or benzene bridges exhibit lamellar, hexagonal or cubic mesophases depending on the surfactant template used in the initial ethanolic solutions.⁵¹ PMO thin

films with a slightly larger organic bridge - a biphenylene group - were also achieved by several research groups, showing periodicity of mesopores in the obtained PMO films.^{42, 52-53} G. A. Ozin's group synthesized some PMO films that possess very low dielectric constant k values due to their high porosity and the high molar ratio of carbon to silicon atoms in the framework.⁵⁴ Inagaki and coworkers recently focused on the preparation of PMO thin films with fluorescent and charge-conducting properties by using organosilica precursors containing oligo(phenylenevinylene) groups.^{26, 55} These studies on synthesizing PMO films on flat substrates are aimed at potential future applications of PMOs in displays, solar cells and microelectronic devices.

Regarding the structural features of PMO thin films, one phenomenon commonly observed is the shrinkage caused by thermal treatment, which is applied to achieve further condensation of the organosilica framework.^{11,13,15} The contraction occurs mainly along the direction perpendicular to the substrate (out of plane), whereas the contraction parallel to the substrate (in plane) is negligible (Figure 1.7). As a consequence, thermal treatment will alter the shape of the mesopores and distort the mesostructure to a certain degree.

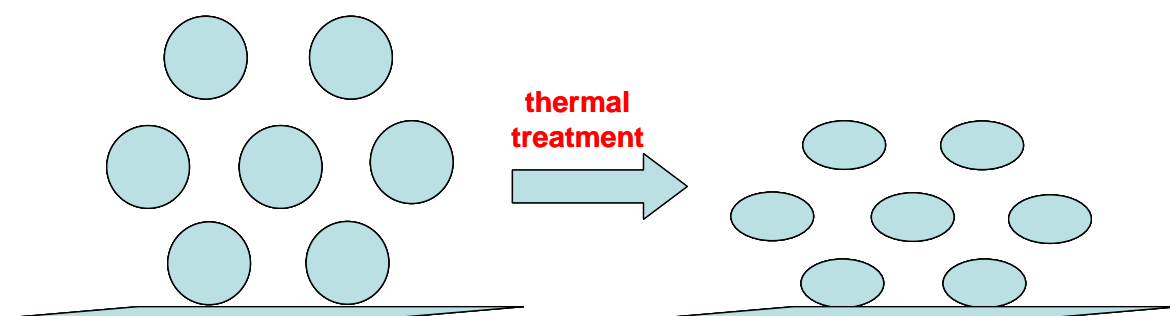


Figure 1.7: Schematic illustration of the shrinkage of a hexagonal mesostructure after a thermal treatment process.

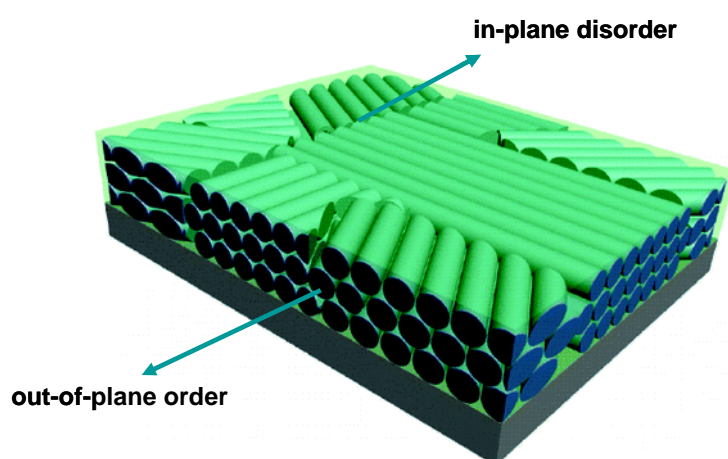


Figure 1.8: Schematic illustration of a mesostructured film with out-of-plane order and in-plane disorder. (Figure adapted from ref. 56.)

The other feature illustrated in Figure 1.8 is that the PMO films are generally composed of domains of mesostructure that exhibit preferential orientation with respect to the substrate surface which is called planar disorder, *i.e.*, they show out-of-plane order but no long-range in-plane order.⁵⁶ In order to realize further control over the domain size and orientation of mesopores in the films, great efforts have been made during the last years including the application of external electric⁵⁷⁻⁵⁸ or magnetic fields⁵⁹⁻⁶⁰, the use of

chemically⁶¹⁻⁶² or lithographically⁶³ treated substrates, etc.. Among those methods, a feasible strategy is to utilize porous anodic alumina membranes (AAMs) as confining hosts and supporting substrates for mesoporous materials.

1.2.2. PMOs Confined in Anodic Alumina Membranes

To date, there are various reports on incorporating mesostructured silica into the tubular channels of anodic alumina membranes (AAMs). By this approach, even a vertical alignment of the mesopores relative to the alumina membrane surface could be realized.⁶⁴⁻⁶⁷ Besides, these types of hierarchical nanostructured composites can offer significant advantages, such as high thermal stability, high aspect ratio of the mesophase system, and applicability to nanofiltration or nanotemplating.

The first case of employing anodic alumina membranes (AAM) as substrate to synthesize mesoporous silica was reported by Yamaguchi and coworkers.⁶⁸ By using the EISA method, the surfactant-templated silica was successfully formed inside each alumina pore, having mesochannels vertically arranged with respect to the AAM surface.

In order to tune the mesophase of mesoporous silica confined in AAM channels, detailed studies were reported including changing the surfactant template,⁶⁹⁻⁷⁰ varying the silica-to-surfactant ratio,⁷¹⁻⁷² making use of additives (*e.g.*, inorganic salts),⁷³ controlling the humidity and temperature during the EISA process,^{66, 74} as well as changing the diameter of the AAM channels.⁷⁵ The reported mesostructures of the confined silica include a 2D hexagonal columnar mesophase (mesopore orientation

along the alumina pore), a 2D hexagonal circular mesophase (mesopore orientation perpendicular to the alumina pore), and a lamellar phase (Figure 1.9).⁴⁷

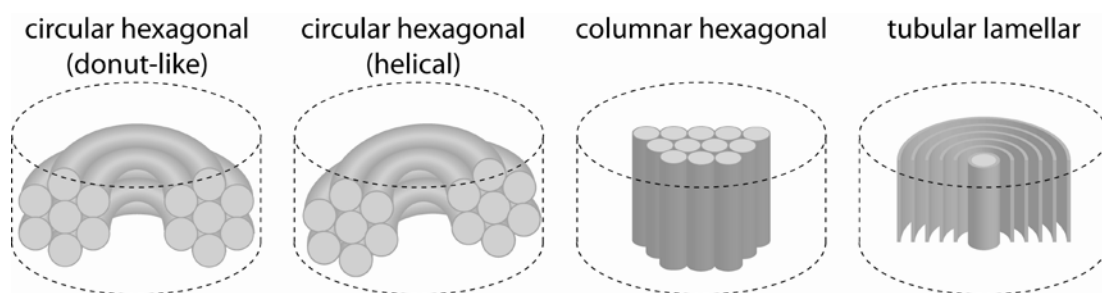


Figure 1.9: Overview over observed silica mesostructures within AAM channels. (Figure adapted from ref. 47.)

Taking advantage of the favorable interaction of silica species with the AAM channel walls found in inorganic silica/AAM systems, it is reasoned that combining organosilica systems with AAM hosts might lead to different mesophase behavior and phase stability and thus open the way to designing novel hierarchical nanosystems based on such PMO materials. The synthesis of PMO material confined within the channels of AAM was initially achieved by using bis(triethoxysilyl)ethane (BTSE) as the organosilica source.²⁸ Two different surfactants, nonionic Brij 56 and ionic CTAB, were used as structure-directing agents (SDA) in an acid-catalyzed EISA process. Brij 56 resulted in the formation of either a hexagonal circular or a cubic mesophase. When using CTAB as the SDA, the only mesophase observed was the hexagonal circular structure. Small-angle X-ray scattering (SAXS) measurements in combination with TEM micrographs were used to investigate the mesostructures of the confined PMO materials in AAM-channels (Figure 1.10).

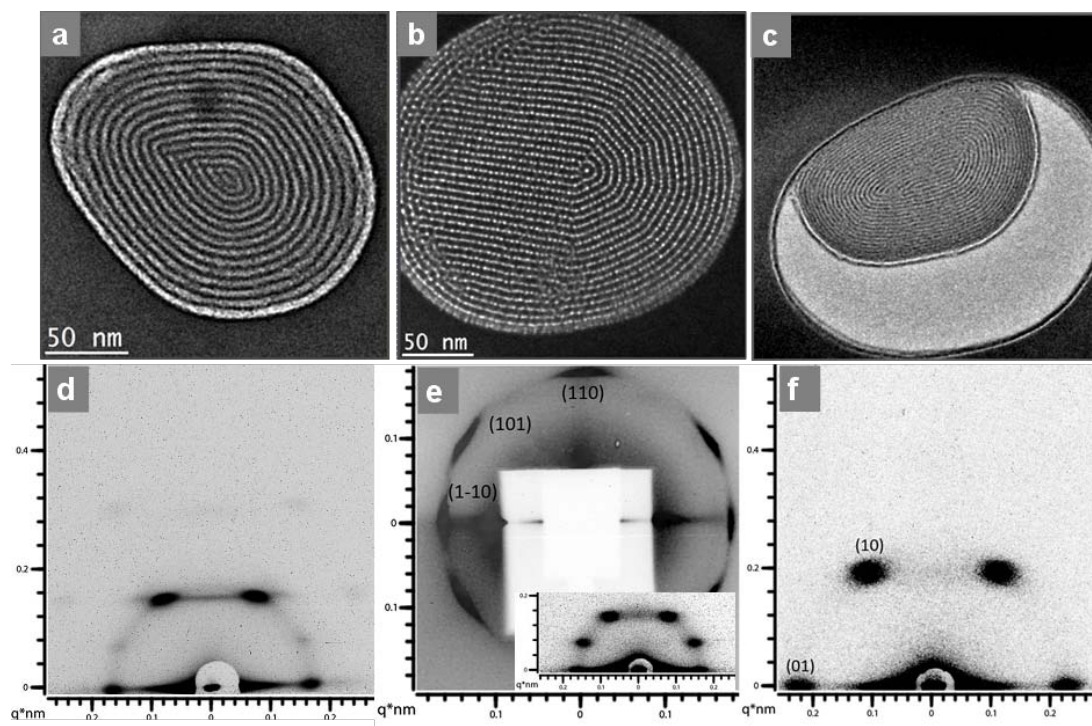


Figure 1.10: TEM micrographs and 2D-SAXS patterns of PMO/AAM composites with hexagonal circular (a, d) and cubic (b, e) structures formed by Brij56 and a circular phase templated by CTAB (c, f). (Figure adapted from ref. 28.)

Besides the ethane-bridged PMO/AAM composite, not much has been reported regarding the synthesis of PMOs containing larger organic units in AAM-channels. The reason might be that it turned out to be very challenging to obtain ordered mesostructures from silsesquioxane precursors with large organic bridges. This type of precursors can show low solubility and high hydrolysis rate leading to almost instant precipitation under common synthesis conditions. Remarkably, recently two new PMO/AAM composites were successfully synthesized by our group (which will be discussed in following chapters), one of which containing biphenylene groups,⁷⁶ the other containing oligo(phenylenevinylene) groups in the PMO framework.⁷⁷ Compared

to previously reported PMO thin films with these two organic units, the PMO materials within the channels of AAM show improved features such as highly ordered and oriented mesostructures as well as good thermal stability and stability against electron-beam irradiation during TEM characterization.

1.3. Photoactive Properties of PMOs with Functional Chromophores

Periodic mesoporous organosilicas with functional chromophores have recently been developed and shown to have promising photoactive properties. A highly efficient light harvesting system based on PMO material has been reported by Inagaki and co-workers. The light-harvesting property is realized by an energy transfer from biphenylene groups in the PMO framework to dye molecules (coumarin-1) that are adsorbed within the PMO meso-channels.⁴¹ Their studies revealed that by increasing the concentration of coumarin-1 in the channels, the emission spectrum gradually shifts from the emission of biphenylene groups at 380 nm to 440-450 nm which is the characteristic emission of coumarin-1 (Figure 1.11). Almost 100% energy transfer efficiency could be achieved when the concentration of the dye was 1.8 mol% (coumarin 1/biphenyl) in PMO films.

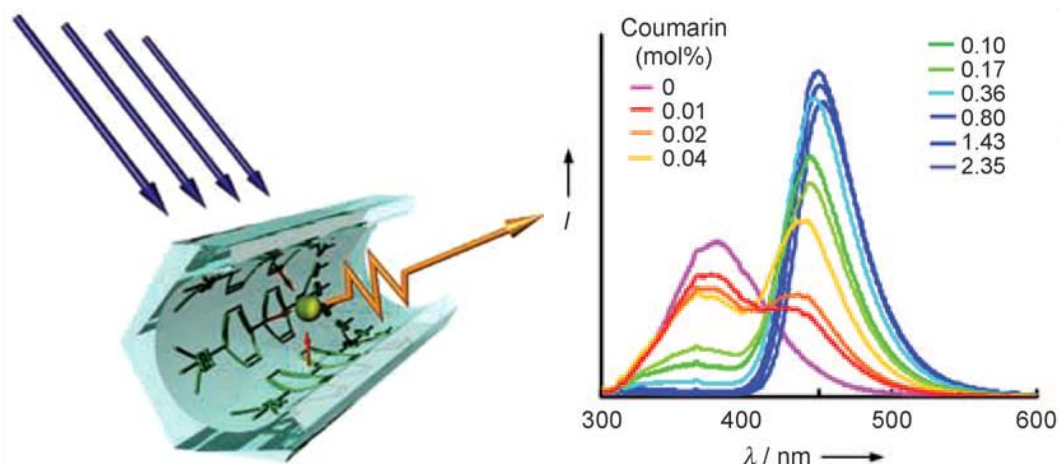


Figure 1.11: Schematic representation of the energy transfer in biphenyl PMO doped with coumarin-1, and the fluorescence spectra of composites with 0-2.35 mol% coumarin - 1/biphenyl molar ratio excited at 270 nm. (Figure adapted from ref. 41.)

This research is the basis for a series of studies of PMO materials containing photoactive groups.⁷⁸⁻⁸⁰ In these recent studies, the light absorption of the obtained PMOs could be extended to the visible light range, which is of considerable interest for the intended applications of these PMOs in photocatalysis and other optoelectronic devices. For example, by synthesizing a new acridone-bridged PMO material, light-harvesting properties could be observed at wavelengths up to 450 nm, indicating the absorption of visible light.⁷⁸

An interesting luminescent PMO material has been obtained by using a 1,3,6,8-tetraphenylpyrene (TPPy)-containing organosilane precursor.⁸¹ The TPPy unit was densely embedded within the framework of thin films exhibiting efficient blue light emission. Furthermore, fluorescent dye doping of this mesostructured film with either green-light-emitting boron-dipyrromethene (Bodipy) or yellow-light-emitting Rhodamine 6G enabled color-tunable photoluminescence over a wide range of the

visible spectrum. Therefore, this kind of luminescent PMO materials could possess significant potential to be applied in light emitting systems. For example, present phosphors on “white” light emitting diodes (LEDs) currently show a slightly bluish color balance, which is perceived as ‘cold’ and uncomfortable, thus tuning their emission spectrum towards ‘warmer’ hues with the assistance of proper PMO material is of great interest.²¹

Besides the light-harvesting and light-emitting properties of the PMOs with chromophoric organic linkers, charge-conductivity could also be achieved with electrically conductive organic linkers. The charge-transporting property of a PMO film with π -conjugated molecules in the pore wall was recently investigated.²⁶ Under the application of a static electric field and upon irradiation with a 337 nm laser pulse, a transient photocurrent was generated and measured at the positive electrode. Carriers were shown to be holes with mobility on the order of $10^{-5} \text{ cm}^2 \text{ V}^{-1} \text{ s}^{-1}$. Although the value is lower than that of well-stacked oligo(phenylenevinylene) systems, this report showed for the first time the possibility of designing an electrically conductive PMO matrix by incorporating large conjugated π -system into the framework (Figure 1.12). This success indicates great potential for designing and synthesizing PMOs containing other similar optoelectroactive molecules.

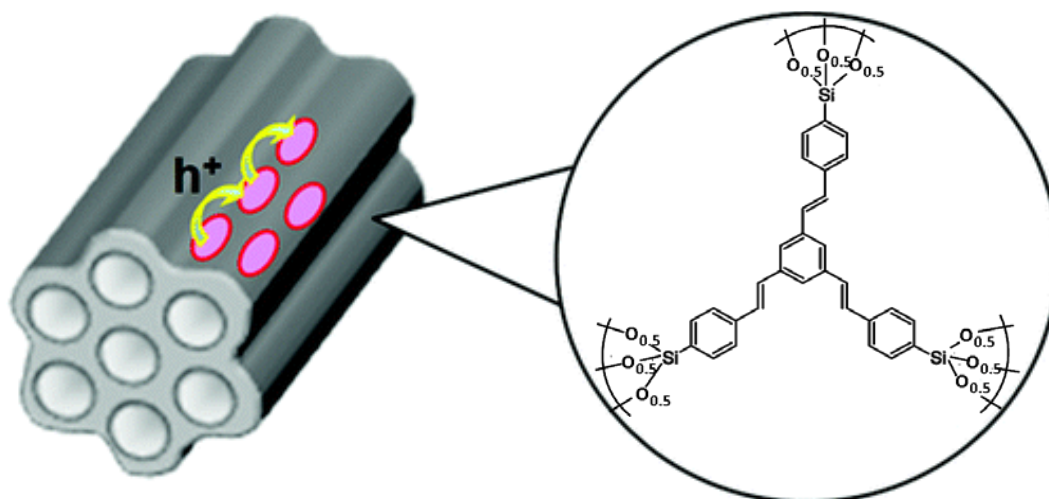


Figure 1.12: Chemical structure of phenylenevinylene-bridged PMO and schematic illustration of the hole-transport process through the PMO framework. (Figure adapted from ref. 26.)

This class of optoelectronically active PMO materials possesses features of high surface area, periodic mesopores as well as photoactive properties such as the absorption and emission of light and conductivity of charges. Thus, such features could lead PMOs into a promising future of being applied in lighting-harvesting systems, OLEDs or solar cells, respectively.

1.4. Chapter References

1. J. Rouquerol, D. Avnir, C. W. Fairbridge, D. H. Everett, J. M. Haynes, N. Pernicone, J. D. F. Ramsay, K. S. W. Sing and K. K. Unger, *Pure Appl. Chem.*, 1994, **66**, 1739-1758.
2. A. Katiyar, S. Yadav, P. G. Smirniotis and N. G. Pinto, *J. Chromatogr. A*, 2006, **1122**, 13-20.

3. F. Di Renzo, H. Cambon and R. Dutartre, *Microporous Mater.*, 1997, **10**, 283-286.
4. T. Yanagisawa, T. Shimizu, K. Kuroda and C. Kato, *Bull. Chem. Soc. Jpn.*, 1990, **63**, 988-992.
5. J. S. Beck, J. C. Vartuli, W. J. Roth, M. E. Leonowicz, C. T. Kresge, K. D. Schmitt, C. T. W. Chu, D. H. Olson and E. W. Sheppard, *J. Amer. Chem. Soc.*, 1992, **114**, 10834-10843.
6. D. Zhao, J. Feng, Q. Huo, N. Melosh, G. H. Fredrickson, B. F. Chmelka and G. D. Stucky, *Science*, 1998, **279**, 548-552.
7. N. Neeraj and M. Eswaramoorthy, *J. Chem. Sci.*, 1998, **110**, 143-149.
8. Z.-X. Li, F.-B. Shi, L.-L. Li, T. Zhang and C.-H. Yan, *Phys. Chem. Chem. Phys.*, 2011, **13**, 2488-2491.
9. X. Jiang, H. Oveisi, Y. Nemoto, N. Suzuki, K. C. W. Wu and Y. Yamauchi, *Dalton Trans.*, 2011, **40**, 10851-10856.
10. I. Kartini, P. Meredith, J. C. D. Da Costa and G. Q. Lu, *J. Sol-Gel Sci. Technol.*, 2004, **31**, 185-189.
11. D. Chen, L. Cao, F. Huang, P. Imperia, Y.-B. Cheng and R. A. Caruso, *J. Amer. Chem. Soc.*, 2010, **132**, 4438-4444.
12. J. M. Szeifert, D. Fattakhova-Rohlfing, D. Georgiadou, V. Kalousek, J. Rathouský, D. Kuang, S. Wenger, S. M. Zakeeruddin, M. Grätzel and T. Bein, *Chem. Mater.*, 2009, **21**, 1260-1265.

1. Introduction

13. J. M. Szeifert, J. M. Feckl, D. Fattakhova-Rohlfing, Y. Liu, V. Kalousek, J. Rathouský and T. Bein, *J. Amer. Chem. Soc.*, 2010, **132**, 12605-12611.
14. D. M. Antonelli and J. Y. Ying, *Angew. Chem. Int. Ed.*, 1996, **35**, 426-430.
15. X. Xu, B. Z. Tian, J. L. Kong, S. Zhang, B. H. Liu and D. Y. Zhao, *Adv. Mater.*, 2003, **15**, 1932-1936.
16. B. Lee, D. Lu, J. N. Kondo and K. Domen, *J. Amer. Chem. Soc.*, 2002, **124**, 11256-11257.
17. D. N. Srivastava, S. Chappel, O. Palchik, A. Zaban and A. Gedanken, *Langmuir*, 2002, **18**, 4160-4164.
18. N. Tatsuda, T. Nakamura, D. Yamamoto, T. Yamazaki, T. Shimada, H. Inoue and K. Yano, *Chem. Mater.*, 2009, **21**, 5252-5257.
19. C. T. Kresge, M. E. Leonowicz, W. J. Roth, J. C. Vartuli and J. S. Beck, *Nature*, 1992, **359**, 710-712.
20. C. J. Brinker and G. W. Scherer, eds., *Sol-Gel Science: The Physics and Chemistry of Sol-Gel Processing*, Academic Press, New York, 1990.
21. F. Hoffmann and M. Fröba, *Chem. Soc. Rev.*, 2011, **40**, 608-620.
22. Q. H. Yang, J. Liu, L. Zhang and C. Li, *J. Mater. Chem.*, 2009, **19**, 1945-1955.
23. V. Rebbin, R. Schmidt and M. Fröba, *Angew. Chem. Int. Ed.*, 2006, **45**, 5210-5214.

24. P. N. Minoofar, R. Hernandez, S. Chia, B. Dunn, J. I. Zink and A. C. Franville, *J. Amer. Chem. Soc.*, 2002, **124**, 14388-14396.
25. R. Hernandez, A. C. Franville, P. Minoofar, B. Dunn and J. I. Zink, *J. Am. Chem. Soc.*, 2001, **123**, 1248-1249.
26. N. Mizoshita, M. Ikai, T. Tani and S. Inagaki, *J. Amer. Chem. Soc.*, 2009, **131**, 14225-14227.
27. F. Hoffmann, M. Cornelius, J. Morell and M. Fröba, *Angew. Chem. Int. Ed.*, 2006, **45**, 3216-3251.
28. A. Keilbach, M. Döblinger, R. Köhn, H. Amenitsch and T. Bein, *Chem. Eur. J.*, 2009, **15**, 6645-6650.
29. B. J. Melde, B. T. Holland, C. F. Blanford and A. Stein, *Chem. Mater.*, 1999, **11**, 3302-3308.
30. S. Inagaki, S. Guan, Y. Fukushima, T. Ohsuna and O. Terasaki, *J. Amer. Chem. Soc.*, 1999, **121**, 9611-9614.
31. T. Asefa, M. J. MacLachlan, N. Coombs and G. A. Ozin, *Nature*, 1999, **402**, 867-871.
32. N. Mizoshita, T. Tani and S. Inagaki, *Chem. Soc. Rev.*, 2011, **40**, 789-800.
33. A. Kuschel and S. Polarz, *J. Am. Chem. Soc.*, 2010, **132**, 6558-6565.
34. M. Park, S. S. Park, M. Selvaraj, D. Y. Zhao and C. S. Ha, *Microporous Mesoporous Mat.*, 2009, **124**, 76-83.

35. C. Li, J. Liu, X. Shi, J. Yang and Q. Yang, *Journal of Physical Chemistry C*, 2007, **111**, 10948-10954.
36. J. Morell, M. Gungerich, G. Wolter, J. Jiao, M. Hunger, P. J. Klar and M. Fröba, *J. Mater. Chem.*, 2006, **16**, 2809-2818.
37. A. Sayari and W. H. Wang, *J. Am. Chem. Soc.*, 2005, **127**, 12194-12195.
38. T. Tani, N. Mizoshita and S. Inagaki, *J. Mater. Chem.*, 2009, **19**, 4451-4456.
39. C. Vercaemst, P. E. de Jongh, J. D. Meeldijk, B. Goderis, F. Verpoort and P. Van Der Voort, *Chem. Commun.*, 2009, 4052-4054.
40. W. Wang, J. E. Lofgreen and G. A. Ozin, *Small*, 2010, **6**, 2634-2642.
41. S. Inagaki, O. Ohtani, Y. Goto, K. Okamoto, M. Ikai, K. Yamanaka, T. Tani and T. Okada, *Angew. Chem. Int. Ed.*, 2009, **48**, 4042-4046.
42. Y. Goto, N. Mizoshita, O. Ohtani, T. Okada, T. Shimada, T. Tani and S. Inagaki, *Chem. Mat.*, 2008, **20**, 4495-4498.
43. Y. F. Hu, K. Qian, P. Yuan, Y. H. Wang and C. Z. Yu, *Mater. Lett.*, 2011, **65**, 21-23.
44. S. Inagaki, S. Guan, T. Ohsuna and O. Terasaki, *Nature*, 2002, **416**, 304-307.
45. C. J. Brinker, Y. F. Lu, A. Sellinger and H. Y. Fan, *Adv. Mater.*, 1999, **11**, 579-585.
46. C. Sanchez, C. Boissière, D. Grosso, C. Laberty and L. Nicole, *Chem. Mater.*, 2008, **20**, 682-737.

1. Introduction

47. B. Platschek, A. Keilbach and T. Bein, *Adv. Mater.*, 2011, **23**, 2395-2412.
48. Y. Yamauchi and K. Kuroda, *Asian J. Chem.*, 2008, **3**, 664-676.
49. <http://www.solgel.com/articles/Nov00/mennig.htm>.
50. http://www.free-photos.biz/images/science/chemistry/solgel_spincoating.jpg.
51. Y. Lu, H. Fan, N. Doke, D. A. Loy, R. A. Assink, D. A. LaVan and C. J. Brinker, *J. Amer. Chem. Soc.*, 2000, **122**, 5258-5261.
52. M. A. Wahab and C. B. He, *J. Nanosci. Nanotechnol.*, 2008, **8**, 6381-6386.
53. M. A. Wahab and C. B. He, *Langmuir*, 2009, **25**, 832-838.
54. B. D. Hatton, K. Landskron, W. Whitnall, D. D. Perovic and G. A. Ozin, *Adv. Funct. Mater.*, 2005, **15**, 823-829.
55. N. Mizoshita, Y. Goto, T. Tani and S. Inagaki, *Adv. Funct. Mater.*, 2008, **18**, 3699-3705.
56. P. Innocenzi, L. Malfatti, T. Kidchob and P. Falcaro, *Chem. Mater.*, 2009, **21**, 2555-2564.
57. M. Trau, N. Yao, E. Kim, Y. Xia, G. M. Whitesides and I. A. Aksay, *Nature*, 1997, **390**, 674-676.
58. K. Kuraoka, Y. Tanaka, M. Yamashita and T. Yazawa, *Chem. Commun.*, 2004, 1198-1199.
59. A. Firouzi, D. J. Schaefer, S. H. Tolbert, G. D. Stucky and B. F. Chmelka, *J. Am. Chem. Soc.*, 1997, **119**, 9466-9477.

60. Y. Yamauchi, M. Sawada, T. Noma, H. Ito, S. Furumi, Y. Sakka and K. Kuroda, *J. Mater. Chem.*, 2005, **15**, 1137-1140.
61. H. Miyata, T. Noma, M. Watanabe and K. Kuroda, *Chem. Mat.*, 2002, **14**, 766-772.
62. H. Miyata, T. Suzuki, A. Fukuoka, T. Sawada, M. Watanabe, T. Noma, K. Takada, T. Mukaide and K. Kuroda, *Nat. Mater.*, 2004, **3**, 651-656.
63. R. L. Rice, D. C. Arnold, M. T. Shaw, D. Iacopina, A. J. Quinn, H. Amenitsch, J. D. Holmes and M. A. Morris, *Adv. Funct. Mater.*, 2007, **17**, 133-141.
64. Z. L. Yang, Z. W. Niu, X. Y. Cao, Z. Z. Yang, Y. F. Lu, Z. B. Hu and C. C. Han, *Angew. Chem., Int. Ed.*, 2003, **42**, 4201-4203.
65. A. Yamaguchi, F. Uejo, T. Yoda, T. Uchida, Y. Tanamura, T. Yamashita and N. Teramae, *Nat. Mater.*, 2004, **3**, 337-341.
66. B. Platschek, N. Petkov and T. Bein, *Angew. Chem. Int. Ed.*, 2006, **45**, 1134-1138.
67. A. Yamaguchi, H. Kaneda, W. S. Fu and N. Teramae, *Adv. Mater.*, 2008, **20**, 1034-1037.
68. A. Yamaguchi, F. Uejo, T. Yoda, T. Uchida, Y. Tanamura, T. Yamashita and N. Teramae, *Nat. Mater.*, 2004, **3**, 337-341.
69. B. Platschek, R. Köhn, M. Döblinger and T. Bein, *Langmuir*, 2008, **24**, 5018-5023.
70. K. J. Lee, S. H. Min and J. Jang, *Small*, 2008, **4**, 1945-1949.

71. B. Platschek, R. Köhn, M. Döblinger and T. Bein, *ChemPhysChem*, 2008, **9**, 2059-2067.
72. D. Wang, R. Kou, Z. Yang, J. He, Z. Yang and Y. Lu, *Chem. Commun.*, 2005, 166-167.
73. B. Platschek, N. Petkov, D. Himsl, S. Zimdars, Z. Li, R. Köhn and T. Bein, *J. Amer. Chem. Soc.*, 2008, **130**, 17362-17371.
74. A. Yamaguchi, H. Kaneda, W. Fu and N. Teramae, *Adv. Mater.*, 2008, **20**, 1034-1037.
75. Y. Wu, G. Cheng, K. Katsov, S. W. Sides, J. Wang, J. Tang, G. H. Fredrickson, M. Moskovits and G. D. Stucky, *Nat. Mater.*, 2004, **3**, 816-822.
76. Y. Li, A. Keilbach, M. Kienle, Y. Goto, S. Inagaki, P. Knochel and T. Bein, *J. Mater. Chem.*, 2011, **21**, 17338-17344.
77. Y. Li, A. Keilbach, N. Mizoshita, S. Inagaki and T. Bein, *in preparation*.
78. H. Takeda, Y. Goto, Y. Maegawa, T. Ohsuna, T. Tani, K. Matsumoto, T. Shimada and S. Inagaki, *Chem. Commun.*, 2009, 6032-6034.
79. H. Takeda, M. Ohashi, T. Tani, O. Ishitani and S. Inagaki, *Inorg. Chem.*, 2010, **49**, 4554-4559.
80. Y. Maegawa, N. Mizoshita, T. Tani and S. Inagaki, *J. Mater. Chem.*, 2010, **20**, 4399-4403.
81. N. Mizoshita, Y. Goto, Y. Maegawa, T. Tani and S. Inagaki, *Chem. Mater.*, 2010, **22**, 2548-2554



2. Characterization

The study of mesostructured materials requires various characterization techniques that are able to detect multiple properties of the synthesized materials, such as mesophase periodicity, porosity, presence of specific molecular species, as well as optical and electronic properties. Small-angle X-ray scattering (SAXS), which provides information on mesostructures, is one of the most frequently used techniques. Besides SAXS, electron microscopy as a complementary technique can provide direct images of the material with nanoscale resolution. The physisorption of nitrogen on the obtained mesoporous material is used to obtain further information on the surface area, the pore volume and the pore size distribution. Nuclear magnetic resonance (NMR) provides information on the chemical environment of a specific atom present within the material. Other techniques which were employed to measure photoactive properties of the synthesized materials are also presented in this chapter, such as UV-Vis spectrophotometry, fluorescence spectroscopy and quantum efficiency measurements.

2.1. X-ray Scattering

X-ray scattering is a non-destructive analytical technique which provides information about periodicity of materials on the atomic to nanometer scale. This method is based on the interaction between a sample and an incident X-ray wave. When the X-ray beam hits a sample, it can interact with the electron cloud of the sample and undergo elastic scattering phenomena. If the electron density in the material is arranged periodically, as *e. g.*, in a crystal lattice, the scattered waves can add up and give rise to constructive and

destructive interference. These interferences can then be recorded as a function of the incident angle of the X-ray beam with respect to the sample.

To visualize the X-ray scattering process, Figure 2.1 displays an X-ray directed with an angle θ onto a system with a lattice-plane distance d . As the X-ray (with a wavelength λ) enters the system, the waves reflected from different planes will have different optical paths towards the detector plane. The difference in path length of two reflected waves is calculated as ' $2d \sin \theta$ '. In case of constructive interference, this difference equals the integer multiples of the wavelength λ , which is known as Bragg's law.

$$2d \sin \theta = n \lambda$$

Bragg's law can be used to obtain the lattice-spacing d of a crystal system.

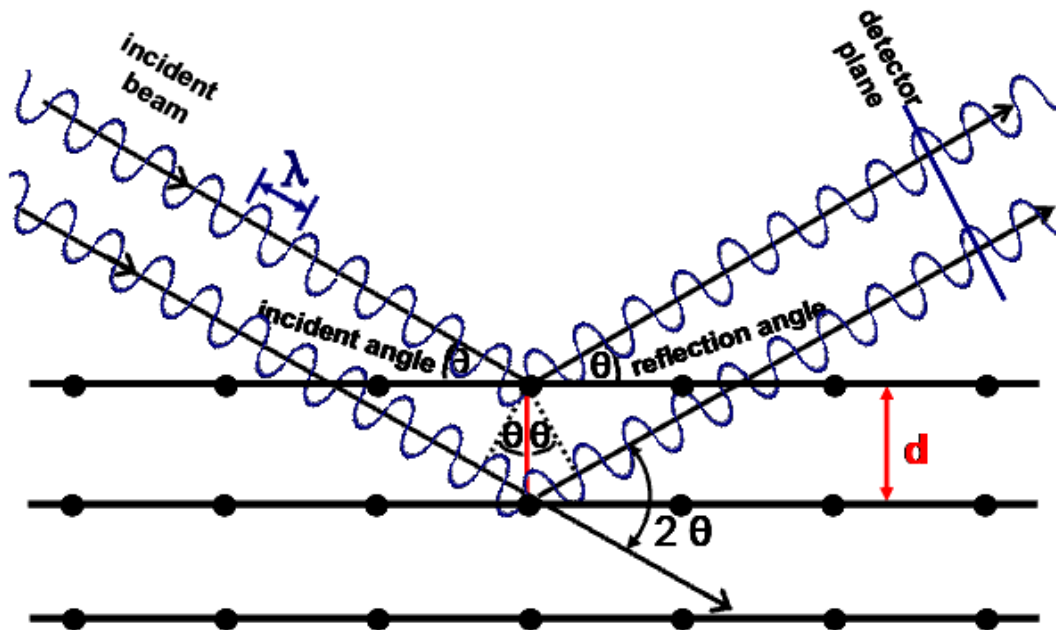


Figure 2.1: Schematic illustration of an X-ray diffraction experiment. Two incident waves are reflected on lattice planes causing constructive interference.

In case of periodic systems that have much larger lattice spacings than the atomic distances found in crystals, the corresponding diffraction angles of constructive interferences are small. Typically, scattering of X-rays at very low angles ($<10^\circ$) is called small angle X-ray scattering (SAXS).¹ SAXS is capable of delivering structural information in the nm-range, *e.g.*, the distance between mesopores and the periodicity of mesostructures. SAXS experiments can be performed either in transmission geometry or in reflection geometry. Compared to the reflection mode, in transmission experiments, the incident X-ray beam is not reflected by the sample, but instead travels through the sample where the diffraction process takes place. SAXS in transmission geometry, however, has disadvantages when measuring thick substrates or thin films, as the scattered X-rays cannot penetrate thick specimens and scattering volume is very small in thin films. Thus, depending on the nature of the sample an appropriate geometry has to be applied for the SAXS experiments. The mesostructured samples investigated in this thesis were usually obtained in the form of substrate-supported films or composite membranes. In case of thin composite membranes, SAXS experiments were performed in the transmission mode, whereas the substrate-supported thin films were measured in the reflection geometry.

Figure 2.2 illustrates the transmission geometry of a SAXS experiment on an anodic alumina membrane (AAM). The sample is placed into the X-ray beam and slightly tilted towards the beam in order to ensure the transmission of X-rays (a tilting angle of 10° was found to be the optimum). The X-rays which pass through the sample without interaction are weakened by a semi-transparent beam stop before detection, while those X-rays scattered from the periodic lattice planes are recorded as a scattering pattern. The position of the scattered X-rays is either recorded as a function of the scattering angle (θ)

2. Characterization

/ degree) or given as the scattering vector (q / nm^{-1}). The scattering angle θ and q -value are correlated through the equation:

$$q \cdot \lambda = 4\pi \cdot \sin\theta$$

Combining with Bragg's law, the lattice-plane-distance d can be calculated by the Bragg equation:¹

$$d = (2\pi/q) \cdot n.$$

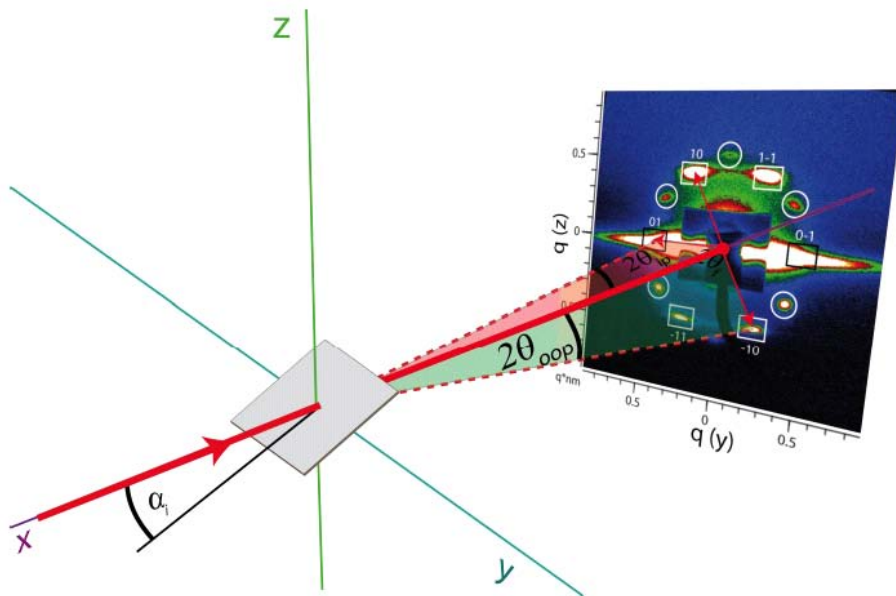


Figure 2.2: Transmission geometry of a SAXS experiment on an anodic alumina membrane (AAM) and the resulting diffraction pattern indexed according to a circular hexagonal structure in the channels of the AAM. (Figure adapted from ref. 2.)

For the substrate-supported film samples, the transmission geometry is not applicable due to the small scattering volume and the thick supporting substrate. Therefore, the SAXS experiments are performed in reflection mode, where the angle of incident

X-rays with respect to the sample surface is kept at a very low value. By varying the incident angle, the penetration depth of the X-rays can be tuned to probe specific regions of the thin film. This method is also called grazing incidence SAXS (GI-SAXS). The point-collimated X-ray beam is incident on the substrate-supported film and the scattered X-rays are recorded by a detector. Figure 2.3 illustrates the reflection geometry and a resulting scattering pattern of an orthorhombic structured thin film.³ The obtained two-dimensional scattering patterns can show reflections from lattice planes that are not only parallel but also tilted with respect to the substrate surface and thus much more information about the structure can be obtained than from one-dimensional diffraction patterns.

2D-SAXS patterns were collected by the SAXSess system from Anton Paar, in combination with a CCD detector system (Roper Scientific). Additionally, 1D scattering patterns were measured on a Bruker D8 Discover with a LynxEye detector. The wavelength of the incident beam was 0.154 nm (Cu-K_α) on both instruments.

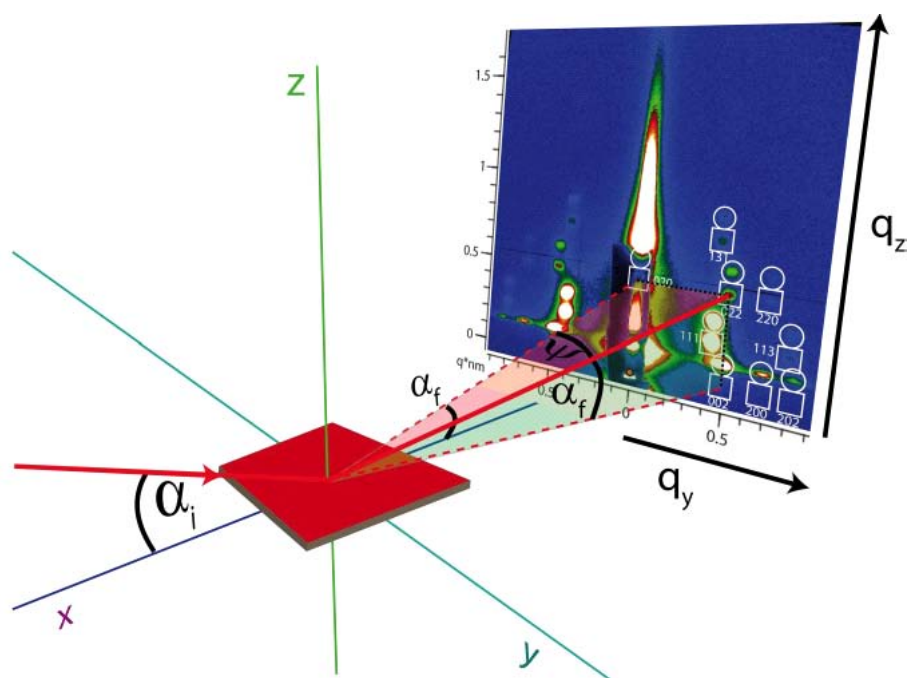


Figure 2.3: Reflection geometry of the SAXS experiment on a substrate-supported film and a resulting pattern indexed according to an orthorhombic mesostructure. The reflections are doubled due to diffraction of the incident beam reflected at the film substrate interface. (Figure adapted from ref. 3.)

2.2. Electron Microscopy

Electron microscopes, as the name implies, use a beam of electrons focused by magnetic lenses to illuminate a specimen and produce a magnified image. As the electrons have wavelengths that are much shorter than those of visible photons, electron microscopes are able to achieve magnifications of up to one million and more. Therefore, electron microscopes are frequently used to obtain structural and compositional information on the nanoscale. Typically, the electrons are emitted by an electron gun, commonly fitted with a tungsten filament cathode as the electron source.

The electron beam is accelerated by an anode and focused onto the specimen by electrostatic and/or electromagnetic lenses. Electron microscopes generally work under high vacuum conditions, in order to avoid beam extinction caused by electron collision with gas molecules. There are different types of electron microscopes. In the following, the concepts behind the scanning electron microscope (SEM) and the transmission electron microscope (TEM) will be described in more detail.

2.2.1. Scanning Electron Microscopy (SEM)

The Scanning Electron Microscopy (SEM) produces magnified images by probing the surface of a sample with a focused electron beam which is scanned across a selected sample area (raster scanning). The SEM technique can provide valuable information about the sample morphology, surface topology and composition of the observed material. In SEM, the electron beam typically has an energy ranging from 0.2 keV to 40 keV. Once the electron beam interacts with the sample, it loses energy that is converted into alternative forms such as heat, light emission, X-ray emission, as well as emission of secondary electrons and backscattered electrons.⁴ The converted energy can be detected by specialized detectors and in most SEMs secondary electron detectors are used to produce final images. A schematic representation of a SEM setup is shown in Figure 2.4.

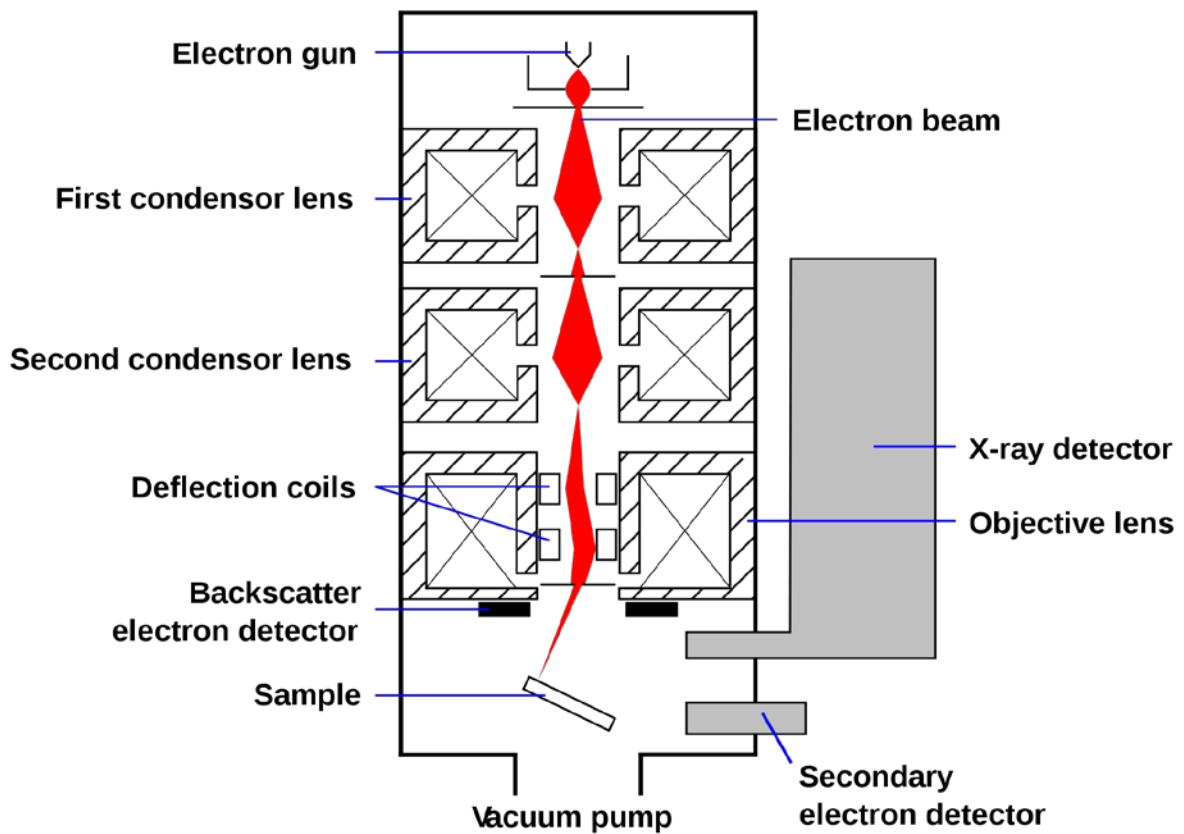


Figure 2.4: Schematic representation of a scanning electron microscope (SEM) equipped with a secondary electron detector, an X-ray detector as well as a backscattered electron detector. (Figure adapted from ref. 5.)

Magnification in an SEM can be adjusted from about 10 to 500,000 times. Unlike optical and transmission electron microscopes, the magnification of an image produced by the SEM is not a function of the power of the objective lens which is used to only focus the electron beam but not to image the specimen.⁶ In SEM, magnification results from the ratio of raster's dimension on the display device to the raster's dimension on the specimen. Assuming the display screen has a fixed size, higher magnification results from reducing the size of the raster scan on the specimen.

2.2.2. Transmission Electron Microscopy

Transmission electron microscopy (TEM) provides a much higher resolution than SEM, and can facilitate the analysis of features at the atomic scale by using an electron beam that has energy in the range of 40 to 400 keV. Unlike SEM which produces images by collecting electrons ejected from or near the surface of the sample, the TEM records images by collecting electrons that are transmitted through the sample. Therefore, specimens for TEM analysis have to be very thin (typically below 100 nm) to allow the electrons to pass through the sample. To obtain a thin specimen from a bulk material, common procedures for sample preparation involve cutting the sample into a thin piece with a diamond saw followed by dimple grinding and ion-beam excavation/milling. The electron beam is focused onto a region close to the border of the excavated hole, where the specimen has a thickness of only tens of nanometers. The transmitted electrons are first focused by the objective lens to form a magnified ‘image’ which is further magnified by the projective lenses to create the final image that can be detected by a fluorescent screen or by a CCD (charge-coupled device) (Figure 2.5).

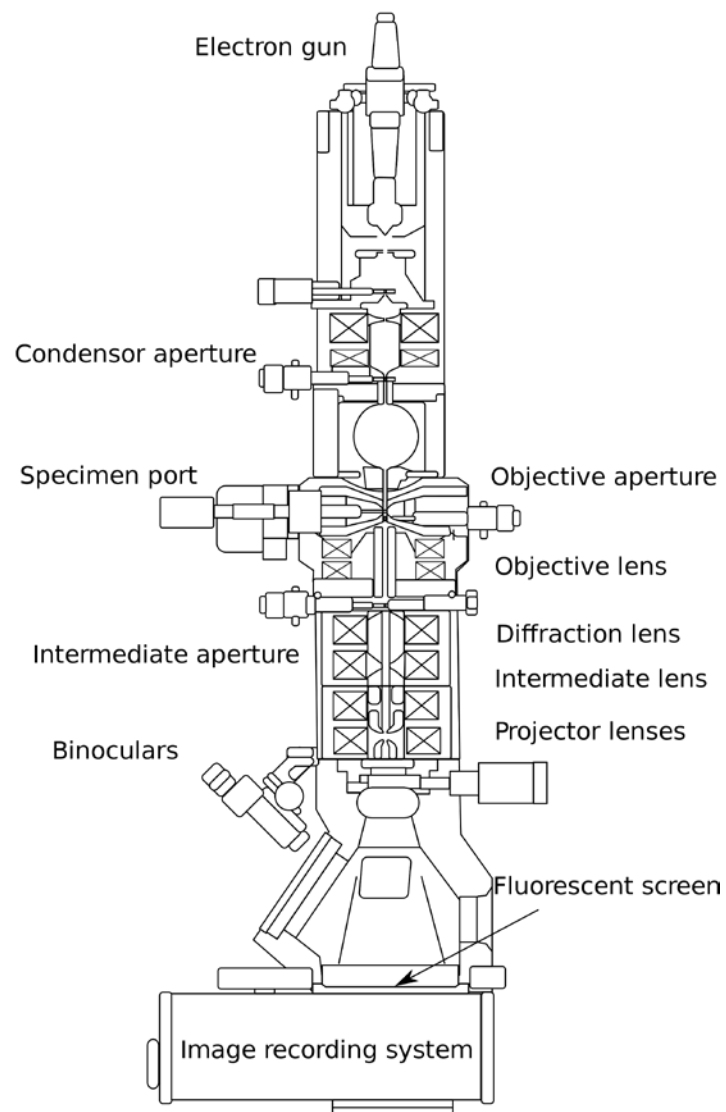


Figure 2.5: Schematic illustration of transmission electron microscopy, containing four main parts - electron source, electromagnetic lens system, specimen holder and imaging system. (Figure adapted from ref. 7.)

A special mode of operation of a TEM is the so-called scanning transmission electron microscopy (STEM) mode. Here, the electron beam is focused into a narrow spot which scans over the sample, and the electrons that go through the sample are detected at a

certain scattering angle. A commonly used detector in STEM is the high angle annular dark field (HAADF) detector which detects the electrons scattered at higher angles. The contrast of such an HAADF image is approximately proportional to the square of the atomic number. Thus, by using the HAADF-STEM imaging technique on mesostructured materials, the contrast between the mesopores and the framework can be highly enhanced compared to conventional TEM.

In this thesis, TEM measurements were made with a JEOL JEM 2011 at an acceleration voltage of 200 kV or with a FEI TITAN 80-300 microscope at an acceleration voltage of 300 kV. HAADF-STEM images were also recorded using the TITAN 80-300 microscope at an acceleration voltage of 300 kV.

2.2.3. Elemental analysis (EDX, EELS)

Energy-dispersive X-ray spectroscopy (EDX) is a technique used to obtain a localized elemental analysis by measuring the X-ray spectra emitted from a specimen bombarded with a focused electron-beam. When an electron beam strikes a specimen, electronic transitions can occur, which results in the emission of X-rays. Due to the unique electronic structure of each element, the corresponding emitted X-rays can be used to identify one element from another. An energy-dispersive spectrometer is used to detect the number and energy of the generated X-rays, which provides information on the elemental composition of the observed specimen.

Electron energy loss spectroscopy (EELS) is often carried out as a technique complementary to the EDX analysis. EELS is an absorption spectroscopy with which we measure the energy loss of the incident electrons following transmission through a

thin specimen. The electron energy loss signals are directly collected with a spectrometer positioned under the specimen. With EELS, it is possible to analyze the elemental composition of the sample and in addition, it can also determine the electronic structure, chemical bonding, valence and conduction band electronic properties.⁸

It is possible to obtain both EDX and EELS spectra with electron microscopes, resulting in a direct correlation of the morphology with the qualitative or quantitative data about the elements present in the sample.

EELS and EDX analysis in this thesis were obtained with the FEI Titan 80-300 electron microscope operated at an acceleration voltage of 300 kV.

2.3. Nitrogen Sorption Measurements

The adsorption and desorption of gas molecules on the surfaces of solid materials is a commonly used method for the characterization of porous materials.⁹⁻¹⁰ The process of adsorption and desorption is usually recorded in the form of sorption isotherms, which are plots of the molar amount of adsorbate versus the relative pressure of the adsorptive p/p_0 (p is the equilibrium pressure, p_0 is the saturation pressure) at constant temperature. From the isotherms, information about the porosity of the material can be obtained, *e.g.*, surface area, pore volume and pore size distribution.

According to IUPAC, the majority of sorption isotherms are grouped into six types shown in Figure 2.6.¹¹ Based on the experimentally obtained isotherm, one can classify the observed material as microporous (pore size below 2 nm), mesoporous (pore size between 2 nm and 50 nm) and macroporous (pore size \geq 50 nm) materials.

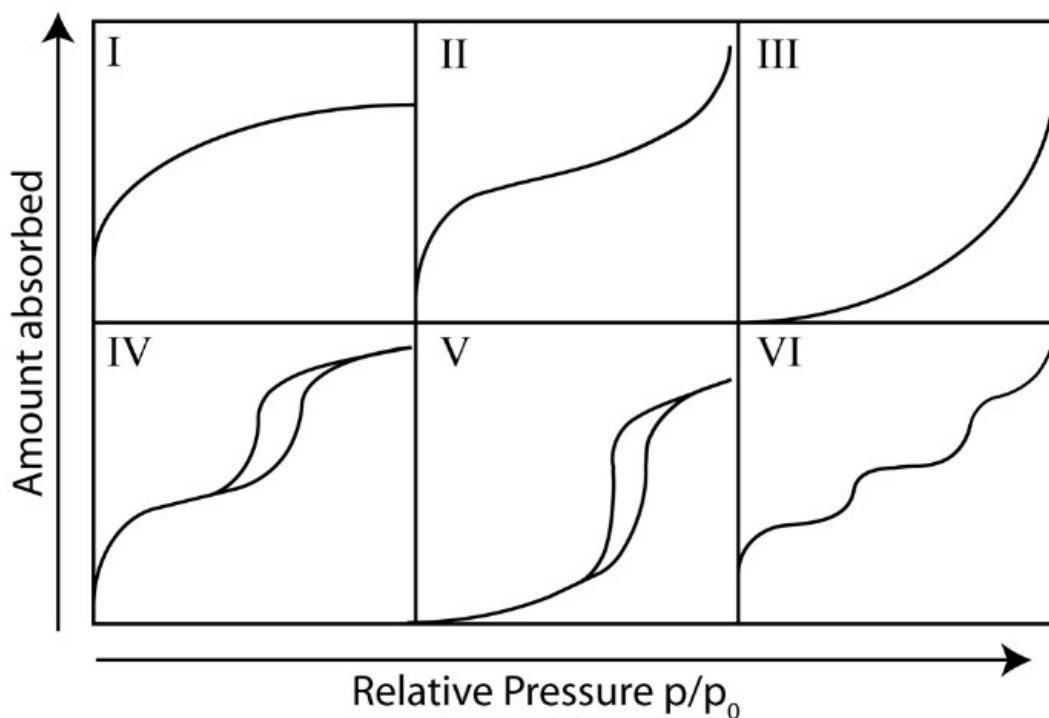


Figure 2.6: Six types of sorption isotherms defined by IUPAC. (Figure adapted from ref. 11.)

Mesoporous materials usually show the type IV isotherms. A frequently observed feature of the Type IV isotherm is its hysteresis loop, which is associated with capillary condensation taking place in mesopores. Some mesoporous materials, in which the interaction between the gas molecules and the porous material is rather weak, are of type V. From such sorption measurements, the porosity of the material such as surface area, pore volume and pore size can be obtained either with calculations derived from classical thermodynamics or with more modern theories based on density functional theory (DFT) or Monte-Carlo methods.

2. Characterization

For the determination of the surface area, the Brunauer-Emmett-Teller (BET) theory is widely used.¹²⁻¹³ The BET theory explains the multilayer adsorption of gas molecules on a solid surface which is based on the following hypotheses:

- (a) there are no interactions between adsorptive molecules in a layer;
- (b) the adsorption enthalpy for all layers is the same except the first layer, where the enthalpy is based on interactions between the solid material and the gas molecules;
- c) at saturation pressure, the number of adsorbed layers becomes infinite.

Using this theory, the surface area of the material can be calculated from the number of adsorbed molecules in the first monolayer. Then the specific surface area of the observed material can be obtained through the following equation

$$a_s (\text{BET}) = n_m^a \cdot L \cdot a_m / m$$

Where n_m^a is the monolayer capacity, m is the mass of the solid material, L is the Avogadro constant, and a_m is the cross-sectional area of the adsorbed gas molecule.

For the evaluation of the pore-size-distribution (PSD) of mesoporous materials, besides the BJH (Barret-Joyer-Halenda) approach which is based on the modified Kelvin equation,¹⁴⁻¹⁵ another quite often used method is based on density functional theory (DFT).¹⁶ Using this theory, a “kernel” is created which consists of hundreds of theoretical, individual isotherms and is used to compare with the experimental isotherm in order to calculate the PSD. For mesoporous organosilica materials, a silica-DFT kernel is quite often used for the PSD analysis.

Another parameter needed to indicate the porosity is the pore volume. It can be calculated from the amount of adsorbate at a value of p/p^0 close to 1, since at this point all the pores in the material are filled.

In this thesis, the sorption experiments were performed with N_2 as adsorptive at its boiling point of 77 K. The measurements were carried out with a NOVA 4000e Surface area & Pore Size Analyzer or an Autosorb-1 by Quantachrome Instruments. All samples were outgassed at 150 °C for 12 hours prior to measurement.

2.4. Nuclear Magnetic Resonance Spectroscopy

Nuclear magnetic resonance (NMR) spectroscopy is applied to determine the physical and chemical properties of atoms or the molecules containing these atoms.¹⁷⁻¹⁸ This technique relies on the phenomenon that atomic nuclei of many elemental isotopes have characteristic spin and behave like small magnets that will align themselves with an external magnetic field. Through exploiting the quantum mechanical magnetic properties of certain atomic nuclei, NMR spectroscopy can provide detailed information about the chemical structure, reaction state and chemical environment of molecules.¹⁹ Specifically, when a sample that contains nuclei possessing spin is placed into a magnetic field and is subjected to a proper radiofrequency (rf) radiation, the atomic nuclei in the lower energy spin state can be excited to the higher energy spin state. The frequency of the rf radiation at which this excitation occurs normally depends on the type of nucleus and also on the chemical environment of the nucleus.²⁰ Since the energy difference between the two spin states is proportional to the strength of the external magnetic field, an NMR spectrum for a sample can be obtained by varying the magnetic field at a constant frequency of rf radiation or by varying rf radiation with the magnetic field kept constant.

For a solid-state sample in which molecules have no or little mobility, the chemical shift anisotropy and the inter-nuclear dipolar coupling could lead to a phenomenon of line broadening in the NMR spectra. One common technique to eliminate this anisotropic effect is the fast rotation of the sample at an angle of 54.7° relative to the electric field, *i.e.*, magic-angle spinning nuclear magnetic resonance (MAS-NMR).²¹ In the case of liquid-state NMR experiments, Brownian motion of the molecules leads to an averaging of anisotropic interactions, thus limiting the line broadening effects.

In this thesis, the solid-state ^{13}C and ^{29}Si NMR measurements were performed using a Bruker Avance III 500 spectrometer which has a magnetic field of 11.74 T (resonance frequencies of 99.4 and 125.8 MHz for ^{29}Si and ^{13}C NMR, respectively).

2.5. Ultraviolet - visible Spectrophotometer

Ultraviolet-visible (UV-Vis) spectrophotometry is a technique used to investigate the ability of a compound to absorb light in the visible, near-UV and near-infrared ranges of the electromagnetic spectrum, *i.e.*, typically at least a range of 800 - 200 nm is covered. The absorption behavior of a molecule relies on its ability to undergo electronic transitions, *i.e.*, electrons in the molecule can be excited from the ground state to a higher energy level with absorption of a certain light energy. Accordingly, a UV-Vis spectrum is a record of the absorbed intensity changing with the wavelength of light.²²⁻²⁴

The UV-Vis spectrometer can be used for both qualitative and quantitative investigations of the samples. The extent of the absorption is proportional to the amount of the species absorbing the light. This linear relationship between the absorbance and concentration of an absorbing species is based on the Beer-Lambert Law which is described as follows:

$$A = \epsilon * b * c$$

Where A is the measured absorbance, it can also be calculated as $A = -\log(I/I_0)$, where I_0 is the intensity of the incident light and I is the light intensity after it passes through the sample; ϵ is a constant known as the wavelength-dependent molar absorptivity; b is the path length of the light in the sample; c is the concentration of the species absorbing the light.

In this thesis, UV-Vis absorption of solutions and films were determined by a Hitachi U-3501 UV-Vis spectrophotometer. In this double-beam spectrometer, a tungsten lamp or a deuterium lamp are used as the light source. A monochromator is employed for separating light of different wavelengths. The monochromatic light is then divided into two beams with a half mirror so that one passes through the sample and the other is used as reference which is unavailable with the single beam spectrometer. The difference of light intensity between reference and sample beam can be detected by a photomultiplier and finally is output as absorbance.

2.6. Fluorescence Spectroscopy

Fluorescence spectroscopy is a type of electromagnetic spectroscopy which is used to obtain fluorescence emitted from a sample and analyze the excited electronic states existing in the investigated species.

In fluorescence spectroscopy, by absorbing a photon a molecule is first excited from its ground electronic state (a low energy level) to one of the various vibrational states in a higher electronic energy level. The excited molecule rapidly loses vibrational energy

due to collision with its environment and falls initially to the lowest vibrational state of the excited state. Then the molecule drops back to the ground state and emits a photon in this process, which results in the fluorescence emission (illustrated in Figure 2.8).²⁵⁻²⁶ At a given excitation wavelength, the plot of emission intensity against wavelength of light is known as the fluorescence emission spectrum.

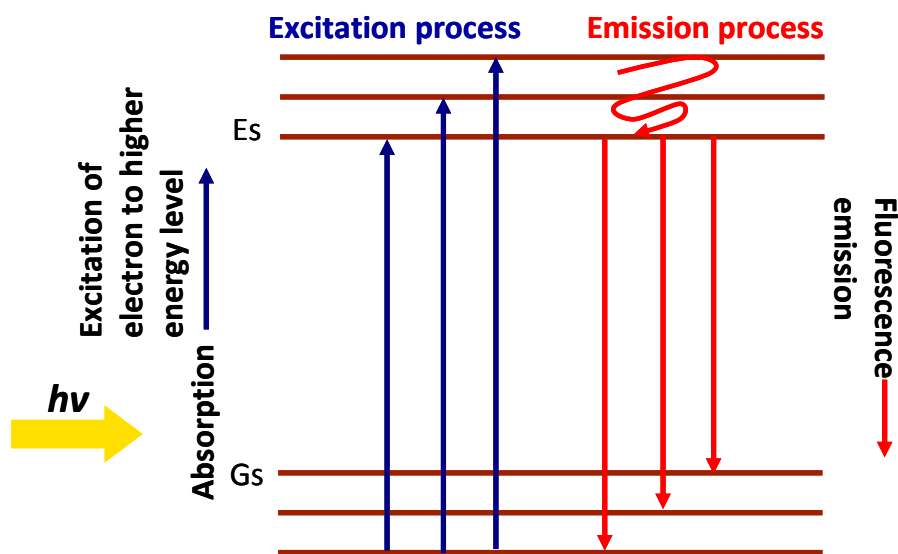


Figure 2.8: Energy levels and electronic transitions of the excitation and emission processes; Gs and Es stand for ground state and excited state, respectively.

In this thesis, Fluorescence spectra were recorded with a fluorescence spectroscopy system (PTI 814 from Photon Technology international), excitation was achieved with a xenon arc lamp.

2.7. External Quantum Efficiency

In the context of photovoltaic systems, quantum efficiency (QE) is an important measurement for a photoactive device as it gives information on the current that a given device will produce when illuminated by light with a particular wavelength.

With optoelectronic devices, one often measures the external quantum efficiency (EQE), which is the ratio of the number of charge carriers collected outside the device to the number of incident photons. Once a photon has been absorbed and has generated an electron-hole pair in the device, these charges can be separated at the electron donor-acceptor junction and collected as current. The EQE behavior therefore is a collective measurement of light harvesting, charge separation and charge collection efficiencies. EQE is often measured over a range of different wavelengths to characterize a device's efficiency at each photon energy.

2.8. Chapter References

1. H. Schnablegger and Y. Singh, *A practical guide to SAXS*, Anton Paar GmbH Austria, Gratz, 2006.
2. J. Schuster, PhD thesis, LMU München, Munich, 2011, p. 31.
3. J. Schuster, PhD thesis, LMU München, Munich, 2011, p. 33.
4. J. W. S. Hearle, J. T. Sparrow and P. M. Cross, *The use of the scanning electron microscope*, Pergamon Press, Oxford; New York, 1972.
5. http://en.wikipedia.org/wiki/File:Schema_MEB_%28en%29.svg.

2. Characterization

6. G. I. Goldstein, D. E. Newbury, P. Echlin, D. C. Joy, C. Fiori and E. Lifshin, *Scanning electron microscopy and x-ray microanalysis*, Plenum Press, New York, 1981.
7. http://en.wikipedia.org/wiki/File:Scheme_TEM_en.svg.
8. S. J. B. Reed, *Electron Microprobe Analysis, 2nd edn*, Cambridge University Press, 1993.
9. S. J. Gregg and K. S. W. Sing, *Adsorption, surface area and porosity*, Academic Press, London, 1982.
10. J. Rouquerol, D. Avnir, C. W. Fairbridge, D. H. Everett, J. H. Haynes, N. Pernicone, J. D. F. Ramsay, K. S. W. Sing and K. K. Unger, *Pure & Appl. Chem*, 1994, **66**, 1739-1758.
11. K. S. W. Sing, D. H. Everett, R. A. W. Haul, L. Moscou, R. A. Pierotti, J. Rouquerol and T. Siemieniewska, *Pure & Appl. Chem*, 1985, **57**, 603-619.
12. S. Brunauer, P. H. Emmett and E. Teller, *J. Am. Chem. Soc.*, 1938, **60**, 309-319.
13. G. Fagerlund, *Materials and Structures*, 1973, **6**, 239-245.
14. E. P. Barrett, L. G. Joyner and P. P. Halenda, *J. Am. Chem. Soc.*, 1951, **73**, 373-380.
15. K. Katsumi, *J. Membr. Sci.*, 1994, **96**, 59-89.
16. S. Lowell, *Characterization of porous solids and powders: surface area, pore size, and density*, Kluwer Academic Publishers, 2004.

2. Characterization

17. J. W. Akitt and B. E. Mann, *NMR and Chemistry*, UK: Stanley Thornes, 2000.
18. J. Keeler, *Understanding NMR Spectroscopy*, John Wiley & Sons, 2005.
19. F. A. Bovey, *Nuclear Magnetic Resonance Spectroscopy*, Academic Press Inc., New York, 1991.
20. T. L. James, *Control* 1998, **27**, 1-31.
21. H. Eckert, *Encyclopedia of materials characterization - Surfaces, Interfaces, Thin Films*, Butterworth-Heinemann Ltd, 1992.
22. D. C. Harris, *Quantitative Chemical Analysis, 7th Ed.*, Freeman, New York, 2007.
23. J. P. Sibilio, *Materials Characterization and Chemical Analysis*, Wiley-VCH, New York, 1996.
24. D. A. Skoog, F. J. Holler and S. R. Crouch, *Principles of Instrumental Analysis, 6th Ed.*, Thomson Brooks/Cole, 2004.
25. A. Sharma and S. G. Schulman, *Introduction to Fluorescence Spectroscopy*, Wiley Interscience, 1999.
26. J. R. Lakowicz, *Principles of Fluorescence Spectroscopy*, Springer US, 2006.



3. Hierarchically Structured Biphenylene-Bridged Periodic Mesoporous Organosilica

This chapter is based on the following publication:

Yan Li, Andreas Keilbach, Marcel Kienle, Yasutomo Goto, Shinji Inagaki, Paul Knochel, and Thomas Bein, *Journal of Materials Chemistry*, **2011**, *21* (43), 17338-17344.

3.1. Introduction

The synthesis of periodic mesoporous organosilica (PMO) materials has attracted much interest since their discovery in 1999.¹⁻³ These materials can be synthesized from alkoxysilyl precursors $(RO)_3SiR'Si(OR)_3$ in the presence of surfactants such as tetraalkylammonium halides or nonionic copolymers acting as structure directing agents. To date, numerous organic groups such as ethylene, thiophene, benzene, biphenylene, naphthalene, or divinylbenzene have been successfully incorporated in the framework of PMOs.⁴⁻⁶ By varying the organic linker group R', mesostructured materials tailored towards specific applications can be prepared. Such applications include catalysis,⁷ adsorbents,⁸ optical⁹⁻¹⁰ and electrical devices.¹¹ Recently, several PMO materials with optical properties have been reported, and among them, PMO thin films show interesting potential for use as fluorescent materials.¹²⁻¹⁵ For example, *Goto et al.* investigated the fluorescence properties of aromatic-bridged PMO films and found that biphenyl-bridged PMO exhibited exceptionally high fluorescence quantum yield (0.45) compared with benzene-, naphthalene-, and anthracene-bridged PMO films

3. Hierarchically Structured Biphenylene-Bridged Periodic Mesoporous Organosilica

(0.03-0.09).¹² A number of studies on biphenyl-bridged PMOs in powder form have been published.¹⁶⁻²³ Biphenyl-bridged PMO was also reported to exhibit excellent light-harvesting antenna properties²⁴ and to be applied to photocatalysis systems for hydrogen evolution from water²⁵ and CO₂ reduction to CO.²⁶

As the biphenyl-bridged PMO materials have such promising catalytic and optical properties, preparing biphenyl PMO as films on surfaces or at interfaces would be beneficial for applications in fields such as nanoscale catalysts, gas sensors, and optical devices. In thin films, which are usually prepared on glass or silicon substrates, the alignment of the mesopore channels is most often parallel to the substrate surface.^{12, 27} However, for certain electrical or optical devices, further control over the mesopore orientation would be desirable.²⁸⁻²⁹ Thus, there have been great efforts during the past years to control the mesoporous domain size and orientation in mesoporous systems. These efforts include application of external electric³⁰⁻³¹ or magnetic fields³²⁻³³, or use of chemically³⁴⁻³⁵ or lithographically²⁹ treated substrates. Among those methods, a feasible approach is to utilize anodic alumina membranes (AAMs) as host for mesoporous materials. For example, by incorporating mesostructured silica into the large channels of AAM, vertical alignment of the mesopores relative to the alumina membranes was achieved.³⁶⁻³⁹ Moreover, these types of hierarchical nanostructures can offer significant advantages over self-supporting thin films, such as higher mechanical stability and high aspect ratios of the mesophase system. While inorganic mesoporous silica has been studied extensively in the confinement of AAM pores,³⁶⁻⁴² there are only a few reports on the synthesis of mesoporous organosilicas confined in AAM channels. Some of us have recently reported the synthesis of ethane-bridged PMO in anodic alumina membranes.⁴³ The observed mesophases include the 2D hexagonal circular, the lamellar, and the cubic *Im-3m* phase. They are – except for the lamellar phase – stable

3. Hierarchically Structured Biphenylene-Bridged Periodic Mesoporous Organosilica

against surfactant removal by solvent extraction or mild calcination protocols. It turned out to be far more challenging to obtain ordered mesostructures of siloxane precursors with the larger biphenylene bridges. This type of precursor shows low solubility and a high hydrolysis rate leading to almost instant precipitation under common synthesis conditions. While there are only few reports on biphenylene-bridged PMO (Bp-PMO) thin films in the literature, we note that Bp-PMO thin films made with the ionic surfactant CTAB can show high order and stability.⁴⁴⁻⁴⁵ However, thin films synthesized with block co-polymers under acidic condition are usually not very stable against surfactant removal and are not highly ordered.¹² Given the favorable interaction of silica species with AAM channel walls found in inorganic silica/AAM systems, we reasoned that combining the biphenyl PMO system with AAMs might lead to different phase behavior and phase stability and thus open the way to designing novel hierarchical nanosystems which might move us closer to the application of Bp-PMO materials as optoelectronic devices.

In this study, we successfully synthesized highly ordered and stable Bp-PMO materials within AAM host systems. The synthesis was based on the evaporation-induced self-assembly (EISA) process.⁴⁶ Thus, 4, 4'-bis(triethoxysilyl)biphenyl (BTEBP) was used as organosilica source in combination with CTAB and F127 as structure directing agents. The resulting hierarchical Bp-PMO systems were characterized by small angle X-ray scattering (SAXS), transmission electron microscopy (TEM), nitrogen sorption and nuclear magnetic resonance (NMR) spectroscopy. In contrast to Bp-PMO thin films, which were reported to be not highly ordered and also electron beam-sensitive,¹² Bp-PMO confined within AAM channels was found to be stable against calcination temperatures of up to 250 °C. The composite materials also showed good stability in the electron beam of the electron microscope. Furthermore, all the oriented Bp-PMO/AAM

hierarchical materials showed fluorescence due to the existence of biphenyl chromophores in the stable organosilica framework.

3.2. Experimental Section

3.2.1. Synthesis of siloxane precursor

4,4'-bis(triethoxysilyl)biphenyl (BTEBP) was synthesized according to a procedure reported by Shea *et al.*⁴⁷ A dry and argon-flushed Schlenk-flask, equipped with a magnetic stirring bar and a septum, was charged with 4,4'-diiodobiphenyl (8.12 g, 20 mmol) and 40 mL THF. After cooling to 0 °C, *i*PrMgCl·LiCl (33.2 mL, 1.32 M in THF, 44 mmol) was added dropwise and stirred for 0.75 h. Then, the reaction mixture was cannulated to neat Si(OEt)₄ (20.8 g, 100 mmol) at 0 °C under argon. The mixture was allowed to warm up to 25 °C within 1.5 h. The crude reaction mixture was diluted with pentane (250 mL) and washed with NH₄Cl solution (5 %, 100 mL). The organic layer was dried (MgSO₄), filtered, and concentrated under reduced pressure. Purification by flash chromatography (pentane/Et₂O, 9:1) yielded 4,4'-bis(triethoxysilyl)biphenyl (3.92 g, 41 %) as a colorless oil. IR (ATR) ν (cm⁻¹) = 2974, 2925, 2886, 1600, 1389, 1295, 1165, 1128, 1094, 1070, 1004, 956, 807, 776, 732. ¹H-NMR (300 MHz, CDCl₃) δ = 7.74 (d, ³*J*(H,H) = 8.3 Hz, 4H, ArH), 7.62 (d, ³*J*(H,H) = 8.3 Hz, 4H, ArH), 3.89 (q, ³*J*(H,H) = 7.0 Hz, 12H, 6 x CH₂CH₃), 1.26 (q, ³*J*(H,H) = 7.0 Hz, 18H, 6 x CH₂CH₃). ¹³C-NMR (75 MHz, CDCl₃) δ = 142.7, 135.3, 129.9, 126.6, 58.8, 18.3. HRMS (EI, *m/z*): calc. for [C₂₄H₃₈O₆Si₂] 478.2207, found: 478.2202.

3.2.2. Preparation of bipenylene-bridged PMO in AAM channels

The synthesis of Bp-PMO confined in AAM channels was achieved by the evaporation-induced self-assembly (EISA) approach. Whatman Anodiscs (47 mm and 25 mm diameter, nominal pore diameter 0.02 μm) were used as porous alumina substrates. SEM measurements showed that these membranes have an effective pore diameter between 150 and 250 nm. 4, 4'-bis(triethoxysilyl)biphenyl (BTEBP) served as organosilica precursor. The ionic surfactant cetyltrimethylammonium bromide (CTAB, Aldrich) as well as nonionic triblock co-polymer Pluronic F127 (Aldrich) were used as structure directing agents (SDA). All chemicals were used without further purification. In the following, the samples are named with the used surfactant followed by the description of formed mesostructure, *e.g.* CTAB-columnar-lamellar indicates that the Bp-PMO within AAM channels is synthesized using CTAB as template and that it has a mesophase mixture of 2D-hexagonal columnar and lamellar structure.

For the preparation of CTAB-columnar-lamellar sample, 0.060 g (0.125 mmol) precursor BTEBP was mixed with 0.6 g of a 3.5 wt% ethanolic solution of CTAB (0.060 mmol) and stirred for 10 min. Then, 0.016 g (0.900 mmol) distilled H₂O was added and the solution was stirred for an additional 10 min. Next, 2.75 μL of 0.1 M HCl (2.75×10^{-4} mmol) were added and the resulting solution was stirred for another 2 h. Finally, the AAM was placed on a Teflon plate and soaked with the above-prepared precursor solution by distributing 0.75 ml of the solution over the whole membrane surface (47 mm diameter). During the EISA-process, the ambient conditions were kept at 45-55% relative humidity and 25 °C.

For the preparation of the F127-circular hexagonal sample, the following, slightly

3. Hierarchically Structured Biphenylene-Bridged Periodic Mesoporous Organosilica

altered protocol was used. First, Pluronic F127 (0.024 g, 0.002 mmol), ethanol (0.459 g), distilled H₂O (0.036 g, 2.0 mmol), and 1 M HCl (2.63 μ L, 2.63×10^{-3} mmol) were added into a small glass vial and stirred for 1 h. Then, 0.060 g BTEBP (0.125 mmol) was added to this solution and stirred for 3 min. Afterwards, a volume of 0.2 mL of the above prepared solution was cast onto the AAM surface (25 mm diameter) and left to dry. During this EISA-process, the ambient conditions were kept at 25-28% relative humidity and 25 °C. The synthesis conditions of the F127-cubic sample followed the same protocol as above with the exception that 0.0024 g LiCl (0.056 mmol) was additionally added to the F127 solution and only 0.10 ml of solution were cast onto the AAM surface (25 mm diameter).

If samples were calcined, the heating rate was 0.5 °C /min below 200 °C and 0.25 °C /min from 200 °C to 250 °C. The annealing periods were 5 h at 120 °C, 5 h at 200 °C and finally 10 h at 250 °C.

3.2.3. Characterization

The samples were characterized with 2D small-angle X-ray scattering (SAXS) using the SAXSess system by Anton Paar in combination with a CCD detector system (Roper Scientific). The wavelength of the incident beam is 0.1541 nm (Cu K α), the sample-detector distance was set to 308 mm. Samples were measured with a tilt angle of 10° with respect to the primary beam. Transmission electron microscopy (TEM) was performed using a JEOL 2011 with an acceleration voltage of 200 kV. Nitrogen sorption measurements were carried out at -196 °C using an Autosorb-1 by Quantachrome Instruments and before the measurements, the samples were degassed at 150 °C for 12 h in vacuum. The Brunauer-Emmett-Teller (BET) surface area was

3. Hierarchically Structured Biphenylene-Bridged Periodic Mesoporous Organosilica

calculated using experimental points at a relative pressure range of $p/p_0 = 0.05-0.20$. The total pore volume was calculated by the N_2 amount adsorbed at the point of $p/p_0 = 0.95$. DFT pore size distributions were calculated using an SiO_2 kernel assuming a cylindrical pore geometry for the F127-circular hexagonal sample and a cylindrical / sphere pore geometry for the F127-cubic sample. Solid-state ^{13}C and ^{29}Si NMR experiments were performed on a Bruker Avance-III 500 spectrometer (11.7 Tesla) operating at frequencies of 125.8 MHz for ^{13}C and 99.4 MHz for ^{29}Si . $^{13}C\{1H\}$ CP-MAS spectra were acquired using a 90° pulse length of 2.5 μs (-1.84 dB) with cross-polarization contact time of 2 ms and a recycle delay of 5 s. $^{29}Si\{1H\}$ CP-MAS experiments were conducted using a 90° pulse length of 2.5 μs (-1.84 dB) with cross-polarization contact time of 5 ms and a recycle delay of 2 s. The fluorescence spectra were measured with a fluorescence spectroscopy system (PTI 814 from Photon Technology international) with a xenon arc lamp.

3.3. Results and Discussion

3.3.1. CTAB-columnar-lamellar Bp-PMO

Using the ionic surfactant cetyltrimethylammonium bromide CTAB as structure directing agent, a phase mixture of the hexagonal columnar and the lamellar phase was obtained within the AAM channels. This can be contrasted to our previous results on CTAB/ethane-bridged PMO/AAM composites that form a 2D-hexagonal circular mesophase.⁴³ This difference could be related to the different character of the organic bridges of the siloxane precursor, such as the hydrophobicity, the flexibility and the size of the bridges, which might lead to different interactions between the SDA (structure

3. Hierarchically Structured Biphenylene-Bridged Periodic Mesoporous Organosilica

directing agents) and the organosilane precursor and thus lead to the formation of different mesophases. 2D small angle X-ray scattering (2D-SAXS) and transmission electron microscopy (TEM) were performed to characterize the mesostructure of the CTAB-columnar-lamellar system. The 2D-SAXS diffraction pattern for this confined Bp-PMO system (Figure 3.1A) shows only in-plane diffractions that correspond to either the hexagonal columnar phase or lamellar structure.

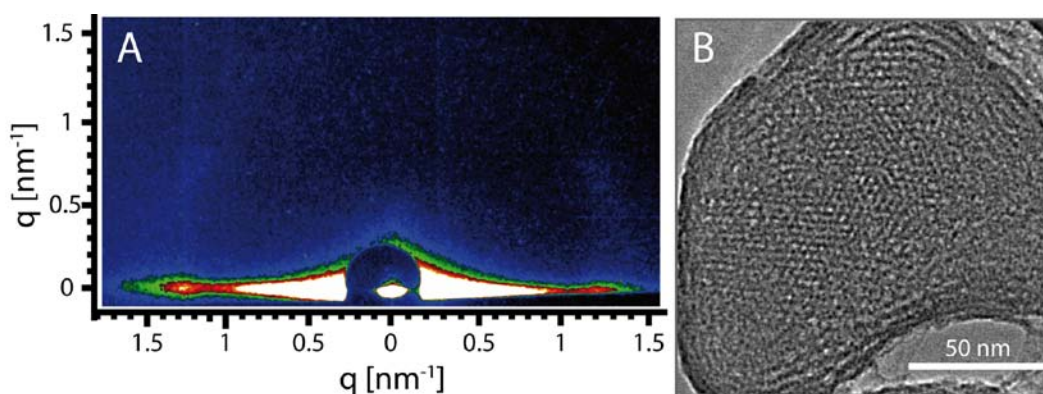


Figure 3.1: A) 2D-SAXS pattern and B) plan-view TEM micrograph of as-prepared CTAB-columnar-lamellar sample representing a mesophase mixture of the columnar and lamellar structure.

The observed d-spacing covers a wide range from 3.7 nm to 5.2 nm. According to previous studies, it is generally possible to distinguish between in-plane diffraction corresponding to the hexagonal phase or to the lamellar structure, as their d-values differ by a factor $\sin(120^\circ)$.⁴⁰ The diffraction spots corresponding to a larger d-spacing (closer to the primary beam) can be assigned to the lamellar phase, and the smaller d-spacing is assigned to the columnar phase, respectively. Additionally, TEM micrographs of the as-prepared CTAB-columnar-lamellar Bp-PMO system confirm the formation of the phase mixture of columnar and lamellar structures. Plan-view TEM micrographs of such samples show that the lamellar phase is preferentially located at the

3. Hierarchically Structured Biphenylene-Bridged Periodic Mesoporous Organosilica

AAM channel wall surrounding the columnar hexagonal phase in the center of the channel (Figure 3.1B). Because of the lamellar structure existing in the system, the mesophase of the CTAB-columnar-lamellar system is not stable after surfactant removal due to the lack of 3-dimensional connection of the lamellar phase. In this case, obtaining good micrographs was difficult because of the shrinkage of the lamellar structure caused by electron beam irradiation (Figure 3.2).

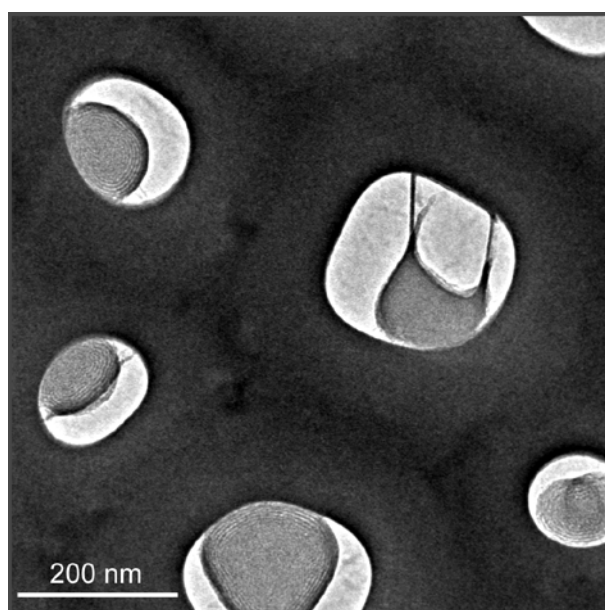


Figure 3.2: Plan-view TEM micrograph of the CTAB-columnar-lamellar Bp-PMO sample, demonstrating the significant shrinkage of the structure due to the existence of a lamellar phase.

3.3.2. F127-circular Bp-PMO

A second mesophase configuration was realized by using the nonionic surfactant pluronic F127 as structure directing agent. Bp-PMO with a 2D-hexagonal circular mesostructure was formed in AAM channels. The diffraction pattern recorded from

3. Hierarchically Structured Biphenylene-Bridged Periodic Mesoporous Organosilica

2D-SAXS measurements (Figure 3.3A) for the as-prepared F127-circular sample shows both in-plane and out-of-plane reflections that can be assigned to a circular hexagonal structure.⁴²⁻⁴³ In order to obtain an open pore system, the sample was calcined in air at 250 °C for 10 h to remove the surfactant template molecules from the mesophase. After calcination, the F127-circular-250 Bp-PMO (F127-circular sample calcined at 250 °C) features a highly ordered mesostructure as observed by 2D-SAXS (Figure 3.4A). The average d-spacing calculated from the diffraction pattern is 12.8 nm, which is in agreement with corresponding TEM results (Figure 3.4B). TEM micrographs of calcined samples also confirmed the preservation of the highly ordered and stable Bp-PMO with a minor shrinkage in the AAM channels after calcination (Figure 3.3B).

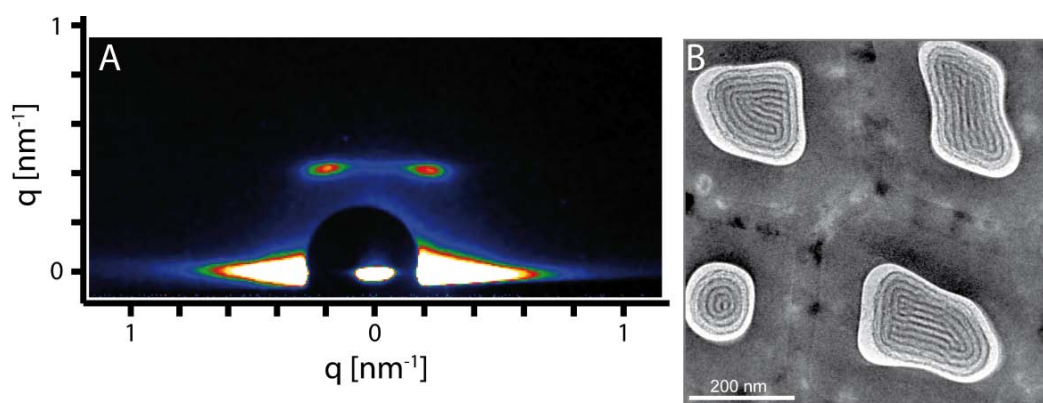


Figure 3.3: A) 2D-SAXS pattern of an as-prepared F127-circular Bp-PMO sample and B) plan-view TEM micrograph showing the preservation of highly-ordered circular structure and minor shrinkage of the structure of a calcined sample F127-circular-250 Bp-PMO.

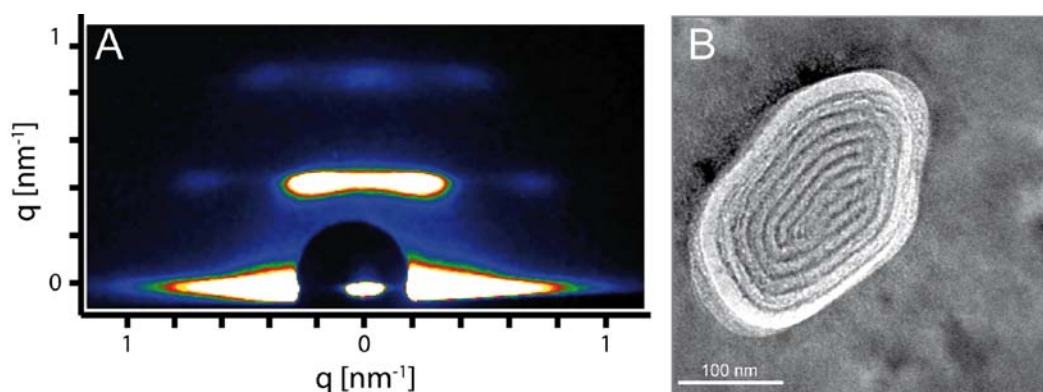


Figure 3.4: A) 2D-SAXS pattern and B) plan-view TEM micrograph showing the highly ordered circular structure of a calcined sample F127-circular-250.

The nitrogen sorption isotherms (Figure 3.5) of F127-circular-250 Bp-PMO show the typical type IV isotherm shape commonly observed for mesoporous materials, as well as a hysteresis loop. The BET surface area calculated from these isotherms is $58 \text{ m}^2 \text{ g}^{-1}$ and the pore volume is $0.072 \text{ cm}^3 \text{ g}^{-1}$ (the mass includes the AAM membrane) which are both similar to other previously reported values for PMO/AAM composites.⁴³ The isotherm shape (hysteresis loop) suggests the existence of ink-bottle shaped pores. This can be confirmed by comparing the DFT pore-size distribution from the adsorption branch (av. pore diameter $\sim 10.5 \text{ nm}$) and the desorption branch (av. pore diameter $\sim 5 \text{ nm}$), both of which show sharp pore size distributions with no significant distribution of the pore entrance sizes visible (Figure 3.6).

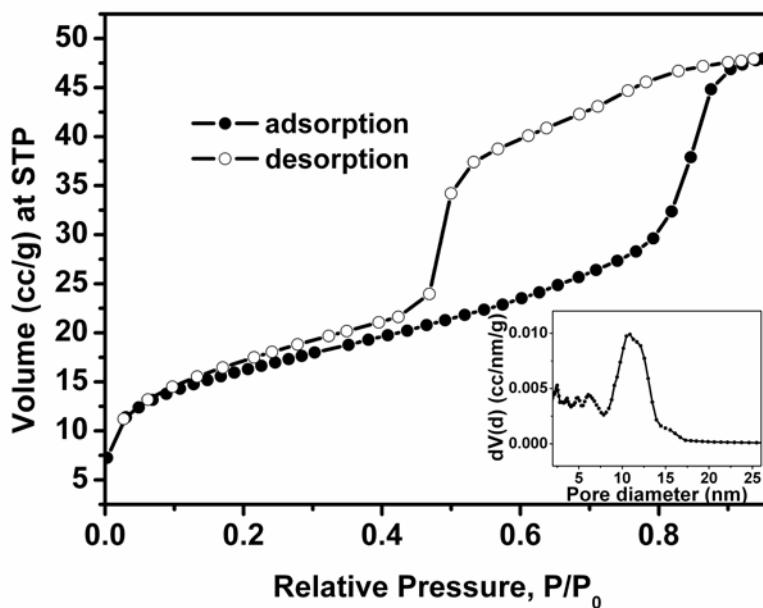


Figure 3.5: Nitrogen adsorption (●) and desorption (○) isotherms of the sample F127-circular-250 Bp-PMO with an inset showing the corresponding pore size distribution calculated with a DFT model from the adsorption branch.

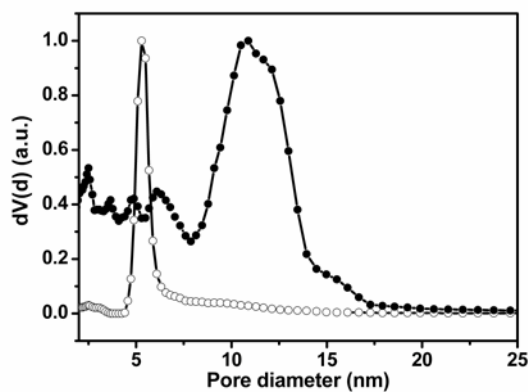


Figure 3.6: DFT pore-size distribution from the adsorption branch (●) and the desorption branch (○) of the sample F127-circular-250 Bp-PMO.

3. Hierarchically Structured Biphenylene-Bridged Periodic Mesoporous Organosilica

The ^{13}C -MAS NMR spectrum (Figure 3.7A) shows that the biphenylene groups are intact in the calcined material. The four aromatic resonances and their side bands are consistent with the results reported for the plain Bp-PMO system.^{16, 19} In addition, there is a weak signal that can be assigned to residual F127 molecules, indicating that the removal of template is not yet fully completed after these calcination conditions. In the ^{29}Si NMR spectrum of the calcined F127-circular-250 sample (Figure 3.7B), we observe strong resonances with high intensity attributed to T^2 -silicon species ($\text{CSi}(\text{OH})(\text{OSi})_2$) at -70.8 ppm and T^3 species ($\text{CSi}(\text{OSi})_3$) at -78.8 ppm. We note that only a minor resonance appears around -99.7 ppm; this signal can be assigned to Q^3 sites,⁴⁸ indicating that most of the Si-C bonds in the framework of the Bp-PMO material are still intact after calcination in air at 250 °C. Compared to Bp-PMO thin films, which were reported to be not highly ordered and electron beam sensitive,¹² the F127-circular Bp-PMO system within AAM channels shows a well-ordered mesopore system with high thermal and electron beam stability. We note that the same synthesis mixture did not result in an ordered mesostructure when deposited as thin film on a glass substrate.

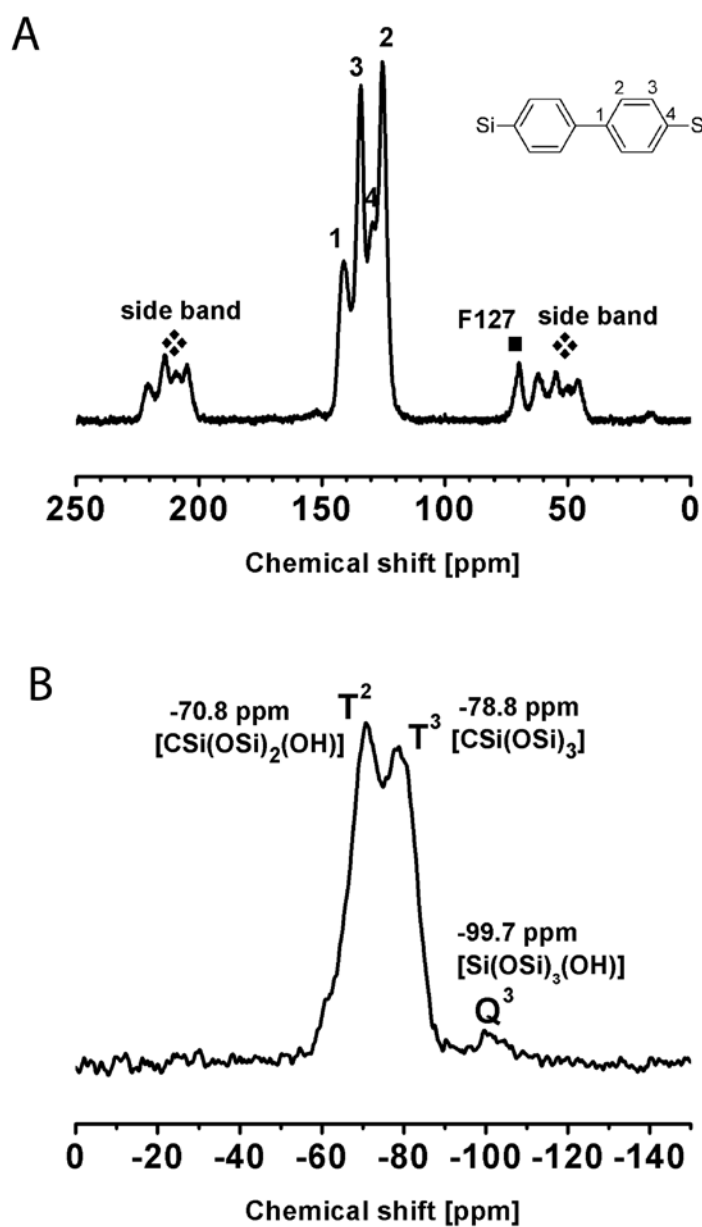


Figure 3.7: A) ^{13}C -MAS NMR and B) ^{29}Si NMR spectra of the calcined F127-circular-250 Bp-PMO sample.

3.3.3. F127-cubic Bp-PMO

Several recent reports have pointed to the profound impact of metal salts on the phase behavior of surfactant-templated mesoporous silica, which was described as “salt-induced phase transformation”.⁴⁹⁻⁵⁴ In an effort to study this effect in our Bp-PMO/AAM systems, we added inorganic salt into the synthesis solution for the F127-circular Bp-PMO system in order to possibly induce a transformation of the hexagonal circular to another mesophase. Lithium chloride was chosen as the inorganic additive because of its significant effect on the micellar hydration and gelation behavior of PEO-PPO-PEO triblock co-polymers in solution.⁵⁵⁻⁵⁶ The added LiCl indeed had a striking impact on the phase behavior, as the resulting PMO/AAM composites now showed a mesophase with cubic *Im-3m* orientation (body centered cubic), which is different from the original 2D hexagonal circular mesophase obtained without salt addition. The 2D-SAXS pattern of F127-cubic-200 Bp-PMO (F127-cubic sample calcined at 200 °C) shows the typical diffractions assigned to the cubic *Im-3m* phase (Figure 3.8A), similar to recent observations with other PMO and mesoporous polymer phases in AAM hosts.^{43, 57} The formation of cubic mesostructure was also confirmed by the following TEM micrographs. Plan-view TEM micrographs obtained from F127-cubic-200 Bp-PMO are displayed in Figure 3.8B. Two orientations, one along [111] (Figure 3.9A) and one along [110] (Figure 3.9B) can be observed. It is noteworthy that even after calcination at 200 °C, the sample shows no shrinkage, which is consistent with the low shrinkage of other cubic mesophases confined in AAM.⁴³ Another reason for the absence of shrinkage might be the added inorganic ions, which have been observed to increase the chemical interactions between organic silica mesophases and the AAM channel surface.⁵⁵

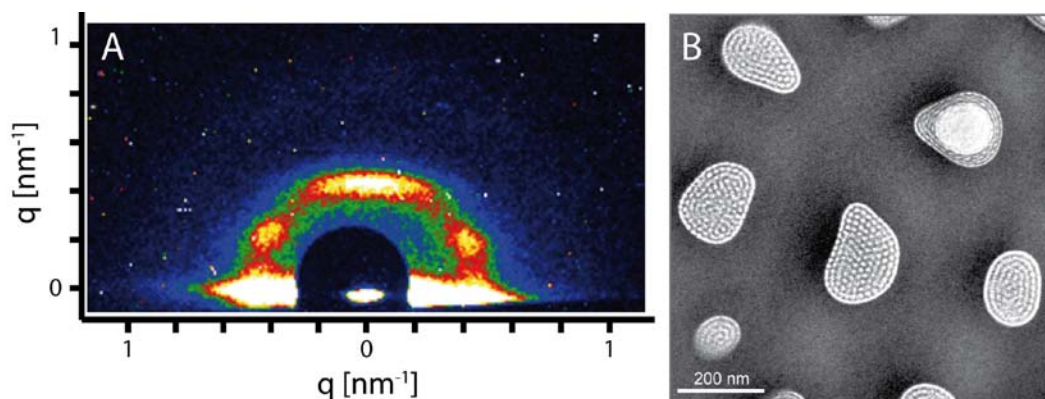


Figure 3.8: A) 2D-SAXS pattern and B) plane-view TEM of the F127-cubic-200 sample representing a highly-ordered cubic structure with absence of shrinkage after calcination at 200 °C

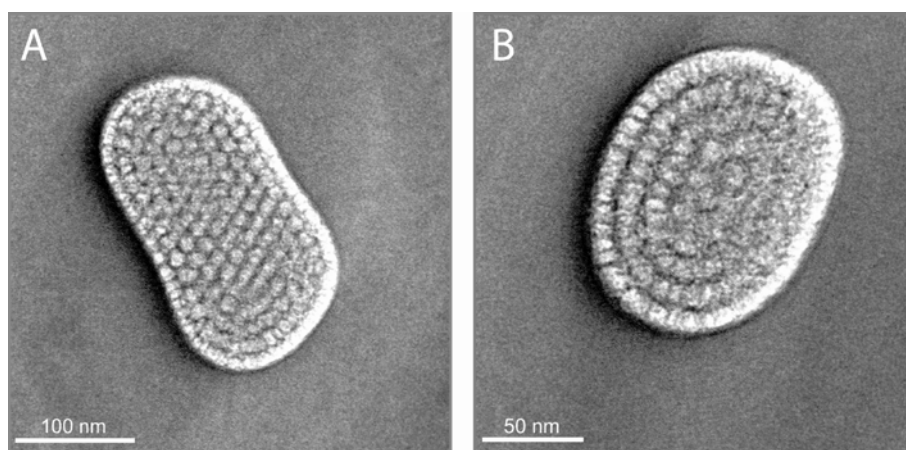


Figure 3.9: TEM micrographs of a F127-cubic-200 Bp-PMO. A) Plan-view along the [111] direction and B) Plan-view along the [110] direction.

The nitrogen sorption isotherm (Figure 3.10) of F127-cubic-250 Bp-PMO (F127-cubic sample calcined at 250 °C) shows the type IV shape with a broad hysteresis loop that is attributed to the existence of bottlenecks connecting pores in the cubic system. We attribute this pore-blocking situation to the incomplete removal of F127 surfactant from those spherical pores in the cubic system. The F127-cubic-250 sample shows a BET

3. Hierarchically Structured Biphenylene-Bridged Periodic Mesoporous Organosilica

surface area of $44 \text{ m}^2 \text{ g}^{-1}$ and a pore volume of $0.053 \text{ cm}^3 \text{ g}^{-1}$, comparable with the values obtained from the circularly structured system F127-circular-250 described above. The pore-size distribution peaks at a pore diameter of 13.8 nm. The ^{13}C and ^{29}Si NMR data (Figure 3.11) of the sample F127-cubic-250 Bp-PMO are consistent with those obtained from the sample F127-circular-250 Bp-PMO. The cubic Im-3m structured Bp-PMO material shows a well-ordered mesophase and thermal stability up to $250 \text{ }^\circ\text{C}$, which is advantageous for possible applications of these Bp-PMO materials.

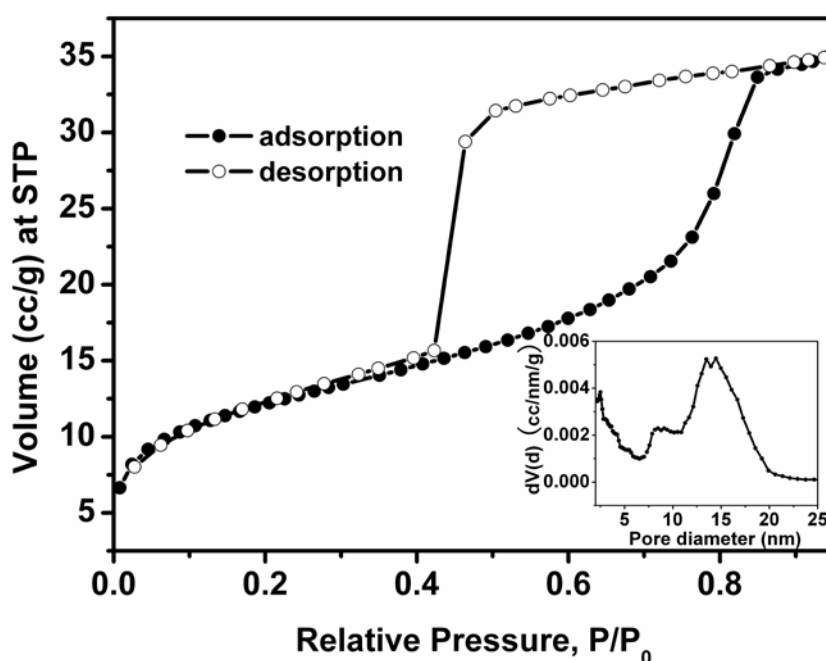


Figure 3.10: Nitrogen adsorption (●) and desorption (○) isotherms of the F127-cubic-250 Bp-PMO with an inside graph showing the corresponding pore size distribution calculated by DFT model from the adsorption branch.

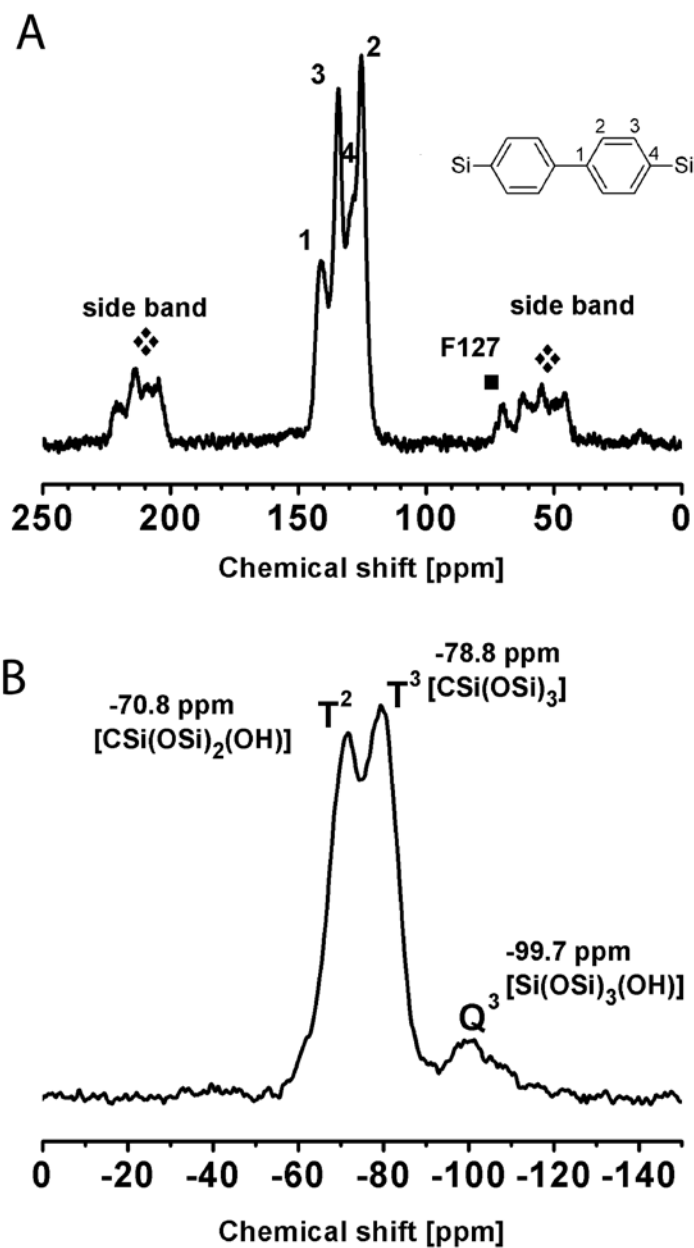


Figure 3.11: A) ^{13}C -MAS NMR and B) ^{29}Si NMR spectra of the calcined F127-cubic-250 Bp-PMO.

We attribute the phase transformation from the 2D hexagonal circular phase to the *Im-3m* cubic phase upon the addition of LiCl to the following mechanism. The presence of Li^+ ions and Cl^- ions can change the micellar hydration behavior of the pluronic F127

3. Hierarchically Structured Biphenylene-Bridged Periodic Mesoporous Organosilica

solution and thus change the curvature of the micelles.^{55-56, 58-59} Specifically, on the one hand the Cl^- ion has the effect of dehydrating hydrophilic groups of F127 micelles and thus decrease the curvature of F127 micelles. On the another hand, hydrated Li^+ ions can form complexes with the PEO chains in the micellar corona region,⁵⁸⁻⁶⁰ which can enlarge the hydrophilic head groups of the F127 micelles. In general, the effect of hydrated Li^+ is stronger than that of Cl^- , such that the size of the hydrophilic head groups of F127 micelles can be increased, which can lead to more hydrophilic F127 micelles with higher curvature. Thus, we propose that the body-centered cubic $Im-3m$ structure with a higher micellar curvature was obtained after addition of LiCl to a solution that originally would result in the 2D hexagonal (circular) structure.

3.3.4. Fluorescent properties

Figure 3.12 shows fluorescence spectra of all the Bp-PMO phases within AAM channels and of a diluted solution of the BTEBP precursor. The fluorescence bands of all the Bp-PMO phases are shifted significantly to longer wavelengths compared to the emission wavelength of the diluted pure precursor solution. This emission behavior is consistent with that of the Bp-PMO thin film on quartz surfaces reported by Goto *et al.*,¹² indicating strong electronic interactions between the aromatic biphenyl groups that exist in the Bp-PMO phases in the AAM channels.

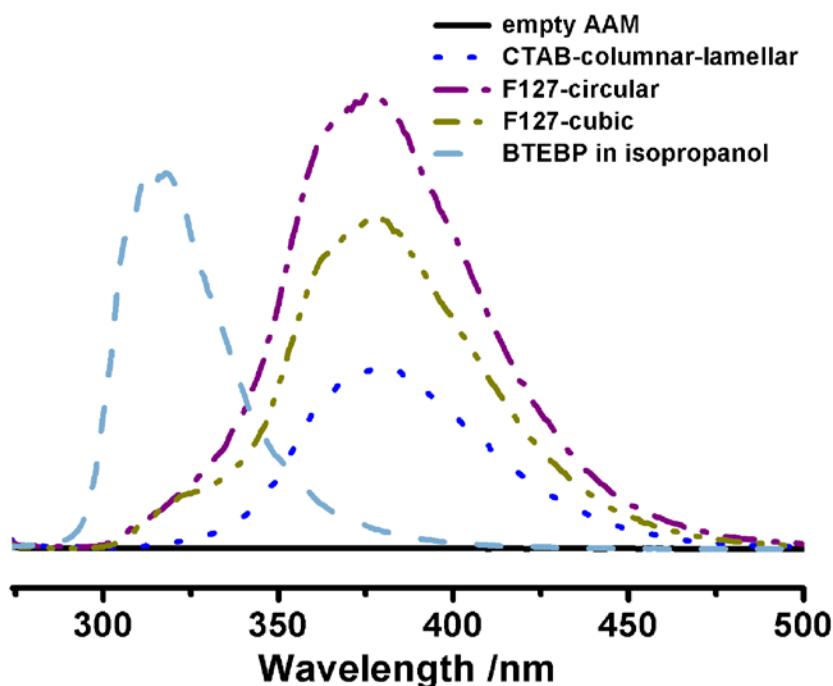


Figure 3.12: Fluorescent spectra (excited at 266 nm) of as-prepared Bp-PMO phases within AAM channels and a diluted BTEBP precursor solution in isopropanol (10^{-5} M) (The intensities are not to scale).

3.4. Conclusions

In summary, different PMO mesophases based on the biphenylene-bridged ethoxysilane BTEBP were successfully synthesized through an evaporation-induced self-assembly (EISA)-process within the pores of anodic alumina membranes. Depending on the surfactant used, different mesophases (Bp-PMO) could be observed. Using CTAB as the structure-directing surfactant, 2D-SAXS experiments and TEM images showed that a phase mixture of 2D-hexagonal columnar and the lamellar mesostructure was formed (sample CTAB-columnar-lamellar Bp-PMO). The lamellar phase appears to be

3. Hierarchically Structured Biphenylene-Bridged Periodic Mesoporous Organosilica

preferentially located close to the alumina walls, while the hexagonal columnar phase is dominant in the center of the channels. This result contrasts with earlier findings for CTAB/ethane-bridged PMO/AAM composites, where a hexagonal circular phase was the only mesophase obtained. When using the block co-polymer F127 as structure directing agent, the hexagonal circular PMO structure was found in the confined environment of the AAM pores. The addition of LiCl to the precursor/F127 solution leads to a striking structural transformation from the hexagonal circular to the body centered cubic (*Im-3m*) mesophase. The resulting composites with circular and cubic mesophases were both structurally stable against calcination in air at temperatures of up to 250 °C, which was also confirmed by ¹³C and ²⁹Si NMR measurements. All the prepared Bp-PMO/AAM hierarchical nanostructures showed fluorescence due to the biphenyl chromophores in the organosilica framework. The energy shift of the fluorescence emission with respect to the precursor molecules points to strong electronic interactions of the chromophores in the confined organosilica network. We therefore anticipate that the stable and oriented Bp-PMO/AAM composites and similar ordered chromophore-containing mesoporous hierarchical nanostructures will offer promise as optoelectronic systems.

3.5. References

1. T. Asefa, M. J. MacLachlan, N. Coombs and G. A. Ozin, *Nature*, 1999, **402**, 867-871.
2. S. Inagaki, S. Guan, Y. Fukushima, T. Ohsuna and O. Terasaki, *J. Am. Chem. Soc.*, 1999, **121**, 9611-9614.

3. Hierarchically Structured Biphenylene-Bridged Periodic Mesoporous Organosilica

3. B. J. Melde, B. T. Holland, C. F. Blanford and A. Stein, *Chem. Mat.*, 1999, **11**, 3302-3308.
4. B. Hatton, K. Landskron, W. Whitnall, D. Perovic and G. A. Ozin, *Acc. Chem. Res.*, 2005, **38**, 305-312.
5. F. Hoffmann, M. Cornelius, J. Morell and M. Fröba, *Angew. Chem., Int. Ed.*, 2006, **45**, 3216-3251.
6. B. D. Hatton, K. Landskron, W. Whitnall, D. D. Perovic and G. A. Ozin, *Adv. Funct. Mater.*, 2005, **15**, 823-829.
7. Q. H. Yang, J. Liu, L. Zhang and C. Li, *J. Mater. Chem.*, 2009, **19**, 1945-1955.
8. V. Rebbin, R. Schmidt and M. Fröba, *Angew. Chem., Int. Ed.*, 2006, **45**, 5210-5214.
9. P. N. Minoofar, R. Hernandez, S. Chia, B. Dunn, J. I. Zink and A. C. Franville, *J. Am. Chem. Soc.*, 2002, **124**, 14388-14396.
10. R. Hernandez, A. C. Franville, P. Minoofar, B. Dunn and J. I. Zink, *J. Am. Chem. Soc.*, 2001, **123**, 1248-1249.
11. N. Mizoshita, M. Ikai, T. Tani and S. Inagaki, *J. Am. Chem. Soc.*, 2009, **131**, 14225-14227.
12. Y. Goto, N. Mizoshita, O. Ohtani, T. Okada, T. Shimada, T. Tani and S. Inagaki, *Chem. Mat.*, 2008, **20**, 4495-4498.
13. N. Mizoshita, Y. Goto, T. Tani and S. Inagaki, *Adv. Funct. Mater.*, 2008, **18**, 3699-3705.

3. Hierarchically Structured Biphenylene-Bridged Periodic Mesoporous Organosilica

14. N. Mizoshita, Y. Goto, T. Tani and S. Inagaki, *Adv. Mater.*, 2009, **21**, 4798-4801.
15. N. Mizoshita, Y. Goto, Y. Maegawa, T. Tani and S. Inagaki, *Chem. Mat.*, 2010, **22**, 2548-2554.
16. M. P. Kapoor, Q. H. Yang and S. Inagaki, *J. Am. Chem. Soc.*, 2002, **124**, 15176-15177.
17. J. Morell, C. V. Teixeira, M. Cornelius, V. Rebbin, M. Tiemann, H. Amenitsch, M. Fröba and M. Linden, *Chem. Mat.*, 2004, **16**, 5564-5566.
18. Y. Yang and A. Sayari, *Chem. Mat.*, 2007, **19**, 4117-4119.
19. M. P. Kapoor, Q. H. Yang, Y. Goto and S. Inagaki, *Chem. Lett.*, 2003, **32**, 914-915.
20. M. Park, S. S. Park, M. Selvaraj, D. Y. Zhao and C. S. Ha, *Microporous Mesoporous Mat.*, 2009, **124**, 76-83.
21. K. J. Balkus, T. J. Pisklak, G. Hundt, J. Sibert and Y. F. Zhang, *Microporous Mesoporous Mat.*, 2008, **112**, 1-13.
22. E. R. Magdaluyo, R. V. R. Virtudazo, L. P. dela Cruz, E. V. Castriciones and H. D. Mendoza, *J. Ceram. Process. Res.*, 2010, **11**, 15-19.
23. F. Hoffmann, M. Guengerich, P. J. Klar and M. Fröba, *J. Phys. Chem. C*, 2007, **111**, 5648-5660.
24. S. Inagaki, O. Ohtani, Y. Goto, K. Okamoto, M. Ikai, K. Yamanaka, T. Tani and T. Okada, *Angew. Chem., Int. Ed.*, 2009, **48**, 4042-4046.

3. Hierarchically Structured Biphenylene-Bridged Periodic Mesoporous Organosilica

25. M. Ohashi, M. Aoki, K. I. Yamanaka, K. Nakajima, T. Ohsuna, T. Tani and S. Inagaki, *Chem.-Eur. J.*, 2009, **15**, 13041-13046.
26. H. Takeda, M. Ohashi, T. Tani, O. Ishitani and S. Inagaki, *Inorg. Chem.*, 2010, **49**, 4554-4559.
27. S. Y. Wu, H. S. Hsueh and M. H. Huang, *Chem. Mat.*, 2007, **19**, 5986-5990.
28. Y. N. Xia, P. D. Yang, Y. G. Sun, Y. Y. Wu, B. Mayers, B. Gates, Y. D. Yin, F. Kim and Y. Q. Yan, *Adv. Mater.*, 2003, **15**, 353-389.
29. R. L. Rice, D. C. Arnold, M. T. Shaw, D. Iacopina, A. J. Quinn, H. Amenitsch, J. D. Holmes and M. A. Morris, *Adv. Funct. Mater.*, 2007, **17**, 133-141.
30. M. Trau, N. Yao, E. Kim, Y. Xia, G. M. Whitesides and I. A. Aksay, *Nature*, 1997, **390**, 674-676.
31. K. Kuraoka, Y. Tanaka, M. Yamashita and T. Yazawa, *Chem. Commun.*, 2004, 1198-1199.
32. A. Firouzi, D. J. Schaefer, S. H. Tolbert, G. D. Stucky and B. F. Chmelka, *J. Am. Chem. Soc.*, 1997, **119**, 9466-9477.
33. Y. Yamauchi, M. Sawada, T. Noma, H. Ito, S. Furumi, Y. Sakka and K. Kuroda, *J. Mater. Chem.*, 2005, **15**, 1137-1140.
34. H. Miyata, T. Noma, M. Watanabe and K. Kuroda, *Chem. Mat.*, 2002, **14**, 766-772.
35. H. Miyata, T. Suzuki, A. Fukuoka, T. Sawada, M. Watanabe, T. Noma, K. Takada, T. Mukaide and K. Kuroda, *Nat. Mater.*, 2004, **3**, 651-656.

3. Hierarchically Structured Biphenylene-Bridged Periodic Mesoporous Organosilica

36. Z. L. Yang, Z. W. Niu, X. Y. Cao, Z. Z. Yang, Y. F. Lu, Z. B. Hu and C. C. Han, *Angew. Chem., Int. Ed.*, 2003, **42**, 4201-4203.
37. A. Yamaguchi, F. Uejo, T. Yoda, T. Uchida, Y. Tanamura, T. Yamashita and N. Teramae, *Nat. Mater.*, 2004, **3**, 337-341.
38. B. Platschek, N. Petkov and T. Bein, *Angew. Chem., Int. Ed.*, 2006, **45**, 1134-1138.
39. A. Yamaguchi, H. Kaneda, W. S. Fu and N. Teramae, *Adv. Mater.*, 2008, **20**, 1034-1037.
40. B. Platschek, R. Köhn, M. Döblinger and T. Bein, *Langmuir*, 2008, **24**, 5018-5023.
41. A. Y. Ku, S. T. Taylor and S. M. Loureiro, *J. Am. Chem. Soc.*, 2005, **127**, 6934-6935.
42. B. Platschek, R. Köhn, M. Döblinger and T. Bein, *ChemPhysChem*, 2008, **9**, 2059-2067.
43. A. Keilbach, M. Döblinger, R. Köhn, H. Amenitsch and T. Bein, *Chem.-Eur. J.*, 2009, **15**, 6645-6650.
44. M. A. Wahab and C. B. He, *J. Nanosci. Nanotechnol.*, 2008, **8**, 6381-6386.
45. M. A. Wahab and C. B. He, *Langmuir*, 2009, **25**, 832-838.
46. C. J. Brinker, Y. F. Lu, A. Sellinger and H. Y. Fan, *Adv. Mater.*, 1999, **11**, 579-585.

3. Hierarchically Structured Biphenylene-Bridged Periodic Mesoporous Organosilica

47. K. J. Shea, D. A. Loy and O. Webster, *J. Am. Chem. Soc.*, 1992, **114**, 6700-6710.
48. C. Breen, J. Madejova and P. Komadel, *J. Mater. Chem.*, 1995, **5**, 469-474.
49. Y. X. Yang, X. P. Qu, Y. R. Chen, X. C. Jia, J. B. Zhang and X. N. Liu, *J. Am. Ceram. Soc.*, 2007, **90**, 2050-2056.
50. C. Z. Yu, B. Z. Tian, J. Fan, G. D. Stucky and D. Y. Zhao, *Chem. Commun.*, 2001, 2726-2727.
51. C. Z. Yu, B. Z. Tian, J. Fan, G. D. Stucky and D. Y. Zhao, *J. Am. Chem. Soc.*, 2002, **124**, 4556-4557.
52. K. Flodstrom, V. Alfredsson and N. Kallrot, *J. Am. Chem. Soc.*, 2003, **125**, 4402-4403.
53. J. W. Tang, C. Z. Yu, X. F. Zhou, X. X. Yan and D. Y. Zhao, *Chem. Commun.*, 2004, 2240-2241.
54. M. Okamoto, Y. Fukukita, M. Haga, K. Toyofuku and N. Mimura, *J. Porous Mater.*, 2009, **16**, 135-140.
55. B. Platschek, N. Petkov, D. Himsl, S. Zimdars, Z. Li, R. Köhn and T. Bein, *J. Am. Chem. Soc.*, 2008, **130**, 17362-17371.
56. R. Ganguly and V. K. Aswal, *J. Phys. Chem. B*, 2008, **112**, 7726-7731.
57. J. Schuster, A. Keilbach, M. Döblinger and T. Bein, *Chem.-Eur. J.*, in press.
58. J. J. Lin and I. J. Cheng, *J. Appl. Polym. Sci.*, 2002, **85**, 612-621.

3. Hierarchically Structured Biphenylene-Bridged Periodic Mesoporous Organosilica

59. Y. Q. Wang, Y. J. Wang, C. M. Yang, G. Z. Lu and F. Schuth, *Langmuir*, 2006, **22**, 5491-5496.
60. P. Alexandridis and J. F. Holzwarth, *Langmuir*, 1997, **13**, 6074-6082.



4. Formation of Hexagonal and Cubic Fluorescent Periodic Mesoporous Organosilicas in the Channels of Anodic Alumina Membranes

4.1. Introduction

Mesoporous organic-inorganic compounds are attractive materials due to their capability of combining the advantages of organic and inorganic building blocks in a single material. These hybrid porous materials feature the versatile functionalities of the organic molecules as well as thermal stability and mechanical robustness of the inorganic parts.¹ Periodic mesoporous organosilicas (PMOs) are such a class of hybrid materials with organic units directly incorporated into the mesoporous silica pore walls, which have attracted much interest since their initial discovery in 1999.²⁻⁴ The method to obtain such mesostructured hybrid materials is by polycondensation of alkoxysilane precursor molecules in the presence of structure directing agents (*e.g.*, surfactants such as tetraalkylammonium halides or nonionic copolymers). The noteworthy point of the PMO materials is the successful integration of versatile organic groups in their pore walls, such as alkyl, double bonded or aromatic systems.⁵⁻⁸ The resulting functional porous materials can interact in different ways with guest molecules that reside in the pores, leading to potential applications of PMOs as catalysts,⁹⁻¹⁰ adsorbents,¹¹⁻¹² and optical¹³⁻¹⁶ systems. During recent years, great efforts have been made towards developing novel PMOs with photoactive or electroactive functions within their frameworks.¹⁷ Recently, a novel PMO material was reported with

4. Formation of Hexagonal and Cubic Fluorescent Periodic Mesoporous Organosilica in the Channels of Anodic Alumina Membranes

oligo(phenylenevinylene) molecules incorporated in the pore walls and was found to be charge-conducting (its charge carrier mobility was on the order of $10^{-5} \text{ cm}^2 \text{ V}^{-1} \text{ s}^{-1}$).¹⁸ This reported PMO was synthesized as film material on flat substrates. The synthesized film had mesopores with diameter of 2.4 nm and possessed a hexagonal packing of the mesochannels judged by indexing the diffraction peaks in the X-ray diffraction pattern. However, direct imaging of such a PMO film by electron microscopy was difficult due to the collapse of the mesostructure under electron-beam irradiation. Therefore, improving the stability of such PMO material, tuning the mesopore size and controlling the mesochannel orientation remain as major issues for further developing its potential.

In order to realize control over the domain size and orientation of mesoporous systems, there have been great efforts during the past years, including application of external electric¹⁹⁻²⁰ or magnetic fields²¹⁻²², or use of chemically²³⁻²⁴ or lithographically²⁵ treated substrates. Moreover, an alternative strategy uses confinement in anisotropic hosts such as porous anodic alumina membranes (AAMs).²⁶ The resulting mesoporous composites were reported to be able to offer high mechanical and thermal stability due to the support of the alumina host. Furthermore, the confinement effects can lead to enhanced control over the resulting mesophase morphologies, with the possibility to realize large single-phase domains and high aspect ratios of mesoporous systems.²⁷⁻³³ Given the favorable interaction of silica species with AAM channel walls found in inorganic silica/AAM systems, we reasoned that combining PMO systems with porous AAM might lead to different phase behavior and phase stability, thus improving the quality of PMO materials and meanwhile opening the way to designing novel hierarchical nanosystems. Based on our previous work on PMO/AAM composite systems,³⁴⁻³⁵ the present study focuses on the synthesis of the reported charge-conducting PMO within

4. Formation of Hexagonal and Cubic Fluorescent Periodic Mesoporous Organosilica in the Channels of Anodic Alumina Membranes

the confinement of AAM channels to achieve a new hierarchical PMO/AAM nanosystem which might move us closer to the application of PMO systems in optoelectronic devices.

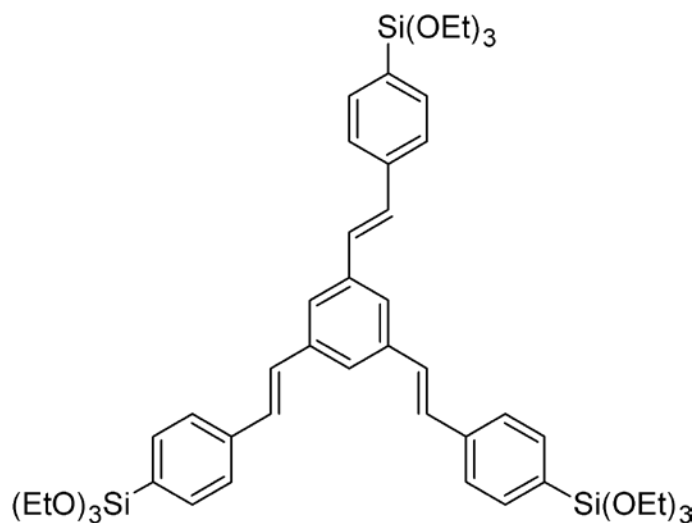
In this study, 1,3,5-tris(4-triethoxysilylstyryl)benzene (a three-armed oligo(phenylenevinylene) organosilane compound, denoted as 3a-OPV) was used as organosilica source to form PMO materials with Pluronic F127 or F108 as structure directing agents. Through a modified evaporation-induced self-assembly (EISA) process,³⁶ highly ordered and stable 3a-OPV-PMO materials were successfully synthesized within AAM host systems. The resulting hierarchical 3a-OPV-PMO/AAM systems were found to be stable against thermal treatment at temperatures of up to 200 °C and also stable in the electron beam of an electron microscope. The pore diameters of the PMO materials were around 10 nm due to the large sizes of the structure directing agents. With such large pore sizes, the resulting PMO materials offer compatibility with many other guest molecules, *i.e.*, the mesochannels of PMOs can accommodate large molecules such as photo-reactive precursors or charge-transporting molecules, so that these PMO materials could offer potential for applications in photocatalytic and photovoltaic fields. Furthermore, all the 3a-OPV-PMO/AAM hierarchical materials showed fluorescence in the visible region due to the strongly interacting phenylenevinylene chromophores in the stable organosilica frameworks.

4.2. Experimental Section

4.2.1. Preparation of 1,3,5-tris(styryl)benzene-bridged PMO in AAM channels

The synthesis of PMO confined in AAM channels was achieved by the evaporation-induced self-assembly (EISA) approach. Whatman Anodiscs (47 mm diameter, 60 μm thickness, 150~250 nm pore diameter) were used as porous alumina substrates. 1,3,5-tris(4-triethoxysilylstyryl)benzene (3a-OPV) (Scheme 4.1) served as organosilica precursor (provided by Toyota Central R&D Laboratories Inc., Japan). Triblock co-polymer F127 (poly(ethylene oxide)-poly(propylene oxide)-poly(ethylene oxide), $\text{EO}_{106}\text{PO}_{70}\text{EO}_{106}$, Sigma-Aldrich) and F108 ($\text{EO}_{132}\text{PO}_{50}\text{EO}_{132}$, Sigma-Aldrich) were used as structure directing agents (SDA). All chemicals were used without further purification. In the following, the 3a-OPV-PMO materials are named with the used SDA followed by the description of the formed mesostructure, *i.e.*, the samples synthesized by F127 and F108 are denoted as F127-circular and F108-cubic, respectively.

4. Formation of Hexagonal and Cubic Fluorescent Periodic Mesoporous Organosilica in the Channels of Anodic Alumina Membranes



Scheme 4.1: Chemical structure of 1,3,5-tris(4-triethoxysilylstyryl)benzene, a three-armed oligo(phenylenevinylene) precursor (denoted as 3a-OPV)

For the preparation of sample F127-circular, 3a-OPV (0.06 g, 0.067 mmol) and F127 (0.06 g, 0.005 mmol) were first dissolved in 2.316 g absolute EtOH. Then, distilled H₂O (0.030 g, 1.7 mmol) was added and the solution was stirred for 10 min. Next, 1 M HCl (4.2 μ L, 4.2×10^{-3} mmol) was added and the resulting solution was stirred for 2 h. Finally, the AAM was placed on a Teflon plate and soaked with the above prepared precursor solution by drop-casting 0.75 ml of the solution over the whole membrane surface (47 mm diameter, with an area of 17 cm²). During the EISA-process, the ambient conditions were kept at 45-55% relative humidity and 25 °C.

For the preparation of sample F108-cubic, the synthesis procedures followed the same protocol as above with the exception that 0.075 g F108 (0.005 mmol) was added to the precursor solution instead of F127.

4. Formation of Hexagonal and Cubic Fluorescent Periodic Mesoporous Organosilica in the Channels of Anodic Alumina Membranes

In order to remove the structure directing agents to get accessible mesopores, the PMO/AAM composites were calcined up to 200 °C with a heating ramp of 0.5 °C /min. Before reaching 200 °C, the samples were kept at 120 °C for 5 h and at last stayed for 10 h at 200 °C.

4.2.2. Characterization

The samples were characterized by 2D small-angle X-ray scattering (2D-SAXS) using the SAXSess system by Anton Paar with a CCD detector (PI-SCX:4300, Roper Scientific). The wavelength of the incident beam is 0.154 nm (Cu K α), the sample-detector distance was set to 308 mm. Samples were measured with a tilt angle of 10° with respect to the primary beam. Transmission electron microscopy (TEM) was performed using a JEOL 2011 with an acceleration voltage of 200 kV. Nitrogen sorption measurements were carried out at -196 °C using an Autosorb-1 by Quantachrome instruments, and before the measurements the samples were degassed at 150 °C for 12 h in vacuum. The Brunauer-Emmett-Teller (BET) surface area was calculated using experimental points at a relative pressure range of $p/p_0 = 0.05-0.20$. The total pore volume was calculated by the N₂ amount adsorbed at the point of $p/p_0 = 0.95$. NLDFT pore size distributions were calculated using an SiO₂ kernel assuming a cylindrical pore geometry for the F127-circular sample and a cylindrical / sphere pore geometry for the F108-cubic sample. Solid-state ¹³C and ²⁹Si NMR experiments were performed on a Bruker Avance-III 500 spectrometer (11.7 Tesla) operating at frequencies of 125.8 MHz for ¹³C and 99.4 MHz for ²⁹Si. ¹³C{1H} CP-MAS spectra were acquired using a 90° pulse length of 2.5 μs (3.7 dB) with cross-polarization contact time of 5 ms and a recycle delay of 2 s. ²⁹Si{1H} CP-MAS experiments were conducted

using a 90° pulse length of 2.5 μ s (2.7 dB) with cross-polarization contact time of 5 ms and a recycle delay of 4 s. The fluorescence spectra were measured with a fluorescence spectroscopy system (PTI 814 from Photon Technology international) with a xenon arc lamp.

4.3. Results and Discussion

4.3.1. F127-circular 3a-OPV-PMO

Using Pluronic F127 as structure directing agent, a circular hexagonal phase was observed within the AAM channels. In order to obtain an open pore system, the composite membranes were mildly calcined up to 200 °C. The highly ordered circular hexagonal structure was identified as the major phase by 2D small angle X-ray scattering (2D-SAXS) measurements. The 2D-SAXS pattern of the calcined sample (Figure 4.1A) shows both in-plane (10) and out-of-plane (01) peaks that are characteristics of a circular hexagonal structure confined in AAM channels.^{34, 37-38} The d-values calculated from the diffraction pattern are 14.5 nm and 15.6 nm, corresponding to d_{10} and d_{01} respectively. The TEM image (Figure 4.1B) of the calcined composite displays an electron-beam stable PMO with a highly-ordered hexagonal circular structure as the predominant phase formed in the AAM channels. The measured d-value is 14 nm, which is smaller than the values resulting from the X-ray diffraction. This can be attributed to the shrinkage of the porous system during the ion milling procedure, which is a crucial step in the TEM specimen preparation, as well as the effect of the exposure to the electron beam under high vacuum in the TEM. We note that the

4. Formation of Hexagonal and Cubic Fluorescent Periodic Mesoporous Organosilica in the Channels of Anodic Alumina Membranes

orientation of the hexagonal mesostructures could be influenced by the size and shape of AAM channels.³⁸ In a small number of the AAM channels, a hexagonal columnar structure was observed as a side phase (*e.g.* the channel on the left side in Figure 4.1B).

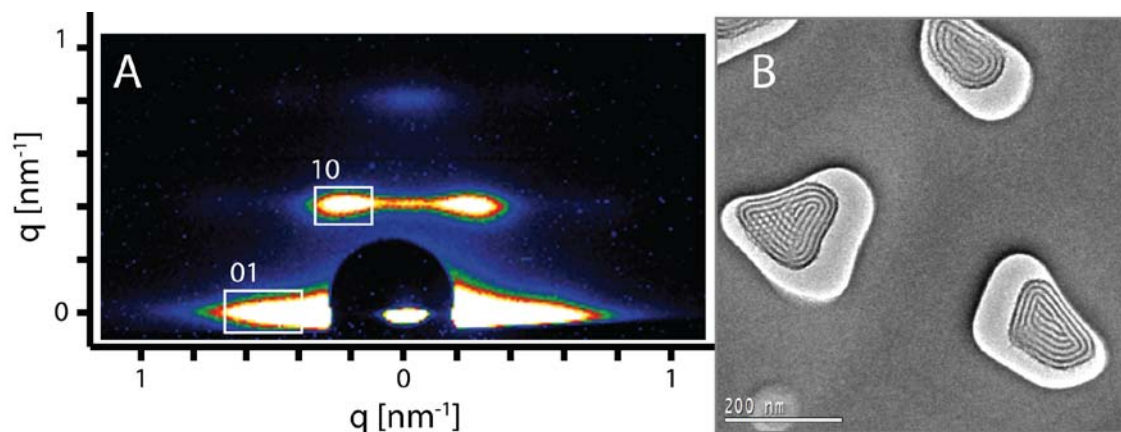


Figure 4.1: A) 2D-SAXS pattern and B) plan-view TEM micrograph of the calcined PMO/AAM composite showing the highly ordered hexagonal circular structure of the 3a-OPV-PMO formed with F127 as structure directing agent.

The nitrogen sorption isotherms (Figure 4.2A) of the calcined F127-circular PMO show the typical type IV isotherm shape commonly observed with mesoporous materials. The Brunauer-Emmett-Teller (BET) surface area calculated from the isotherm is $57.3 \text{ m}^2 \text{ g}^{-1}$ and the pore volume is $0.073 \text{ cm}^3 \text{ g}^{-1}$ (the mass for the calculation includes the AAM host). The isotherm has a large hysteresis loop suggesting the existence of ink-bottle shaped pores in the PMO material. This can be confirmed by comparing the DFT pore-size distributions from the adsorption branch (av. pore diameter $\sim 9.4 \text{ nm}$) and the desorption branch (av. pore diameter $\sim 5.3 \text{ nm}$), both of which show sharp pore size distributions (Figure 4.2B).

4. Formation of Hexagonal and Cubic Fluorescent Periodic Mesoporous Organosilica in the Channels of Anodic Alumina Membranes

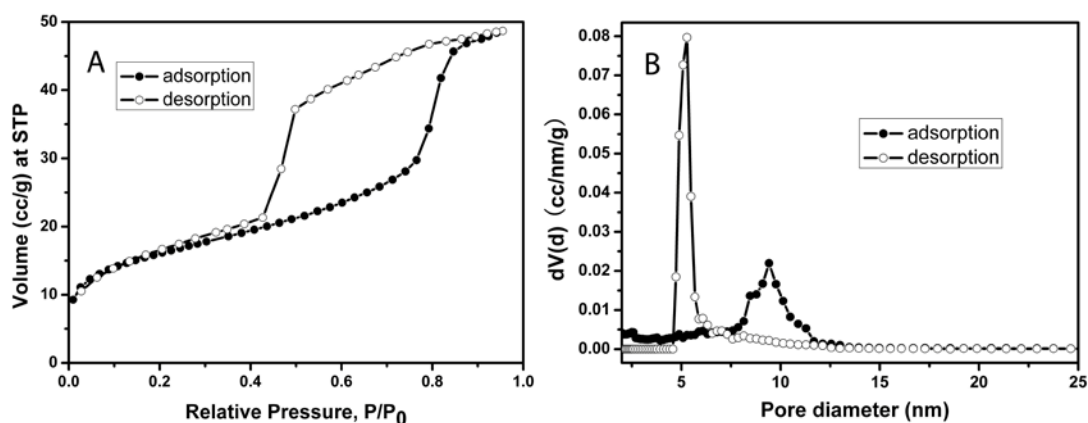


Figure 4.2: A) Nitrogen adsorption (●) and desorption (○) isotherms of the calcined F127-circular sample and B) pore size distributions calculated by a DFT model from both the adsorption branch (●) and desorption branch (○) by using an SiO₂ kernel assuming a cylindrical pore geometry.

In the ¹³C-MAS NMR spectrum (Figure 4.3A), the peaks at around 130 ppm and their spinning side bands (indicated by asterisk) correspond to the 1,3,5-tris(styryl)benzene group, suggesting the preservation of the organic units in the calcined F127-circular PMO material. In addition, weak signals (at 17.6 and 75.3 ppm) can be attributed to small amounts of residual F127 molecules, indicating the incomplete removal of the structure directing agent. This incomplete removal of F127 possibly caused partial blocking of the large mesopores and thus led to the ink-bottle shaped pores, which is in agreement with the above nitrogen sorption result. The ²⁹Si NMR spectrum (Figure 4.3B) shows resonances attributed to T²-silicon species (CSi(OSi)₂(OH)) at -71.3 ppm and T³ species (CSi(OSi)₃) at -80.2 ppm, suggesting a high degree of polycondensation of the organosilane precursors in the formed PMO pore walls. It is also noteworthy that no resonance appears in the Q-site region (around 100 ppm), indicating that the Si-C

4. Formation of Hexagonal and Cubic Fluorescent Periodic Mesoporous Organosilica in the Channels of Anodic Alumina Membranes

bonds were kept intact in the framework of the 3a-OPV-PMO material under all the conditions of preparation and thermal treatment.

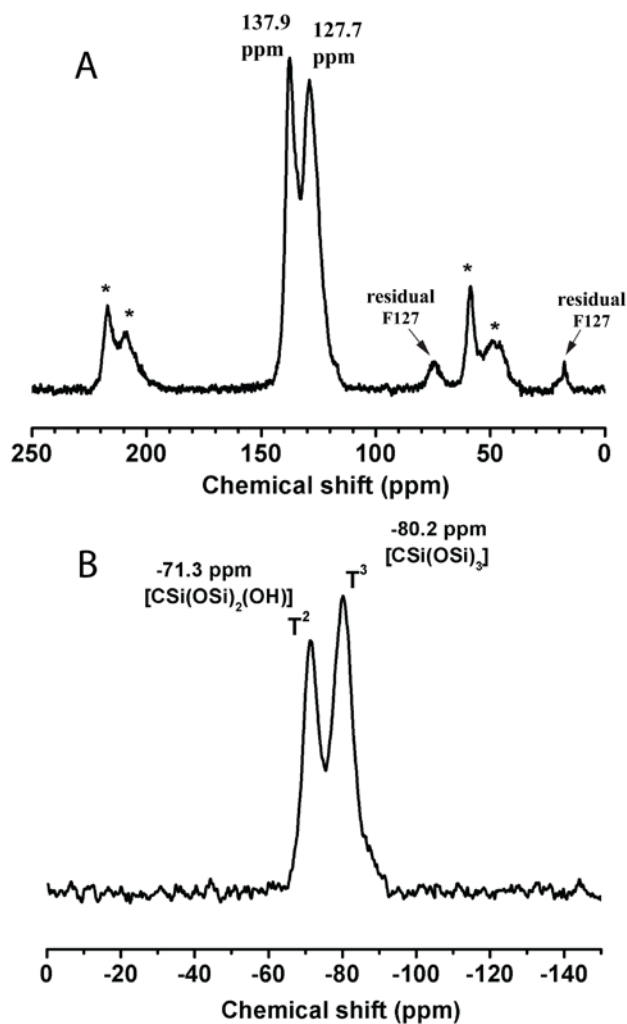


Figure 4.3: A) ^{13}C -MAS NMR and B) ^{29}Si NMR spectra of the calcined F127-circular sample, showing the almost complete removal of the surfactant F127, the highly condensed Si-O-Si network and the preserved Si-C bonds in the obtained stable PMO material. (Signals marked with asterisk denote the spinning side bands of the tris(styryl)benzene groups)

4.3.2. F108-cubic 3a-OPV-PMO

A second mesophase was created by using the triblock co-polymer F108 as structure directing agent. Compared to Pluronic F127 ($\text{EO}_{106}\text{PO}_{70}\text{EO}_{106}$), template F108 ($\text{EO}_{132}\text{PO}_{50}\text{EO}_{132}$) is a relatively hydrophilic surfactant with longer hydrophilic EO chains and shorter hydrophobic PO parts, which leads to micelles with higher curvature in the solution.³⁹ Thus, we reasoned that after replacing F127 with F108 into a solution that originally could result in a 2D hexagonal (circular) structure, a new structure would be formed. 2D-SAXS measurements were carried out to identify the mesostructure of the PMO templated by F108. The SAXS diffraction pattern recorded from the calcined sample shows the typical diffractions assigned to a body centered cubic *Im-3m* phase (Figure 4.4A), similar to recent observations with other cubic phases in AAM hosts,^{34-35,} ³⁸ indicating that 3a-OPV-PMO with a cubic structure was formed. The formation of the cubic mesostructure was also confirmed by the TEM micrographs. The averaging d-value resulting from the SAXS pattern is 17.4 nm, which is in good agreement with the value ($d_{110} = 17$ nm) measured from TEM image. A plan-view TEM micrograph obtained from the calcined F108-cubic sample is displayed in Figure 4.4B. It is remarkable that the F108-cubic PMO material within the AAM channels shows minor shrinkage; we attribute this to the three-dimensional connection existing in the cubic structure combined with the spatial confinement in the AAM host.

The porosity properties were determined by nitrogen sorption. Figure 4.5 depicts the isotherms of the calcined F108-cubic sample, showing the type IV shape with a very wide adsorption-desorption hysteresis that is attributed to large mesopores connected by smaller open windows in the cubic system. The BET surface area of the calcined

4. Formation of Hexagonal and Cubic Fluorescent Periodic Mesoporous Organosilica in the Channels of Anodic Alumina Membranes

F108-cubic composite is $37 \text{ m}^2 \text{ g}^{-1}$ and the pore volume is $0.071 \text{ cm}^3 \text{ g}^{-1}$ (the mass includes the AAM membrane). The pore-size distribution (calculated from the adsorption branch) shows a pore diameter of 14.0 nm . The ^{13}C and ^{29}Si NMR data (Figure 4.6) of the calcined F108-cubic sample are consistent with those obtained from the F127-circular system. All the characterization results show that a body centered cubic 3a-OPV-PMO is successfully formed with electron beam stability as well as thermal stability up to $200 \text{ }^\circ\text{C}$.

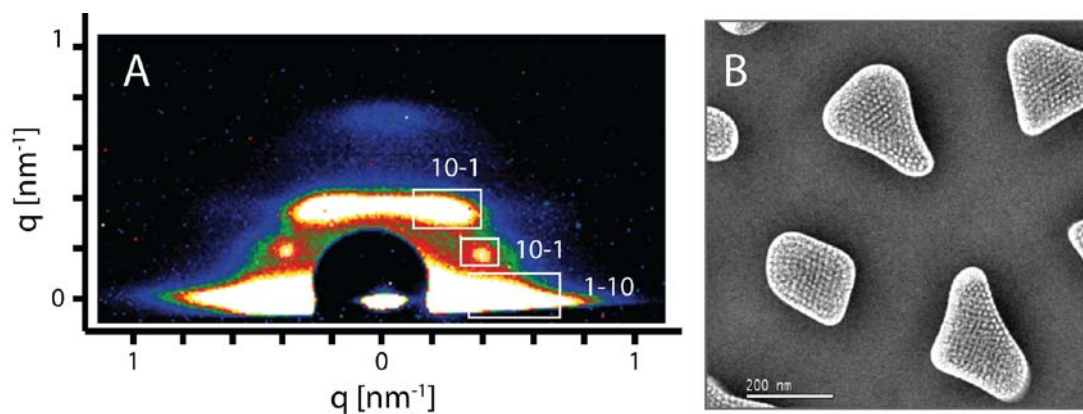


Figure 4.4: A) 2D-SAXS pattern and B) plan-view TEM micrograph of the calcined F108-cubic PMO, representing a highly-ordered body centered cubic structure with only minor shrinkage after thermal treatment.

4. Formation of Hexagonal and Cubic Fluorescent Periodic Mesoporous Organosilica in the Channels of Anodic Alumina Membranes

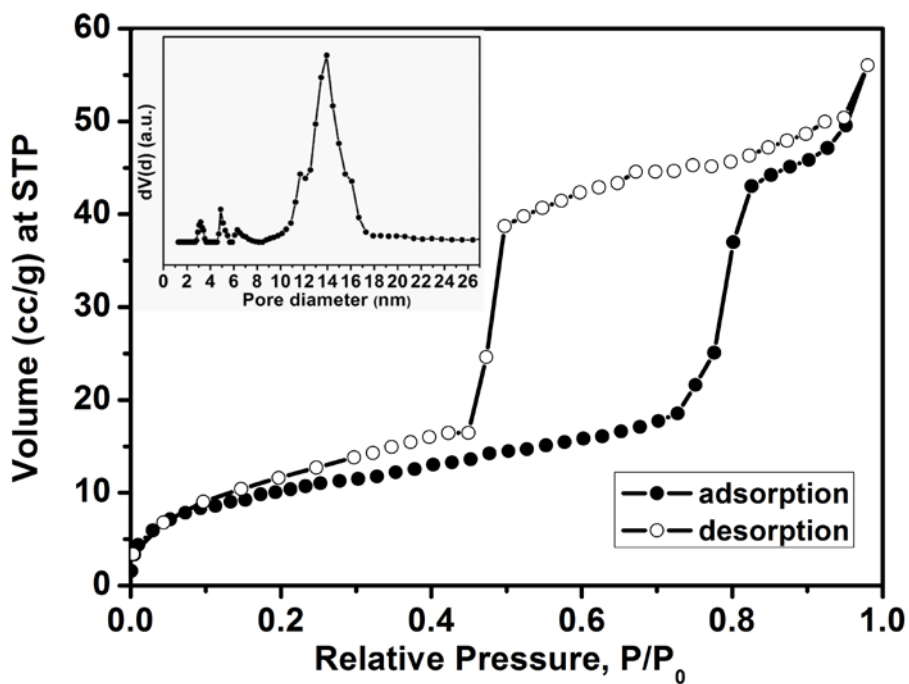


Figure 4.5: Nitrogen sorption isotherms of the calcined F108-cubic sample with an inset graph showing the corresponding pore size distribution calculated with a DFT model using the adsorption branch with a SiO_2 kernel assuming a cylindrical / spherical pore geometry.

4. Formation of Hexagonal and Cubic Fluorescent Periodic Mesoporous Organosilica in the Channels of Anodic Alumina Membranes

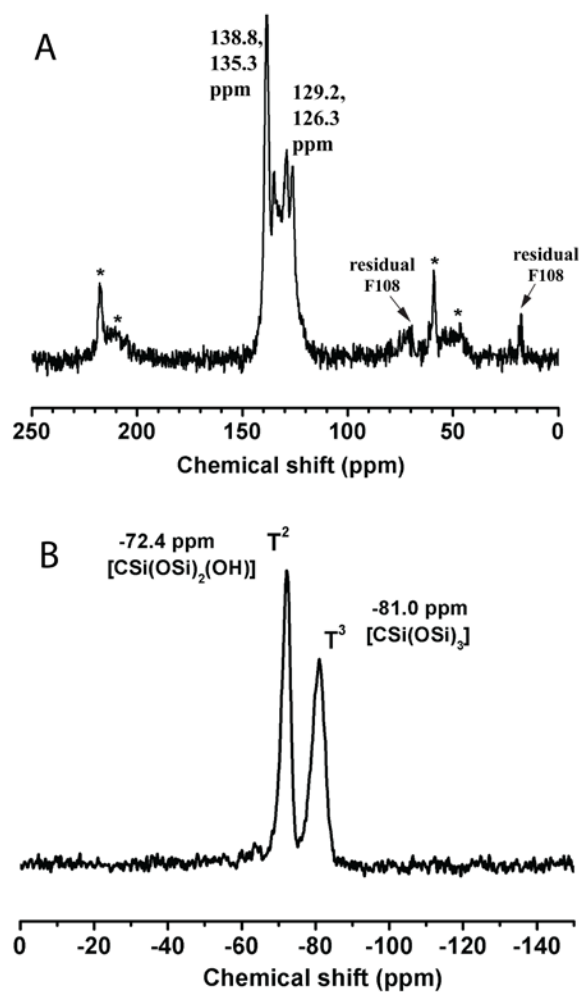


Figure 4.6: A) ^{13}C -MAS NMR and B) ^{29}Si NMR spectra of the calcined F108-cubic sample, showing the almost complete removal of the template Pluronic F108 and the high degree of condensation of the Si-O-Si network. (Signals marked with asterisk denote the spinning side bands.)

4.3.3. Fluorescence emission of 3a-OPV-PMO/AAM composites

Fluorescence emission spectra were recorded from both 3a-OPV-PMO/AAM composites and a diluted isopropanol solution of the 3a-OPV precursor (Figure 4.7).

4. Formation of Hexagonal and Cubic Fluorescent Periodic Mesoporous Organosilica in the Channels of Anodic Alumina Membranes

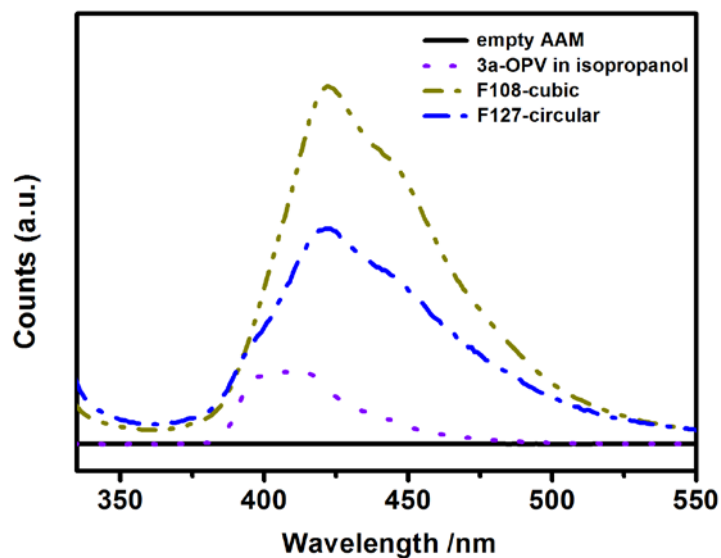


Figure 4.7: Fluorescence spectra (excited at 320 nm) of circular and cubic-structured 3a-OPV-PMO confined in AAM channels and a diluted 3a-OPV precursor solution in isopropanol (10^{-5} M) (The intensities are not to scale).

The resulting hierarchically structured 3a-OPV-PMO/AAM composites were observed to be fluorescent in the visible light region. The fluorescence emission bands of both circular and cubic PMO/AAM composites peak at a wavelength of 422 nm, which indicates a slight shift to longer wavelength with respect to the fluorescence emission of the diluted precursor solution (10^{-5} M in isopropanol) which peaks at 410 nm. The broadening and energy shift of the emission bands of the obtained PMOs indicate that the phenylenevinylene chromophores in the confined organosilica networks are still active and have strong intermolecular electronic interactions.

4.4. Conclusions

In summary, periodic mesoporous organosilica materials with the phenylenevinylene moiety (3a-OPV-PMO) were successfully synthesized within the tubular channels of anodic alumina membranes through an evaporation-induced self-assembly (EISA) process. Depending on different structure directing agents, different mesophases could be observed. 2D-SAXS experiments and TEM measurements carried out on the calcined sample templated by Pluronic F127 showed that a 2D-hexagonal circular phase was predominantly formed within AAM channels, and a hexagonal columnar structure as an additional phase was observed as well. When using template F108, which can form micelles with higher curvature than Pluronic F127, a body centered cubic (*Im-3m*) mesophase was achieved in the confined environment of the AAM channels. It is noteworthy that the resulting circular and cubic 3a-OPV-PMO/AAM composites were both structurally stable against thermal treatments at temperatures of up to 200 °C and also stable in the electron beam of the electron microscope, which is a remarkable enhancement over the previously reported flat-substrate supported 3a-OPV-PMO films. All the synthesized hierarchically nanostructured 3a-OPV-PMO/AAM composites were observed to be fluorescent in the visible light region. The fluorescence emission of the PMO/AAM composites showed a red-shift compared to that of the precursor molecule solution, indicating strong electronic interactions between the phenylenevinylene chromophores in the condensed organosilica networks. The success of achieving such stable, fluorescent and highly oriented mesoporous 3a-OPV-PMO materials suggests that these PMO/AAM composites and similar chromophore-containing hierarchical nanostructures might offer potential as hierarchical optoelectronic systems.

4.5. References

1. F. Hoffmann and M. Fröba, *Chem. Soc. Rev.*, 2011, **40**, 608-620.
2. B. J. Melde, B. T. Holland, C. F. Blanford and A. Stein, *Chem. Mater.*, 1999, **11**, 3302-3308.
3. S. Inagaki, S. Guan, Y. Fukushima, T. Ohsuna and O. Terasaki, *J. Am. Chem. Soc.*, 1999, **121**, 9611-9614.
4. T. Asefa, M. J. MacLachlan, N. Coombs and G. A. Ozin, *Nature*, 1999, **402**, 867-871.
5. J. Morell, M. Gungerich, G. Wolter, J. Jiao, M. Hunger, P. J. Klar and M. Froba, *J. Mater. Chem.*, 2006, **16**, 2809-2818.
6. A. Sayari and W. H. Wang, *J. Am. Chem. Soc.*, 2005, **127**, 12194-12195.
7. T. Tani, N. Mizoshita and S. Inagaki, *J. Mater. Chem.*, 2009, **19**, 4451-4456.
8. C. Vercaemst, P. E. de Jongh, J. D. Meeldijk, B. Goderis, F. Verpoort and P. Van Der Voort, *Chem. Commun.*, 2009, 4052-4054.
9. Q. H. Yang, J. Liu, L. Zhang and C. Li, *J. Mater. Chem.*, 2009, **19**, 1945-1955.
10. A. Kuschel and S. Polarz, *J. Am. Chem. Soc.*, 2010, **132**, 6558-6565.
11. M. Park, S. S. Park, M. Selvaraj, D. Y. Zhao and C. S. Ha, *Microporous Mesoporous Mater.*, 2009, **124**, 76-83.

4. Formation of Hexagonal and Cubic Fluorescent Periodic Mesoporous Organosilica in the Channels of Anodic Alumina Membranes

12. C. Li, J. Liu, X. Shi, J. Yang and Q. Yang, *J. Phys. Chem. C*, 2007, **111**, 10948-10954.
13. S. Inagaki, O. Ohtani, Y. Goto, K. Okamoto, M. Ikai, K. Yamanaka, T. Tani and T. Okada, *Angew. Chem. Int. Ed.*, 2009, **48**, 4042-4046.
14. R. Hernandez, A. C. Franville, P. Minoofar, B. Dunn and J. I. Zink, *J. Am. Chem. Soc.*, 2001, **123**, 1248-1249.
15. P. N. Minoofar, R. Hernandez, S. Chia, B. Dunn, J. I. Zink and A. C. Franville, *J. Am. Chem. Soc.*, 2002, **124**, 14388-14396.
16. N. Mizoshita, Y. Goto, T. Tani and S. Inagaki, *Adv. Funct. Mater.*, 2008, **18**, 3699-3705.
17. W. Wang, J. E. Lofgreen and G. A. Ozin, *Small*, 2010, **6**, 2621.
18. N. Mizoshita, M. Ikai, T. Tani and S. Inagaki, *J. Am. Chem. Soc.*, 2009, **131**, 14225-14227.
19. K. Kuraoka, Y. Tanaka, M. Yamashita and T. Yazawa, *Chem. Commun.*, 2004, 1198-1199.
20. M. Trau, N. Yao, E. Kim, Y. Xia, G. M. Whitesides and I. A. Aksay, *Nature*, 1997, **390**, 674-676.
21. A. Firouzi, D. J. Schaefer, S. H. Tolbert, G. D. Stucky and B. F. Chmelka, *J. Am. Chem. Soc.*, 1997, **119**, 9466-9477.

4. Formation of Hexagonal and Cubic Fluorescent Periodic Mesoporous Organosilica in the Channels of Anodic Alumina Membranes

22. Y. Yamauchi, M. Sawada, T. Noma, H. Ito, S. Furumi, Y. Sakka and K. Kuroda, *J. Mater. Chem.*, 2005, **15**, 1137-1140.
23. H. Miyata, T. Noma, M. Watanabe and K. Kuroda, *Chem. Mater.*, 2002, **14**, 766-772.
24. H. Miyata, T. Suzuki, A. Fukuoka, T. Sawada, M. Watanabe, T. Noma, K. Takada, T. Mukaide and K. Kuroda, *Nat. Mater.*, 2004, **3**, 651-656.
25. R. L. Rice, D. C. Arnold, M. T. Shaw, D. Iacopina, A. J. Quinn, H. Amenitsch, J. D. Holmes and M. A. Morris, *Adv. Funct. Mater.*, 2007, **17**, 133-141.
26. B. Platschek, A. Keilbach and T. Bein, *Adv. Mater.*, 2011, **23**, 2395-2412.
27. A. Y. Ku, S. T. Taylor and S. M. Loureiro, *J. Am. Chem. Soc.*, 2005, **127**, 6934-6935.
28. B. Platschek, N. Petkov and T. Bein, *Angew. Chem. Int. Ed.*, 2006, **45**, 1134-1138.
29. B. Platschek, N. Petkov, D. Himsl, S. Zimdars, Z. Li, R. Köhn and T. Bein, *J. Am. Chem. Soc.*, 2008, **130**, 17362-17371.
30. A. Yamaguchi, H. Kaneda, W. S. Fu and N. Teramae, *Adv. Mater.*, 2008, **20**, 1034-1037.
31. B. Yao, D. Fleming, M. A. Morris and S. E. Lawrence, *Chem. Mater.*, 2004, **16**, 4851-+.

4. Formation of Hexagonal and Cubic Fluorescent Periodic Mesoporous Organosilica in the Channels of Anodic Alumina Membranes

32. Y. Y. Wu, G. S. Cheng, K. Katsov, S. W. Sides, J. F. Wang, J. Tang, G. H. Fredrickson, M. Moskovits and G. D. Stucky, *Nat. Mater.*, 2004, **3**, 816-822.
33. K. Maeda, K. Ichinose, T. Yamazaki and T. Suzuki, *Microporous Mesoporous Mater.*, 2008, **112**, 603-611.
34. A. Keilbach, M. Döblinger, R. Köhn, H. Amenitsch and T. Bein, *Chem. Eur. J.*, 2009, **15**, 6645-6650.
35. Y. Li, A. Keilbach, M. Kienle, Y. Goto, S. Inagaki, P. Knochel and T. Bein, *J. Mater. Chem.*, 2011, **21**, 17338-17344.
36. C. J. Brinker, Y. F. Lu, A. Sellinger and H. Y. Fan, *Adv. Mater.*, 1999, **11**, 579-585.
37. B. Platschek, R. Köhn, M. Döblinger and T. Bein, *ChemPhysChem*, 2008, **9**, 2059-2067.
38. J. Schuster, A. Keilbach, R. Köhn, M. Döblinger, T. Dörfler, T. Dennenwaldt and T. Bein, *Chem. Eur. J.*, 2011, **17**, 9463-9470.
39. Y. Q. Wang, Y. J. Wang, C. M. Yang, G. Z. Lu and F. Schuth, *Langmuir*, 2006, **22**, 5491-5496.

5. A Periodic Mesoporous Organosilica with Phthalocyanine Macrocyces Exhibiting Optoelectronic Properties

This chapter is based on a collaboration with Prof. Dirk Trauner and Florian Löbermann in the organic chemistry division of LMU. The synthesis of the organosilane precursor was done there.

5.1. Introduction

Phthalocyanines are large, π -conjugated macrocycles which have received considerable attention due to their unique electrical and optical properties as well as their chemical and thermal stability.¹⁻³ The combination of these properties is of great interest for a number of applications, such as photovoltaics,⁴⁻⁷ electrical conductors,⁸⁻¹⁰ chemical sensors,¹¹⁻¹³ nonlinear optics,¹⁴⁻¹⁶ and photocatalysis.¹⁷⁻²⁰ Hence, recently much effort has been put in designing and synthesizing novel materials containing phthalocyanine macrocycles. For example, a phthalocyanine-based metal-organic framework (MOF) was synthesized and shown to be useful in gas adsorption due to its porous structure.²¹ The first phthalocyanine based covalent organic framework (COF) was described by Dichtel and coworkers.²² Besides, a metallophthalocyanine COF was reported to exhibit considerable charge carrier mobility and photoconductivity.²³ The phthalocyanine moiety has also been accommodated within the robust mesoporous silica matrix.²⁴⁻²⁸ However, in these reported porous silica materials, the phthalocyanine molecules were either inside the mesopores as guest molecules, or as a layer on the inner-surface of the

5. A Periodic Mesoporous Organosilica with Phthalocyanine Macrocycles Exhibiting Optoelectronic Properties

mesopores, both of which can reduce or block access to the pores and thus lead to rather low porosity of the mesoporous systems. So far all reported phthalocyanine-based porous materials only have small pore sizes of less than 5 nm. This fact strongly constrains the possibilities of incorporating larger guest molecules into the mesopores and thus can limit the potential applications of these phthalocyanine-containing porous materials. Besides, the reported phthalocyanine based porous materials in most cases are obtained as powders, which makes integration into devices difficult. Therefore, creating phthalocyanine-containing porous films with large accessible pores will significantly expand the scope of their possible applications.

Periodic mesoporous organosilicas (PMOs) define a class of porous materials that possess accessible mesopores as well as tunable organic functional pore-walls. Synthesis and application of PMO materials have attracted much interest since their discovery in 1999.²⁹⁻³¹ PMO films can be synthesized through the evaporation-induced self-assembly (EISA) process.³²⁻³⁵ In the presence of surfactant template, the condensation of alkoxy-silyl precursors $R'[Si(OR)]_n$ ($n \geq 2$) can lead to a PMO framework with organic linker groups R' uniformly distributed within the pore walls. To date, numerous organic groups such as ethylene, thiophene, benzene, biphenylene, naphthalene, or divinylbenzene have been successfully incorporated in the framework of PMOs.³⁶⁻³⁹ We note that it is rather challenging to obtain ordered mesostructures from alkoxy-silyl precursors with bulky organic linkers, as this type of precursor often shows low solubility and high hydrolysis rates leading to almost instant precipitation under common synthesis conditions. Sometimes a certain amount of inorganic silica precursor such as tetraethyl orthosilicate (TEOS) is needed to assist the bulky organic precursor in forming an ordered mesostructure. Mizoshita et al.⁴⁰ reported that with the

5. A Periodic Mesoporous Organosilica with Phthalocyanine Macrocycles Exhibiting Optoelectronic Properties

addition of 50-80 wt% of TEOS based on the total weight of precursors, the synthesis of a PMO material containing large tetraphenylpyrene bridges was achieved.

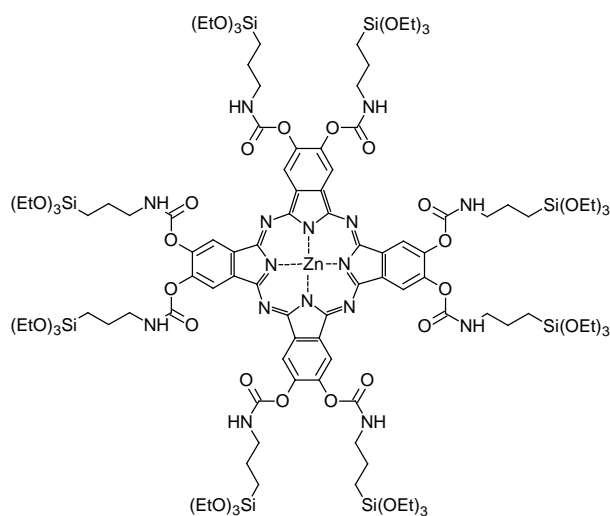
Based on the above considerations, in this work we designed a novel ethoxysilyl precursor with a phthalocyanine chromophore and successfully synthesized phthalocyanine-based PMO films. Thus, 2,3,9,10,16,17,23,24-octa[(3-triethoxysilylpropylaminocarbonyloxy) phthalocyaninato zinc (II)] was the synthesized organic precursor, triblock co-polymer Pluronic F108 was the surfactant template and 50 wt % tetraethyl orthosilicate (TEOS) was added to assist in forming the mesostructure. Through the EISA process, highly ordered mesoporous films (denoted as Pc-Si-PMO) were successfully synthesized. With a view toward their porosity as well as the periodicity and orientation of the mesostructure, the resulting Pc-Si-PMO materials were thoroughly characterized by 1D and 2D small angle X-ray diffraction techniques, transmission electron microscopy (TEM) and nitrogen sorption measurements. After surfactant extraction, the obtained PMO film features an orthorhombic porous structure with cage-like pores of 17 nm in diameter, connected through 7 nm windows. It was confirmed by energy dispersive X-ray spectroscopy (EDX), electron energy loss spectroscopy (EELS) and nuclear magnetic resonance (NMR) spectroscopy that the phthalocyanine molecules are preserved after being incorporated in the PMO pore-walls. Furthermore, the optoelectronic activities of the Pc-Si-PMO film material were investigated in the presence of electron-conducting guest species, showing photoactive and hole-conducting properties due to the phthalocyanine moieties covalently bonded in the stable organosilica pore walls.

5.2. Experimental Section

5.2.1. Preparation of phthalocyanine-bridged PMO films

The synthesis of phthalocyanine-bridged PMO films was achieved by the evaporation-induced self-assembly (EISA) approach.^{32,41} The amount of 0.050 g phthalocyanine-bridged precursor (Scheme 5.1, synthetic procedures in Appendix A-1), 0.050 g TEOS and 0.060 g F108 were first dissolved in a mixture of 2 ml ethanol and 0.2 ml tetrahydrofuran (THF). Next, 0.066 ml of 0.1 M HCl was added and the resulting solution was stirred at room temperature for 20 h. Finally, the aged sol was spin-coated on glass slides (2 cm × 2 cm) at a spinning-rate of 3000 rpm with an acceleration of 2905 rpm/s for 30 s. Evaporation of the volatile agents (ethanol, THF, HCl) from the sol mixture resulted in homogeneous films on the glass slides. Afterwards the films were dried in air at room temperature for 24 h (denoted as Pc-Si-PMO-as prepared). The dried films were then heated in flowing N₂ with a ramp of 1°C/min to 120 °C and kept at this temperature for 5 h (denoted as Pc-Si-PMO-120 °C). Finally the surfactant template Pluronic F108 was extracted by supercritical CO₂ at 88 bar and 60 °C for 2 h (denoted as extracted Pc-Si-PMO).

5. A Periodic Mesoporous Organosilica with Phthalocyanine Macrocycles Exhibiting Optoelectronic Properties



Scheme 5.1: Chemical structure of the ethoxysilyl precursor 2,3,9,10,16,17,23,24-octa [(3-triethoxysilylpropylaminocarbonyloxy) phthalocyaninato zinc (II)].

5.2.2. Structure Characterization

The samples were characterized with X-ray diffraction (XRD) measurements using a Bruker D8 Discover with Ni-filtered $\text{CuK}\alpha$ -radiation (0.154 nm) and a position-sensitive detector (LynxEye). For two-dimensional grazing-incidence small angle X-ray scattering (2D-GISAXS) characterization, a SAXSess system by Anton Paar ($\text{CuK}\alpha$ -radiation, sample-detector distance 306.7 mm) with a CCD detector (PI-SCX:4300, Roper Scientific) was used. The samples were measured for 10 h with a tilt angle of 0.27° with respect to the primary beam. Transmission electron microscopy (TEM) was performed using a FEI Titan 80-300 instrument equipped with a field emission gun operated at 300 kV. Energy dispersive X-ray spectroscopy (EDXS) and electron energy loss spectroscopy (EELS) were performed using the same FEI Titan 80-300 instrument. Scanning electron microscopy images were recorded on a JEOL

JSM-6500F FE-SEM operating at 4 kV acceleration voltage and using the secondary electron signal. Nitrogen sorption measurements were carried out at -196 °C using an Autosorb-1 by Quantachrome Instruments; the sample was degassed at 150 °C for 12 h in vacuum before the measurement. For this purpose thicker films were synthesized by drop-casting solutions identical to those for Pc-Si-PMO on flat glass substrates. The thick films (after the same thermal treatment) were scratched off from the glass slides and extracted by supercritical CO₂ before the nitrogen sorption measurement. The Brunauer-Emmett-Teller (BET) surface area was calculated using experimental points at a relative pressure range of $p/p_0 = 0.05-0.20$. The total pore volume was calculated by the N₂ amount adsorbed at the highest p/p_0 ($p/p_0 = 0.98$). NLDFT pore size distributions were calculated from both the adsorption and desorption branches using a SiO₂ kernel assuming cylindrical/spherical pore geometry for the sample. Solid-state ¹³C and ²⁹Si NMR experiments were performed on a Bruker Avance-III 500 spectrometer (11.7 Tesla) operating at frequencies of 125.8 MHz for ¹³C and 99.4 MHz for ²⁹Si. ¹³C{1H} CP-MAS spectra were acquired using a 90° pulse length of 2.5 μs (3.7 dB) with cross-polarization contact time of 5 ms and a recycle delay of 2 s. ²⁹Si{1H} CP-MAS experiments were conducted using a 90° pulse length of 2.5 μs (3.7 dB) with cross-polarization contact time of 5 ms and a recycle delay of 2 s.

5.2.3. Photoelectrochemical Characterization

Pc-Si-PMO films were synthesized on indium tin oxide coated glass (VisionTek, 150 nm ITO, 12-15 ohms/sq).

5. A Periodic Mesoporous Organosilica with Phthalocyanine Macrocycles Exhibiting Optoelectronic Properties

UV-Vis measurements were performed on a Hitachi U3501 spectrophotometer equipped with an integrating sphere. Absorbance spectra were recorded in transmission geometry with plain ITO as reference.

For the measurements in an electrolyte, the ITO substrates were cut into pieces of 1 cm \times 1.5 cm. A 5 mm wide contact area on one side of the substrate was masked during the deposition of the PMO film, resulting in an active area of 1 cm². After extraction of the Pluronic template the blank part of the ITO was contacted with a copper wire using silver paste and then this contact area was sealed with poly(dimethylsiloxane) in order to avoid direct contact between the ITO and the electrolyte. Photoelectrochemical measurements were performed with the Pc-Si-PMO film as working electrode and a platinum wire as counter electrode in an aqueous electrolyte containing either 0.1 M KNO₃ or 0.1 M KNO₃ and 1 mM H₂O₂.

Solid-state devices were fabricated on patterned ITO substrates. After deposition of the PMO layer and subsequent extraction of the template, the films (1.5 cm \times 1.5 cm) were immersed overnight into a solution of [6, 6]-phenyl-C₆₁-butyric acid methyl ester (PCBM, 3 mg/ml in chlorobenzene to enhance the infiltration of the PCBM into the mesopores (each film in 5 ml PCBM solution). The films were then taken from this solution and immediately spun at 1000 rpm with an acceleration of 996 rpm/s for 60 s, which resulted in a thin and homogeneous layer of PCBM on top of the PMO film. Finally, 70 nm thick silver contacts were sputter-deposited through a shadow mask, yielding an active area of 16 mm². The samples were illuminated through a 12 mm² mask and measured in air. As a comparison, bilayer samples made from non-porous

5. A Periodic Mesoporous Organosilica with Phthalocyanine Macrocycles Exhibiting Optoelectronic Properties

films were prepared in a similar way as described above with the exception that no TEOS and F108 were added to the initial precursor solution.

For recording current transients the samples were illuminated with white light from an AM1.5G solar simulator (Solar Light Model 16S) at 100 mW/cm^2 , which was modulated using a shutter. Lower light intensities were realized with a set of calibrated reflective neutral density filters. The signal was detected using a low noise preamplifier (Femto DLPCA-200) and an oscilloscope (Tektronix DPO2012).

External quantum efficiency (EQE) measurements were performed at short circuit. Monochromatic light was obtained from a 150 W xenon lamp in combination with a monochromator and order-sorting filters. The slits were adjusted such that the FWHM was 5 nm at a light intensity of approximately 2 mW/cm^2 . All light intensities were calibrated with a Fraunhofer ISE certified silicon reference cell equipped with a KG5 filter. The monochromatic light was modulated using an optical chopper at a frequency of 4 Hz for measurements with an electrolyte and 12 Hz in case of the solid state devices. The signal was detected via a low noise pre-amplifier (Femto DLPCA-200) and a lock-in amplifier (Signal Recovery 7265). The modulation frequency was chosen as a tradeoff between signal amplitude and measurement duration. Although the signal amplitude changed only by about 10 % when changing the modulation frequency from 0.1 Hz to 40 Hz, we do not argue that the EQE values presented in this work represent a steady-state current.

5.3. Results and Discussion

5.3.1. Mesostructured phthalocyanine-bridged PMO films

With the triblock co-polymer F108 acting as structure-directing agent, mesostructured organosilica films were obtained by acidic sol-gel polycondensation of the phthalocyanine-containing organic precursor and TEOS molecules. The periodic mesostructure of the film was characterized by means of small angle XRD, as shown in Figure 5.1. The reflection position of as-prepared material along the film normal corresponds to $d = 11.6$ nm. The d -value decreases to 9.2 nm after thermal treatment at 120 °C for 5 h and to 8.7 nm after template extraction with CO₂. Such shrinkage along the substrate normal is common for mesoporous thin films after template removal.⁴¹⁻⁴⁴ The peak widths indicate a variation of the d -values of around 0.5 nm, which can be expected for such a flexible material. After template removal, the reflection intensities increase in comparison to as-prepared material, as a result of the better X-ray contrast.

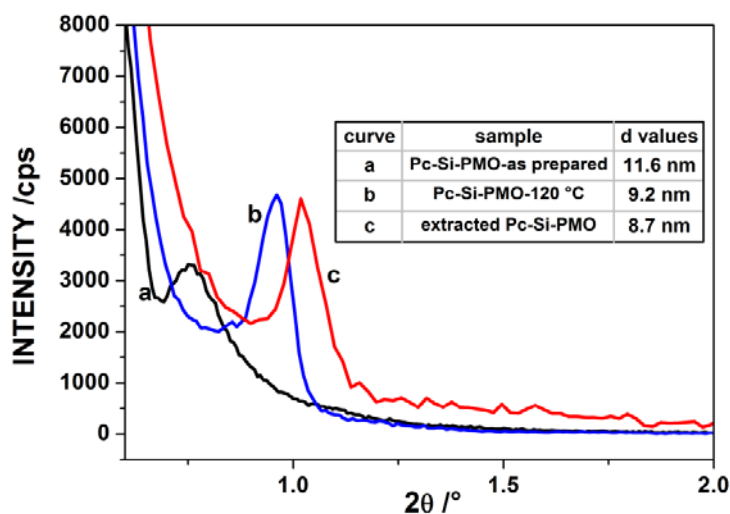


Figure 5.1: X-ray diffraction patterns of the PC-Si-PMO films, (a) as-synthesized, (b) after thermal treatment at 120 °C, (c) after extraction with CO₂.

For further characterization with TEM and 2D-GISAXS, films obtained after template extraction with CO₂ were used. TEM cross sections of the films (Figure 5.2) show their high degree of structural order and thicknesses of around 160 nm. Image analysis shows that the d-values along the film normal vary between 8.3 nm and 9.6 nm, the film shrinkage appears to be more pronounced toward the film surface. Regarding zone axis orientations, lateral d-values of 14.0 nm (Figure 5.2 a) and 8.2 nm (Figure 5.2 b) were measured. If an initial body-centered cubic structure is assumed before film shrinkage, an orthorhombic structure with *Fmmm* symmetry results after shrinkage along the film normal, with the following lattice constants: $a = 19.9$ nm, $b = 17.8$ nm, $c = 28.1$ nm, corresponding to a film shrinkage of 37% (see details below in caption of Figure 5.3). The basis vectors **a** and **c** are parallel to the film and **b** is along the film normal (Figure 5.3). Films possessing the above space group and orientation with respect to the

5. A Periodic Mesoporous Organosilica with Phthalocyanine Macrocycles Exhibiting Optoelectronic Properties

substrate are common for mesoporous carbons and metal oxides after uniaxial shrinkage.⁴⁵⁻⁴⁹ In accordance with this structure model, the TEM images of Figures 5.2 a) and 5.2 b) can be interpreted as structure projections along [100] and [101], respectively.

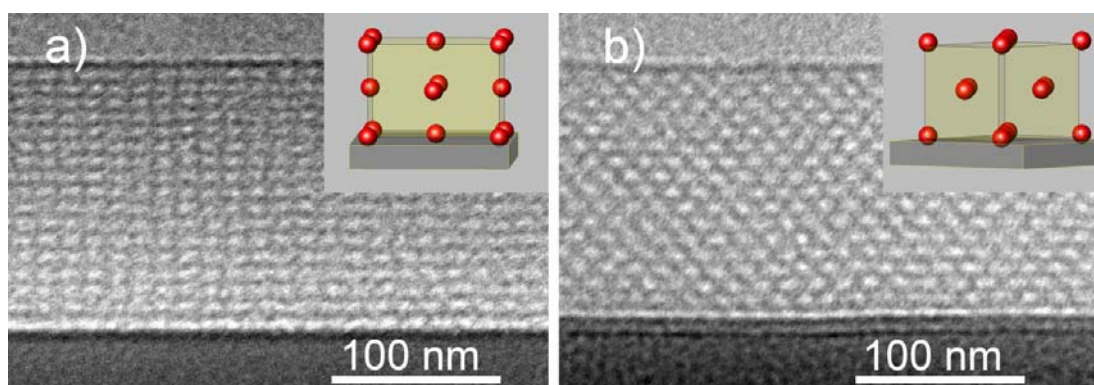


Figure 5.2: Cross section TEM images of the extracted PC-Si-PMO film. The insets show corresponding orientations of the structure model. (a) The average lattice plane distance measured along the film normal is 9.1 nm, along the film substrate it is 14.0 nm. For the structure model in [100] projection as shown in the inset, these values correspond to d_{020} and d_{002} respectively. (b) The average lattice plane distance measured along the film normal is 8.8 nm, along the film substrate it is 8.2 nm. For the structure model in [101] projection as shown in the inset, these values correspond to d_{020} and d_{20-2} respectively.

5. A Periodic Mesoporous Organosilica with Phthalocyanine Macrocycles Exhibiting Optoelectronic Properties

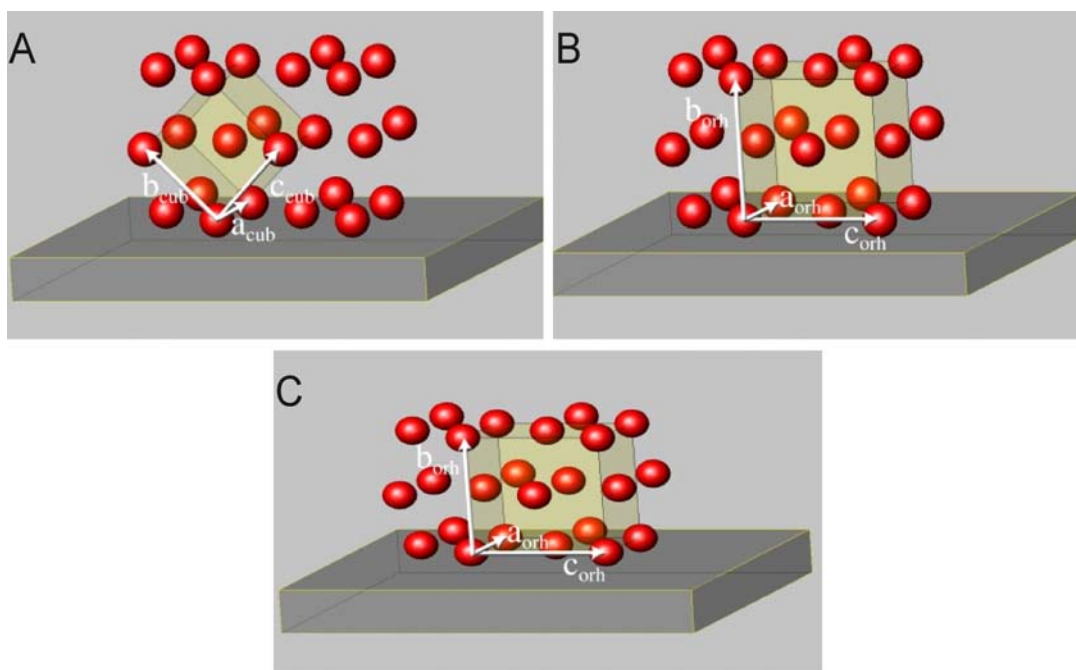


Figure 5.3: Relationship of the mesoporous structure models in the cubic and the orthorhombic setting with respect to the substrate. A) The initial cubic $Im\bar{3}m$ structure, with the face diagonal of the unit cell $[011]_{\text{cub}}$ along the film normal. B) the initial structure described in an orthorhombic setting with $Fmmm$ symmetry and $[010]_{\text{orh}}$ along the film normal. The lattice basis vectors change as follows: $\mathbf{a}_{\text{orh}} = \mathbf{a}_{\text{cub}}$, $\mathbf{b}_{\text{orh}} = (\mathbf{b}_{\text{cub}} + \mathbf{c}_{\text{cub}})$, and $\mathbf{c}_{\text{orh}} = \mathbf{c}_{\text{cub}} - \mathbf{b}_{\text{cub}}$. C) After uniaxial shrinkage, \mathbf{a}_{orh} and \mathbf{c}_{orh} remain constant, with the fixed ratio of $c_{\text{orh}} = 1.41 a_{\text{orh}}$, while b_{orh} is decreasing by a shrinkage factor. The lattice parameters of the structure model imply an initial cubic lattice parameter of $a_{\text{cub}} = 19.9$ nm and a film shrinkage by 37%.

The 2D GISAXS pattern of a CO_2 -extracted film shown in Figure 5.4 is in agreement with space group, orientation, and lattice parameters of the structure model inferred from TEM. The presence of the elements expected from the synthesis was confirmed by energy dispersive X-ray spectroscopy (EDXS) and electron energy loss spectroscopy (EELS). Because of their large relative amounts and the specific sensitivity of EELS,

5. A Periodic Mesoporous Organosilica with Phthalocyanine Macrocycles Exhibiting Optoelectronic Properties

the elemental ratio of nitrogen to oxygen was quantified. The nitrogen to oxygen ratio of 0.31 ± 0.03 determined from five EEL spectra is in very good agreement with the value of 0.3 calculated based on the ratio between precursors in the synthesis. For more details, see Appendix A-2.

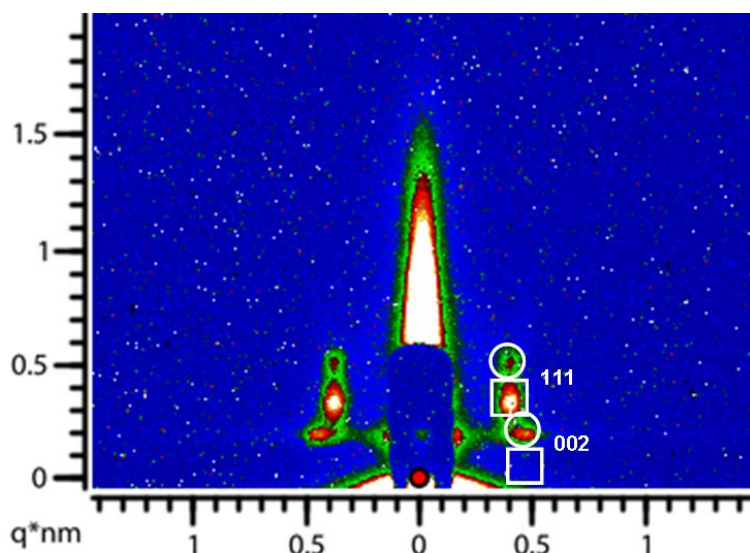


Figure 5.4: 2D-GISAXS diffraction pattern of the CO₂ extracted film. The reflections are doubled due to diffraction of the incident beam reflected at the film-substrate interface. Hence, reflections on top of each other (one circle and one square) belong to the same indexing. The lower empty square denotes the 002 reflection position according to the *Fmmm* structure model. As it is below the sample ‘horizon’, the reflection intensity is fully absorbed by the sample. The measured d-values of 12.1 nm and 13.7 nm agree very well with the values expected for the structure model, with $d_{111} = 12.0$ nm and $d_{002} = 14.0$ nm.

The porosity of the extracted phthalocyanine-bridged PMO material was examined by a nitrogen sorption measurement of scratched-off films. The nitrogen sorption isotherms (Figure 5.5) show the typical type IV isotherm shape commonly observed for

5. A Periodic Mesoporous Organosilica with Phthalocyanine Macrocycles Exhibiting Optoelectronic Properties

mesoporous materials. The Brunauer-Emmett-Teller (BET) surface area calculated from these isotherms is $379 \text{ m}^2 \text{ g}^{-1}$ and the pore volume is $0.69 \text{ cm}^3 \text{ g}^{-1}$. The isotherm shape with a hysteresis loop suggests the existence of cage-like pores. This can be confirmed by comparing the DFT pore-size distributions from the adsorption branch (av. pore diameter of 17 nm) and the desorption branch (av. pore diameter of 7 nm) (inset of Figure 5.5). The cage-like pores result from the interconnected spherical micelles of the triblock co-polymers in the initial cubic structure. The pore diameter from the desorption branch (7 nm) represents the window size, while the 17 nm from the adsorption branch are related to the cage diameter. Similar porosity properties with cage-like pores were also found for mesoporous carbon films with the *Fmmm* symmetry, although with much smaller pore sizes.⁴⁸

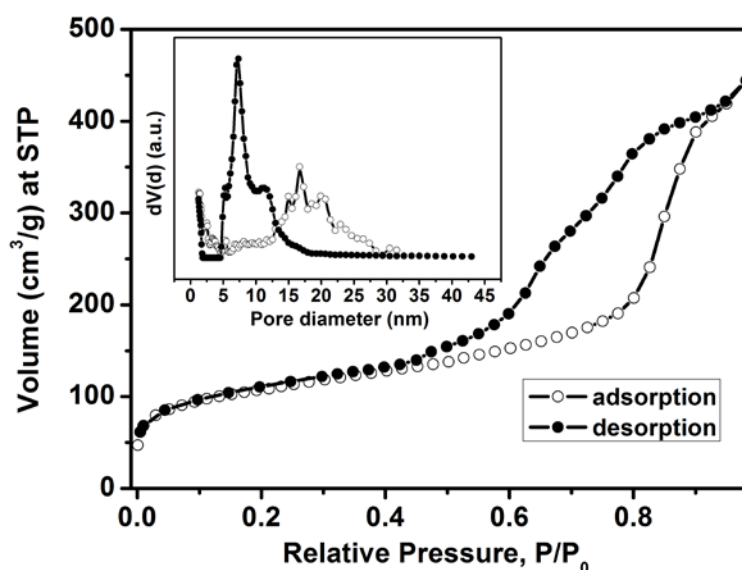


Figure 5.5: Nitrogen adsorption (○) and desorption (●) isotherms of the extracted Pc-Si-PMO sample with an inset showing NLDFT pore size distributions calculated from both the adsorption branch (○) and desorption branch (●) using a SiO₂ kernel assuming cylindrical/spherical pore geometry for the sample.

5.3.2. Framework constitution of the phthalocyanine-bridged PMO films

Energy dispersive X-Ray spectroscopy (EDXS) and electron energy loss spectroscopy (EELS) confirm the presence of the elements that are expected to be in the Pc-Si-PMO films. To obtain more detailed information about the local chemical environment of the PMO material, the extracted Pc-Si-PMO material was examined with solid-state NMR spectroscopy of both ^{13}C and ^{29}Si nuclei (Figure 5.6). The signals in the ^{13}C -MAS NMR spectrum of the extracted material can be assigned to the corresponding carbon atoms of the phthalocyanine bridges (Figure 5.6A), which are consistent with the results reported for phthalocyanine systems.⁵⁰⁻⁵⁴ The signals at 8.76 ppm (C1), 22.0 ppm (C2), 43.68 ppm (C3) and 118.7 ppm (C4) could be assigned correspondingly to the carbon atoms existing in the propyl isocyanate moiety.⁵⁵⁻⁵⁸ The detected chemical shifts in the range of 100 - 160 ppm represent the resonances from the carbon atoms in the aromatic ring of the phthalocyanine moiety. The ^{13}C -MAS NMR proves that the phthalocyanine organic group in the precursor is robust enough to survive the synthesis and extraction conditions. In the solid state ^{29}Si NMR spectrum (Figure 5.6B), resonances at -49.3, -58.1 and -66.3 ppm are representative of T-type organosilica species [$\text{T}^n = \text{RSi}(\text{OSi})_n(\text{OH})_{3-n}$], which could be assigned to T^1 , T^2 , T^3 units of the condensed silsesquioxane moieties.^{56, 59} The presence of the characteristic Q signals [$\text{Q}^n = \text{Si}(\text{OSi})_n(\text{OH})_{4-n}$] at -91.1 (Q^2), -100.6 (Q^3) and -109.9 ppm (Q^4) shows the condensation state of the silica species in the framework.^{58, 60} Based on both the ^{13}C and ^{29}Si NMR spectra, we conclude that the organic phthalocyanine moieties are covalently integrated into the condensed silica walls of the PMO material.

5. A Periodic Mesoporous Organosilica with Phthalocyanine Macrocycles Exhibiting Optoelectronic Properties

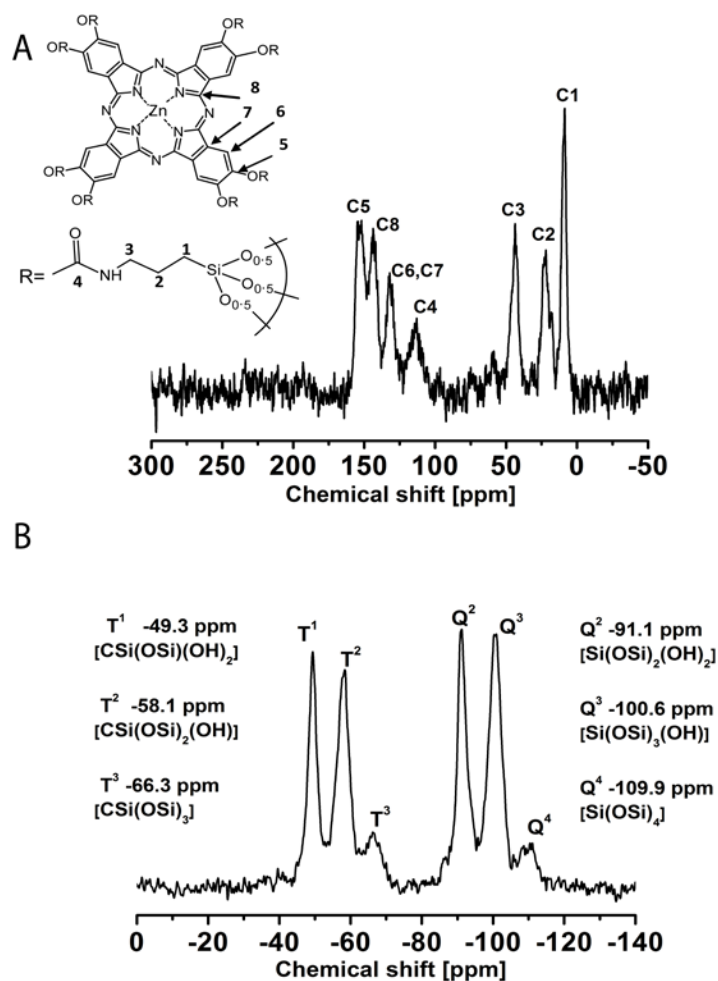


Figure 5.6: A) ^{13}C -MAS NMR and B) ^{29}Si NMR spectra of the extracted Pc-Si-PMO material.

5.3.3. UV-Vis absorption properties

Figure 5.7 shows UV-Vis absorbance spectra of an extracted Pc-Si-PMO film and of a diluted solution of the organosilane precursor molecules in THF. The absorption spectrum of the dilute THF solution of the precursor is typical for non-aggregated phthalocyanines.^{54, 61-63} Specifically, the two distinguished peaks at 603 and 667 nm located within the broad absorption band from 550 to 700 nm (Q band) are

5. A Periodic Mesoporous Organosilica with Phthalocyanine Macrocycles Exhibiting Optoelectronic Properties

characteristic of monomeric phthalocyanine macrocycles. Meanwhile, the Q band of the extracted Pc-Si-PMO film is broadened and red-shifted (625 and 685 nm) compared to that of the diluted precursor solution. Additionally, the B band of the extracted PMO film peaking at 338 nm is blue-shifted by 10 nm from that (348 nm) of the precursor monomers.

The blue shift of the B band and the broadening behavior of the Q bands normally indicate the formation of H-aggregates (face to face aggregates) of phthalocyanine units.⁶⁴⁻⁶⁵ As no other evidence could be obtained to confirm the formation of H-aggregates, we cautiously deduce that in the mesoporous Pc-Si-PMO framework the phthalocyanine moieties could be densely packed resulting strong electronic interactions between each other.

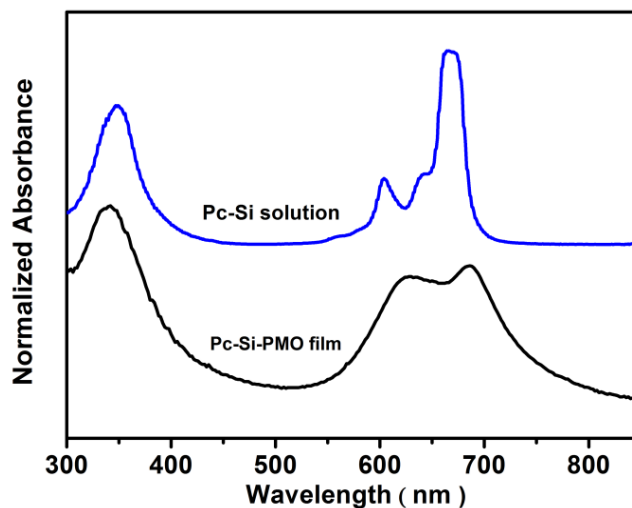
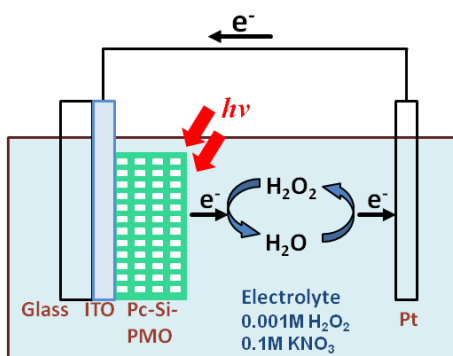


Figure 5.7: UV-Vis absorption spectra of a template-extracted mesostructured Pc-Si-PMO film (black curve) and that of a diluted solution containing 10^{-5} M phthalocyanine-bridged precursor in THF (blue curve). For clarity, an offset is added to the blue curve.

5.3.4. Optoelectronic behavior

In order to investigate the photoactive and electronic properties of the Pc-Si-PMO films we prepared samples on ITO-coated glass substrates. Figure 5.8 shows the time-resolved photocurrent response and the spectrally resolved response of such an extracted Pc-Si-PMO film (160 nm thick), measured in a two-electrode configuration with the sample connected as working electrode and a Pt counter-electrode in an aqueous electrolyte containing either 0.1 M KNO₃ or 0.1 M KNO₃ and 1 mM H₂O₂ (set-up illustrated in Scheme 5.2).



Scheme 5.2: Illustration of the set-up for photoelectrochemical experiments in electrolyte containing 0.1 M KNO₃ and 1 mM H₂O₂.

We recorded current transients at different intensities of simulated solar light (Figure 5.8A). Upon illumination a current pulse is generated, which quickly decays to a lower steady-state current. The sign of the photocurrent denotes that the electrons are transferred to the electrolyte, whereas the holes are transported within the Pc-Si-PMO film which is consequently a p-type semiconductor.⁶⁶⁻⁶⁹ Switching off the light results in a pulse of similar amplitude, but opposite sign. As expected, the steady-state current is

5. A Periodic Mesoporous Organosilica with Phthalocyanine Macrocycles Exhibiting Optoelectronic Properties

zero in this case. These anodic and cathodic current spikes are well-known for phthalocyanine films in electrolytes and could originate from charging and discharging of surface states.^{66, 68-69} A similar behavior of current transients under illumination, in which an initially higher current decays to a lower stable current, could also originate from limitations in charge transport. To analyze whether a transport limitation was present in our films we extrapolated the transients recorded at various light intensities to full sun illumination (inset of Figure 5.8A). If the current was limited by slow charge transport, one would expect the extrapolated current from the low light intensity measurements to be higher and the initial decay less pronounced. Since all four curves are exactly on top of each other, we can conclude that the current response of the Pc-Si-PMO film scales linearly with light intensity and therefore there seems to be no severe bottleneck in charge transport.

The spectrum of the external quantum efficiency (EQE) which is the ratio of collected electrons to incident photons closely resembles the absorption spectrum of the sample, suggesting that indeed the Pc-Si-PMO is the origin of the photocurrent (Figure 5.8B). Addition of 1 mM H₂O₂ to the electrolyte helps to reduce recombination of photogenerated holes in the Pc-Si-PMO film with electrons from the electrolyte and therefore yields a higher photocurrent without affecting the shape of the spectrum.

5. A Periodic Mesoporous Organosilica with Phthalocyanine Macrocycles Exhibiting Optoelectronic Properties

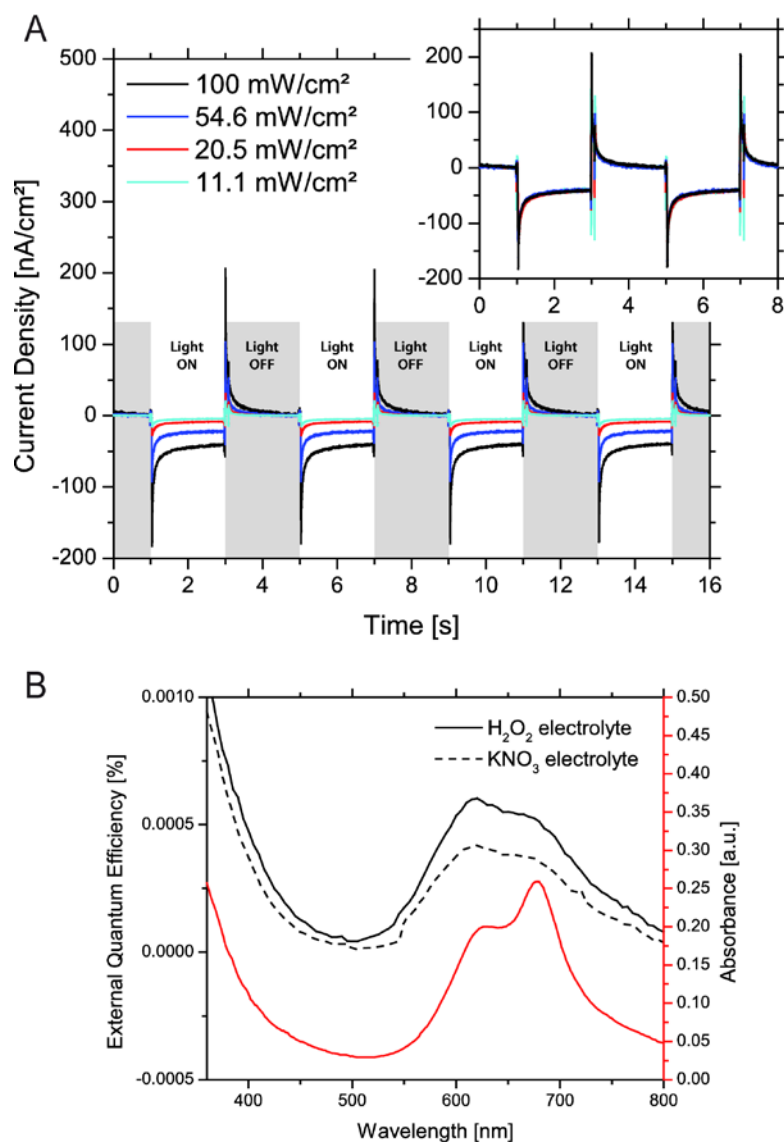
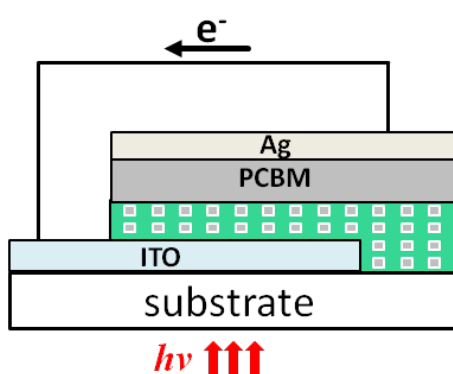


Figure 5.8: A) Time-resolved photocurrent response of the extracted Pc-Si-PMO film deposited on ITO in an aqueous electrolyte containing 0.1 M KNO₃ (active area is 1 cm²). The experiment was carried out using simulated AM1.5G solar light of different light intensity. Inset: Photocurrent transients normalized to 100 mW/cm² irradiance. B) External quantum efficiency in two different electrolytes (0.1 M KNO₃ and 0.1 M KNO₃ with 1 mM H₂O₂) and UV-Vis spectrum of the Pc-Si-PMO film. Illumination was from the film side in both measurements.

5. A Periodic Mesoporous Organosilica with Phthalocyanine Macrocycles Exhibiting Optoelectronic Properties

We also combined the p-type phthalocyanine-based PMO films with an electron acceptor to form a three-dimensional solid-state heterojunction by soaking the extracted mesoporous films in a solution of PCBM for infiltration of the electron-transporting species into the mesopores. Subsequent spin-coating of the PCBM solution results in an additional PCBM overlayer, which is required for avoiding contact between the Ag back electrode and the p-type material (device configuration illustrated in Scheme 5.3).



Scheme 5.3: Illustration of the configuration of the solid-state device with mesostructured PMO film. The porous green layer on the surface of ITO represents the Pc-Si-PMO film.

The external quantum efficiency of the solid state device follows the absorbance of the Pc-Si-PMO/PCBM composite (Figure 5.9A). Compared to the measurements in an electrolyte the photocurrent response in the blue and UV part of the spectrum is much higher, which might be due to a contribution of the PCBM. The observed photocurrent seems to be a superposition of (i) excitons generated in the Pc-Si-PMO followed by electron injection into the PCBM, and (ii) excitons generated upon light absorption by the PCBM followed by hole injection into the Pc-Si-PMO.

5. A Periodic Mesoporous Organosilica with Phthalocyanine Macrocycles Exhibiting Optoelectronic Properties

In order to assess the influence of the mesostructure on the photovoltaic performance, we compared the mesostructured samples to their bilayer counterparts. Strikingly, the response of the bilayer device is far more than one order of magnitude lower than the EQE of the structured device (note that the response of the bilayer structure was multiplied by 10 for clarity) (Figure 5.9B). These data strongly suggest that only excitons generated in the vicinity of the interface can diffuse to the heterojunction and get separated. If the heterojunction is flat, the region where light absorption can produce separated charge carriers does not extend far from the interface. Therefore the measured current is extremely low. Since the EQE of the mesostructured, but otherwise identical device is remarkably higher, we can conclude that through the infiltration with PCBM a three-dimensional junction is formed, which can harvest photogenerated excitations from a much larger volume. We note that in the EQE spectrum of the bilayer device the optical fingerprint of the phthalocyanine framework between 600 nm and 700 nm is not clearly visible. A possible explanation for this is that when illuminating the sample through the substrate, the light has to pass the phthalocyanine layer and thus the light intensity close to the interface, where current can be generated, is lower at wavelengths where the phthalocyanine absorbs strongly. In case of the mesostructured device, the heterojunction extends into the Pc-Si-PMO layer, rendering more of the phthalocyanine material electronically active and thus the light filtering effect is less pronounced.

5. A Periodic Mesoporous Organosilica with Phthalocyanine Macrocycles Exhibiting Optoelectronic Properties

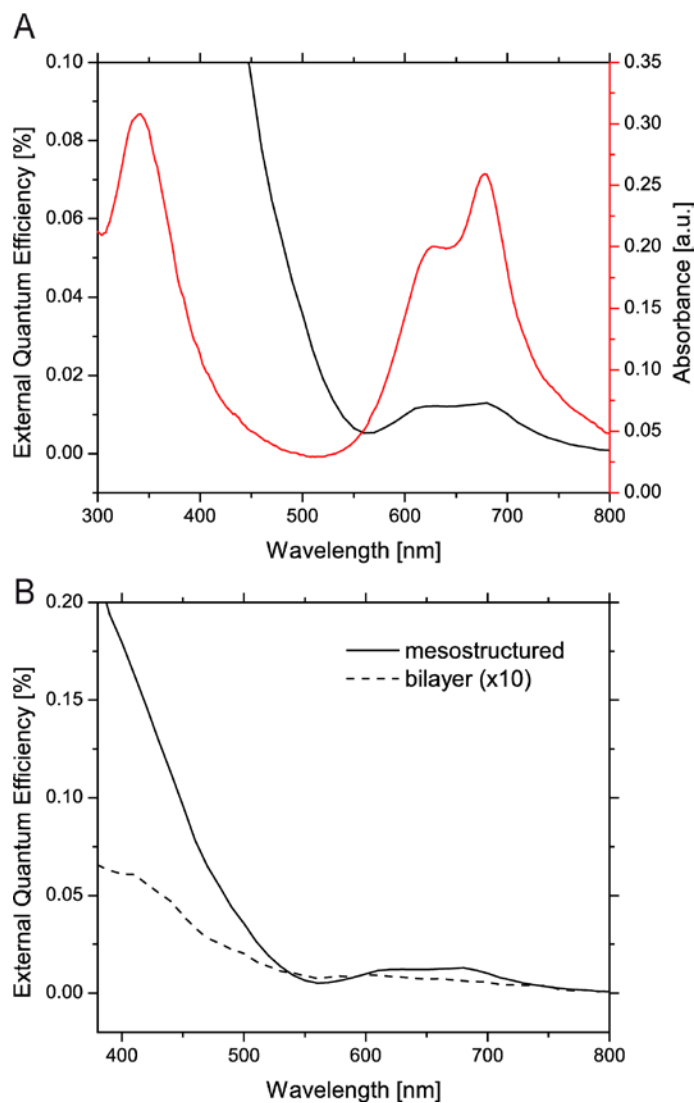


Figure 5.9: A) External quantum efficiency (black) and absorbance (red) spectra of the mesoporous Pc-Si-PMO/PCBM device and B) Comparison between the mesostructured Pc-Si-PMO/PCBM device and a non-porous bilayer counterpart. The EQE of the bilayer device was multiplied by 10 for better visibility.

5.4. Conclusion

In this work, a periodic mesoporous organosilica film material based on zinc-phthalocyanine macrocycles was successfully synthesized through an evaporation-induced self-assembly process using the triblock co-polymer F108 as template. XRD, 2D-GISAXS measurements and TEM of the extracted Pc-Si-PMO film showed that an orthorhombic porous structure was obtained on flat substrates. EDX, EELS and solid state NMR results confirmed the existence of zinc-phthalocyanine organic units in the condensed organosilica frameworks. The obtained Pc-Si-PMO material with cage-like pores of 17 nm in diameter showed a BET surface area of $379 \text{ m}^2 \text{ g}^{-1}$ and a pore volume of $0.69 \text{ cm}^3 \text{ g}^{-1}$. The UV-Vis absorbance spectrum of the PMO film exhibits a broad absorption band owing to strongly interacting phthalocyanine moieties in the organosilica pore walls. An investigation of the optoelectronic properties of the Pc-Si-PMO film in an aqueous electrolyte showed light-induced charge generation capability and hole-transporting character. Through a comparison of the mesostructured Pc-Si-PMO/PCBM devices with their bilayer counterparts we found that the photoactive heterojunction indeed extends into the porous Pc-Si-PMO framework and thus the structured devices can collect excitons from a much larger volume and consequently produce a more than tenfold increased photocurrent. Based on these results we anticipate that zinc-phthalocyanine-based PMO frameworks and similar opto-electroactive moiety-containing PMO materials can serve as highly ordered model systems for device architectures in organic photovoltaics.

5.5. References

1. T. H. Wei, D. J. Hagan, M. J. Sence, E. W. Vanstryland, J. W. Perry and D. R. Coulter, *Appl. Phys. B*, 1992, **54**, 46-51.
2. F. H. T. Moser, A. L. , *The Phthalocyanines, Vol. 2, CRC Press: Boca Raton, Fla.*, 1983.
3. P. H. Erk, H. , *The Porphyrin Handbook; Academic Press: New York* , 2003, **19**, 105-149.
4. J. G. Xue, B. P. Rand, S. Uchida and S. R. Forrest, *Adv. Mater.*, 2005, **17**, 66-71.
5. S. Pfuetzner, J. Meiss, A. Petrich, M. Riede and K. Leo, *Appl. Phys. Lett.*, 2009, **94**, 253303.
6. S. Pfuetzner, J. Meiss, A. Petrich, M. Riede and K. Leo, *Appl. Phys. Lett.*, 2009, **94**, 223307.
7. D. Placencia, W. N. Wang, R. C. Shallcross, K. W. Nebesny, M. Brumbach and N. R. Armstrong, *Adv. Funct. Mater.*, 2009, **19**, 1913-1921.
8. T. Inabe, *J. Porphyr. Phthalocyanines*, 2001, **5**, 3-12.
9. T. Inabe, T. Asari, H. Hasegawa, M. Matsuda, E. H. Gacho, N. Matsumura, S. Takeda, K. Takeda and T. Naito, *Synth. Met.*, 2003, **133**, 515-518.
10. A. T. Oza, S. G. Patel, R. G. Patel, S. M. Prajapati and R. Vaidya, *Thin Solid Films*, 2005, **477**, 153-161.

5. A Periodic Mesoporous Organosilica with Phthalocyanine Macrocycles Exhibiting Optoelectronic Properties

11. A. Generosi, B. Paci, V. R. Albertini, P. Perfetti, A. M. Paoletti, G. Pennesi, G. Rossi and R. Caminiti, *Appl. Phys. Lett.*, 2005, **87**.
12. A. Generosi, B. Paci, V. R. Albertini, P. Perfetti, A. M. Paoletti, G. Pennesi, G. Rossi and R. Caminiti, *Appl. Phys. Lett.*, 2006, **88**.
13. Z. G. Kong, W. L. Li, G. B. Che, B. Chu, D. F. Bi, L. L. Han, L. L. Chen, Z. Z. Hu and Z. Q. Zhang, *Appl. Phys. Lett.*, 2006, **89**.
14. H. Manaa, A. Al Mulla, S. Makhseed, M. Al-Sawah and J. Samuel, *Opt. Mater.*, 2009, **32**, 108-114.
15. Y. X. Li, J. H. Zhu, Y. Chen, J. J. Zhang, J. Wang, B. Zhang, Y. He and W. J. Blau, *Nanotechnology*, 2011, **22**.
16. H. Manaa, A. Tuhl, J. Samuel, A. Al-Mulla, N. A. Al-Awadi and S. Makhseed, *Opt. Commun.*, 2011, **284**, 450-454.
17. Z. C. Guo, B. Chen, M. Y. Zhang, J. B. Mu, C. L. Shao and Y. C. Liu, *J. Colloid Interface Sci.*, 2010, **348**, 37-42.
18. T. B. Ogunbayo and T. Nyokong, *J. Mol. Struct.*, 2010, **973**, 96-103.
19. X. Q. Li, L. F. Liu, S. Z. Kang, J. Mu and G. D. Li, *Appl. Surf. Sci.*, 2011, **257**, 5950-5956.
20. T. B. Ogunbayo, E. Antunes and T. Nyokong, *J. Mol. Catal. A-Chem.*, 2011, **334**, 123-129.

5. A Periodic Mesoporous Organosilica with Phthalocyanine Macrocycles Exhibiting Optoelectronic Properties

21. C. H. Lee, R. Filler, J. Lee, J. Li and B. K. Mandal, *Renew. Energy*, 2010, **35**, 1592-1595.
22. E. L. Spitler and W. R. Dichtel, *Nat. Chem.*, 2010, **2**, 672-677.
23. X. S. Ding, J. Guo, X. A. Feng, Y. Honsho, J. D. Guo, S. Seki, P. Maitarad, A. Saeki, S. Nagase and D. L. Jiang, *Angew. Chem. Int. Ed.*, 2011, **50**, 1289-1293.
24. T. Z. Ren, Z. Y. Yuan and B. L. Su, *Colloids Surf., A*, 2007, **300**, 79-87.
25. M. Pirouzmand, M. M. Amini and N. Safari, *J. Colloid Interface Sci.*, 2008, **319**, 199-205.
26. X. B. Lu, H. Wang and R. He, *J. Mol. Catal. A-Chem.*, 2002, **186**, 33-42.
27. J. T. Li, L. M. Guo and J. L. Shi, *Phys. Chem. Chem. Phys.*, 2010, **12**, 5109-5114.
28. H. J. Kim, K. J. Shin, M. K. Han, K. An, J. K. Lee, I. Honma and H. Kim, *Scr. Mater.*, 2009, **61**, 1137-1140.
29. T. Asefa, M. J. MacLachlan, N. Coombs and G. A. Ozin, *Nature*, 1999, **402**, 867-871.
30. S. Inagaki, S. Guan, Y. Fukushima, T. Ohsuna and O. Terasaki, *J. Am. Chem. Soc.*, 1999, **121**, 9611-9614.
31. B. J. Melde, B. T. Holland, C. F. Blanford and A. Stein, *Chem. Mat.*, 1999, **11**, 3302-3308.

5. A Periodic Mesoporous Organosilica with Phthalocyanine Macrocycles Exhibiting Optoelectronic Properties

32. C. J. Brinker, Y. F. Lu, A. Sellinger and H. Y. Fan, *Adv. Mater.*, 1999, **11**, 579-585.
33. Y. Goto, N. Mizoshita, O. Ohtani, T. Okada, T. Shimada, T. Tani and S. Inagaki, *Chem. Mater.*, 2008, **20**, 4495-4498.
34. M. A. Wahab and C. B. He, *J. Nanosci. Nanotechno.*, 2008, **8**, 6381-6386.
35. M. A. Wahab and C. B. He, *Langmuir*, 2009, **25**, 832-838.
36. J. Morell, M. Gungerich, G. Wolter, J. Jiao, M. Hunger, P. J. Klar and M. Froba, *Journal of Materials Chemistry*, 2006, **16**, 2809-2818.
37. A. Sayari and W. H. Wang, *Journal of the American Chemical Society*, 2005, **127**, 12194-12195.
38. H. Takeda, Y. Goto, Y. Maegawa, T. Ohsuna, T. Tani, K. Matsumoto, T. Shimada and S. Inagaki, *Chem. Commun.*, 2009, 6032-6034.
39. C. Vercaemst, P. E. de Jongh, J. D. Meeldijk, B. Goderis, F. Verpoort and P. Van Der Voort, *Chemical Communications*, 2009, 4052-4054.
40. N. Mizoshita, Y. Goto, Y. Maegawa, T. Tani and S. Inagaki, *Chem. Mater.*, 2010, **22**, 2548-2554.
41. N. Mizoshita, M. Ikai, T. Tani and S. Inagaki, *J. Am. Chem. Soc.*, 2009, **131**, 14225-14227.
42. H. Miyata and K. Kuroda, *Chem. Mater.*, 1999, **12**, 49-54.

5. A Periodic Mesoporous Organosilica with Phthalocyanine Macrocycles Exhibiting Optoelectronic Properties

43. E. Ortel, T. Reier, P. Strasser and R. Kraehnert, *Chem. Mater.*, 2011, **23**, 3201-3209.
44. J. Schuster, R. Köhn, A. Keilbach, M. Döblinger, H. Amenitsch and T. Bein, *Chem. Mater.*, 2009, **21**, 5754-5762.
45. M. P. Tate, V. N. Urade, J. D. Kowalski, T. C. Wei, B. D. Hamilton, B. W. Eggiman and H. W. Hillhouse, *J. Phys. Chem. B*, 2006, **110**, 9882-9892.
46. P. Falcaro, D. Grosso, H. Amenitsch and P. Innocenzi, *J. Phys. Chem. B*, 2004, **108**, 10942-10948.
47. L. Song, D. Feng, C. G. Campbell, D. Gu, A. M. Forster, K. G. Yager, N. Fredin, H.-J. Lee, R. L. Jones, D. Zhao and B. D. Vogt, *Journal of Materials Chemistry*, 2010, **20**, 1691-1701.
48. S. Tanaka, Y. Katayama, M. P. Tate, H. W. Hillhouse and Y. Miyake, *Journal of Materials Chemistry*, 2007, **17**, 3639-3645.
49. J. Schuster, R. Köhn, M. Döblinger, A. Keilbach, H. Amenitsch and T. Bein, *J. Am. Chem. Soc.*, 2012, doi: 10.1021/ja208941s.
50. T. Enokida, *Jpn. J. Appl. Phys.*, 1992, **31**, 1135-1136.
51. M. N. K. Harish, J. Keshavayya, K. R. V. Reddy, H. R. Mallikarjuna, R. A. S. Ali and T. Rajesh, *J. Coord. Chem.*, 2010, **63**, 4050-4060.
52. C. F. Vannostrum, A. W. Bosman, G. H. Gelinck, P. G. Schouten, J. M. Warman, A. P. M. Kentgens, M. A. C. Devillers, A. Meijerink, S. J. Picken, U. Sohling, A. J. Schouten and R. J. M. Nolte, *Chem. Eur. J.*, 1995, **1**, 171-182.

5. A Periodic Mesoporous Organosilica with Phthalocyanine Macrocycles Exhibiting Optoelectronic Properties

53. M. A. Shaibat, L. B. Casabianca, D. Y. Siberio-Perez, A. J. Matzger and Y. Ishii, *J. Phys. Chem. B*, 2010, **114**, 4400-4406.
54. M. B. Kılıçaslan, F. Ağin and H. Kantekin, *J. Coord. Chem.*, 2010, **63**, 861-867.
55. J. D. Bass and A. Katz, *Chem. Mater.*, 2003, **15**, 2757-2763.
56. B. Radi, R. M. Wellard and G. A. George, *Macromolecules*, 2010, **43**, 9957-9963.
57. B. Yan and D. H. Ma, *J. Solid State Chem.*, 2006, **179**, 2059-2066.
58. B. Francis, D. B. A. Raj and M. L. P. Reddy, *Dalton Trans*, 2010, **39**, 8084-8092.
59. M. Takafuji, N. Azuma, K. Miyamoto, S. Maeda and H. Ihara, *Langmuir*, 2009, **25**, 8428-8433.
60. X. Elias, R. Pleixats, M. W. C. Man and J. J. E. Moreau, *Adv. Synth. Catal.*, 2007, **349**, 1701-1713.
61. K. Bayo, J. C. Mossoyan and G. V. Ouedraogo, *Spectrochim. Acta, Part A*, 2004, **60**, 653-657.
62. D. K. Modibane and T. Nyokong, *Polyhedron*, 2009, **28**, 1475-1480.
63. K. Nagao, *Coord. Chem. Rev.*, 2002, **227**, 129-152.
64. E. L. Spitler and W. R. Dichtel, *Nat. Chem.*, 2010, **2**, 672-677.

5. A Periodic Mesoporous Organosilica with Phthalocyanine Macrocycles Exhibiting Optoelectronic Properties

65. X. Ding, J. Guo, X. Feng, Y. Honsho, J. Guo, S. Seki, P. Maitarad, A. Saeki, S. Nagase and D. Jiang, *Angew. Chem. Int. Ed.*, 2011, **50**, 1289-1293.
66. T. Oekermann, D. Schlettwein and N. I. Jaeger, *J. Electroanal. Chem.*, 1999, **462**, 222-234.
67. R. J. C. Brown and A. R. Kucernak, *J. Solid State Electrochem.*, 2005, **9**, 459-468.
68. T. Oekermann, D. Schlettwein and N. I. Jaeger, *J. Phys. Chem. B*, 2001, **105**, 9524-9532.
69. D. Schlettwein, E. Karmann, T. Oekermann and H. Yanagi, *Electrochim. Acta*, 2000, **45**, 4697-4704

6. Optoelectronically Active Periodic Mesoporous Organosilica Films Containing Porphyrin Chromophores

This chapter is based on a collaboration with Prof. Dirk Trauner and Florian Löbermann in the organic chemistry division of LMU. The synthesis of the organosilane precursor was done there.

6.1. Introduction

The great interest in developing mesoporous organic-inorganic hybrid materials arises from the expectation that the assembly of organic and inorganic building blocks in a single material can combine their particular properties and advantages.¹ As a result, such hybrid porous materials can have versatile organic functionalities and excellent mechanical and thermal stabilities, enabling their applications as catalyst, catalysis supports, nanoscale inclusion vessels and adsorbents.² Periodic mesoporous organosilicas (PMOs) are a class of porous materials that can achieve the combination of organic units and inorganic cross-linking parts within their periodically structured frameworks.³⁻⁵ PMO materials are normally synthesized by polycondensation of alkoxy-silyl precursors $R'[Si(OR)]_n$ ($n \geq 2$) in the presence of surfactant templates such as tetraalkylammonium halides or nonionic copolymers. To date, numerous organic units from small aliphatic and aromatic groups to larger functional groups have been successfully incorporated in the framework of PMO materials.⁶⁻¹³ In PMOs, each individual organic group R' is covalently bonded to two or more silicon atoms, such

6. Optoelectronically Active Periodic Mesoporous organosilica Film Containing Porphyrin Chromophores

that the bridging organic unit is an integral part of the pore walls, rendering the mesopores well accessible for guest molecules. Therefore their periodically arranged mesochannels as well as the great diversity of intrinsically functionalized pore walls could lead to potential applications of PMOs in areas such as catalysis,¹⁴⁻¹⁶ adsorbents¹⁷⁻¹⁸, and optical systems¹⁹⁻²².

Recent developments of PMO materials include the incorporation of electroactive organic species within their frameworks, aimed towards controlled energy and charge transfer.²³⁻²⁴ For example, Inagaki and coworkers have synthesized a novel PMO film containing π -conjugated phenylenevinylene molecules in its mesostructured framework and investigated its charge transport properties.²³ This reported PMO thin film had accessible mesopores with a diameter of 2.4 nm and possessed hexagonal packing of the mesochannels. For the first time, the observed charge-carrier mobility in the obtained film (on the order of $10^{-5} \text{ cm}^2 \text{ V}^{-1} \text{ s}^{-1}$) showed the possibility of designing semiconducting PMO materials. Given the charge-transporting ability of numerous π -conjugated systems, we reasoned that incorporating such conjugated organic units in the alkoxysilyl precursors might result in novel PMO materials with interesting photoactive and charge-conducting properties. As π -conjugated porphyrin molecules are well known to possess related electrical and optical properties, integrating porphyrin units into organosilica frameworks might lead to the desired PMO materials. However, alkoxysilyl precursors with bulky organic bridges are not easily integrated into periodic mesostructures, as this type of precursor can show low solubility and high hydrolysis rates leading to almost instant precipitation under common synthesis conditions.

Here we show that under optimized synthesis conditions a judiciously designed ethoxysilyl porphyrin macrocycle precursor can be used to successfully synthesize periodic mesoporous organosilica films without the addition of any other silica source. These porphyrin-bridged PMO films (denoted as Por-PMO) were prepared by an evaporation-induced self-assembly method with triblock co-polymer Pluronic F127 as structure-directing agent. The resulting PMO film was stable against mild thermal treatment of up to 120 °C. Besides, after template removal with ethanol, the extracted Por-PMO film showed stability against electron-beam irradiation during TEM characterization and was observed to possess an orthorhombic porous structure. Nitrogen sorption experiments on the extracted PMO material gave a surface area of 364 m² g⁻¹ and a pore size of 15 nm. Furthermore, the optoelectronic activities of the synthesized PMO films were investigated in the presence of electron-accepting species, showing light-induced charge generation and hole-transporting capability.

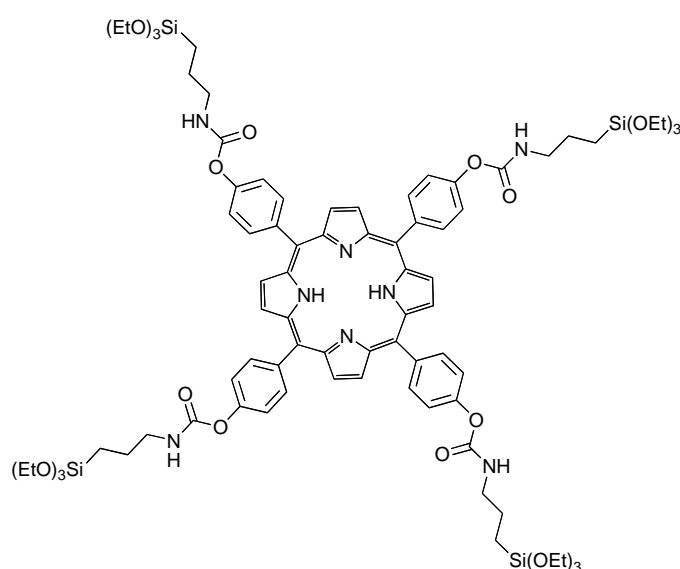
6.2. Experimental Section

6.2.1. Preparation of porphyrin-based PMO films

Porphyrin-based PMO films were synthesized by the evaporation-induced self-assembly (EISA) approach.²⁵ 0.075 g (0.045 mmol) porphyrin-containing precursor (Scheme 6.1, synthetic procedures in Appendix, A-3) and 0.075 g (0.006 mmol) Pluronic F127 were first dissolved in 2.4 ml ethanol. Next, 0.08 ml of 0.1 M HCl (8.0×10^{-3} mmol) were added and the resulting solution was stirred at room temperature for 4 h. Finally, the aged sol was spin-coated on glass slides (2 cm × 2 cm) at a spinning-rate of 3000 rpm

6. Optoelectronically Active Periodic Mesoporous organosilica Film Containing Porphyrin Chromophores

with an acceleration of 2905 rpm/s for 30 s. The obtained films were dried in air at room temperature overnight (denoted as Por-PMO-as prepared). In order to remove the surfactant template F127, the films were then heated in flowing N₂ with a ramp of 1°C/min to 120 °C and kept at this temperature for 5 h (denoted as Por-PMO-120 °C) and finally refluxed in absolute ethanol for 2 h to remove the surfactant F127 (denoted as extracted Por-PMO).



Scheme 6.1: Chemical structure of the ethoxysilyl precursor containing porphyrin macrocycles.

6.2.2. Structural Characterization

The samples were characterized with X-ray diffraction (XRD) measurements using a Bruker D8 Discover with Ni-filtered CuK_α-radiation (0.154 nm) and a position-sensitive detector (LynxEye). For two-dimensional grazing-incidence small angle X-ray scattering (2D-GISAXS) characterization, a SAXSess system by Anton Paar (CuK_α-radiation,

6. Optoelectronically Active Periodic Mesoporous organosilica Film Containing Porphyrin Chromophores

sample-detector distance 306.7 mm) with a CCD detector (PI-SCX:4300, Roper Scientific) was used. The samples were measured for 10 h with a tilt angle of 0.27° with respect to the primary beam. Transmission electron microscopy (TEM) was performed using a FEI Titan 80-300 instrument equipped with a field emission gun operated at 300 kV. Nitrogen sorption measurements were carried out at -196°C using an Autosorb-1 by Quantachrome Instruments, and before the measurements the samples were degassed at 150°C for 12 h in vacuum. For this purpose thicker films were synthesized by drop-casting the same solutions as for Por-PMO on flat glass substrates. After thermal treatment, the thick films were scratched off from the glass slides and refluxed in absolute ethanol to removal surfactant template before the nitrogen sorption measurement. The Brunauer-Emmett-Teller (BET) surface area was calculated using experimental points at a relative pressure range of $p/p_0 = 0.05-0.20$. The total pore volume was calculated by the N_2 amount adsorbed at the highest p/p_0 ($p/p_0 = 0.98$). NLDFT pore size distributions were calculated from the adsorption branch using a SiO_2 kernel assuming cylindrical/spherical pore geometry for the sample. Solid-state ^{13}C and ^{29}Si NMR experiments were performed on a Bruker Avance-III 500 spectrometer (11.7 Tesla) operating at frequencies of 125.8 MHz for ^{13}C and 99.4 MHz for ^{29}Si . $^{13}\text{C}\{1\text{H}\}$ CP-MAS spectra were acquired using a 90° pulse length of $2.5\ \mu\text{s}$ (3.7 dB) with cross-polarization contact time of 5 ms and a recycle delay of 2 s. $^{29}\text{Si}\{1\text{H}\}$ CP-MAS experiments were conducted using a 90° pulse length of $2.5\ \mu\text{s}$ (3.7 dB) with cross-polarization contact time of 5 ms and a recycle delay of 2 s.

6.2.3. Photoelectrochemical Characterization

Por-PMO films were synthesized on indium tin oxide coated glass (VisionTek, 150 nm ITO, 12-15 ohms/sq).

UV-Vis measurements were performed on a Hitachi U3501 spectrophotometer equipped with an integrating sphere. Absorbance spectra were recorded in transmission geometry with plain ITO as reference.

For the measurements in an electrolyte, the ITO substrates were cut into pieces of 1 cm × 1.5 cm. A 5 mm wide contact area on one side of the substrate was masked during the deposition of the PMO film, resulting in an active area of 1 cm². After extraction of the template the blank part of the ITO was contacted with a copper wire using silver paste and then this contact area was sealed with poly(dimethylsiloxane) in order to avoid direct contact between the ITO and the electrolyte. Photoelectrochemical measurements were performed with the Por-PMO film as working electrode and a platinum wire as counter electrode in an aqueous electrolyte containing 0.1 M KNO₃ and 1 mM H₂O₂.

Solid-state devices were fabricated on patterned ITO substrates. After deposition of the PMO layer and subsequent extraction of the template, the films (1.5 cm × 1.5 cm) were immersed overnight into a solution of [6, 6]-phenyl-C₆₁-butyric acid methyl ester (PCBM, 3 mg/ml in chlorobenzene) to enhance the infiltration of the PCBM into the mesopores (each film in 5 ml PCBM solution). The films were then taken from this solution and immediately spun at 1000 rpm with an acceleration of 996 rpm/s for 60 s, which resulted in a thin and homogeneous layer of PCBM on top of the PMO film. Finally, 70 nm thick silver contacts were sputter-deposited through a shadow mask,

6. Optoelectronically Active Periodic Mesoporous organosilica Film Containing Porphyrin Chromophores

yielding an active area of 16 mm². The samples were illuminated through a 12 mm² mask and measured in air.

For recording current transients the samples were illuminated with white light from an AM1.5G solar simulator (Solar Light Model 16S) at 100 mW/cm², which was modulated by a shutter. Illumination was carried out from the film side in the case of measurements in an electrolyte and through the ITO substrate in case of the solid-state devices. Lower light intensities were realized with a set of calibrated reflective neutral density filters. The signal was recorded using a low noise preamplifier (Femto DLPCA-200) and an oscilloscope (Tektronix DPO2012).

External quantum efficiency (EQE) measurements were performed at short circuit. Monochromatic light was obtained from a 150 W xenon lamp in combination with a monochromator and order-sorting filters. The slits were adjusted such that the FWHM was 5 nm at a light intensity of approximately 2 mW/cm². All light intensities were calibrated with a Fraunhofer ISE certified silicon reference cell equipped with a KG5 filter. The monochromatic light was modulated using an optical chopper at a frequency of 4 Hz for measurements with an electrolyte and 12 Hz in case of the solid state devices. The signal was detected via a low noise pre-amplifier (Femto DLPCA-200) and a lock-in amplifier (Signal Recovery 7265). The modulation frequency was chosen slow enough such that the current response of the sample was square-like.

6.3. Results and discussion

6.3.1. Mesostructured porphyrin-bridged PMO films

Figure 6.1 shows the XRD patterns of the synthesized Por-PMO films. The film deposited from the precursor solution gives a diffraction peak at $2\theta = 0.86^\circ$, indicating the formation of a periodic mesostructure with a d-spacing of 10.2 nm. After a thermal treatment at 120 °C followed by solvent extraction, the diffraction peaks are shifted to 0.92° and 1.33° respectively, corresponding to d-spacings of 9.5 and 6.6 nm. The decreased d-spacings indicate a film shrinkage along the substrate normal, which is commonly observed for mesoporous thin films after template removal.^{23, 26-28}

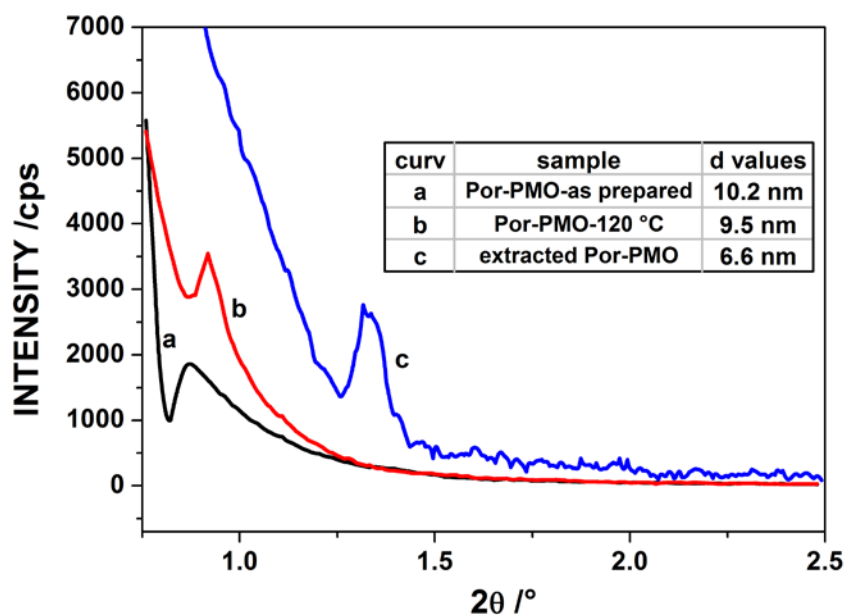


Figure 6.1: Small-angle X-ray diffractions of the Por-PMO films, (a) as prepared, (b) after thermal treatment at 120 °C for 5 hours, (c) after extraction with ethanol. The intensity of the extracted Por-PMO film was multiplied by 2 for better visibility.

6. Optoelectronically Active Periodic Mesoporous organosilica Film Containing Porphyrin Chromophores

The 2D-GISAXS pattern of the extracted Por-PMO film resembled those observed for many mesoporous films after 1D shrinkage.²⁹⁻³⁰ It can be indexed with an orthorhombic unit cell ($Fmmm$) with the (010) plane parallel to the substrate (Figure 6.2). Mesoporous silica and carbon films with a similar face-centred orthorhombic symmetry prepared with the same structure directing agent (Pluronic F127) have also been reported.³¹⁻³⁴ The reflections in the GISAXS pattern are doubled due to diffraction of the incidence beam reflected at the film-substrate interface. Hence, reflections on top of each other (one circle and one square) belong to the same indexing. The lower empty square denotes the 002 reflection position. As it is below the sample 'horizon', the reflection intensity is fully absorbed by the sample. The lattice constants for the extracted Por-PMO film determined by XRD methods are $a = 17.5$ nm, $b = 13.2$ nm, and $c = 24.8$ nm. The basis vectors \mathbf{a} and \mathbf{c} are parallel to the film and \mathbf{b} is along the film normal (Figure 6.2).

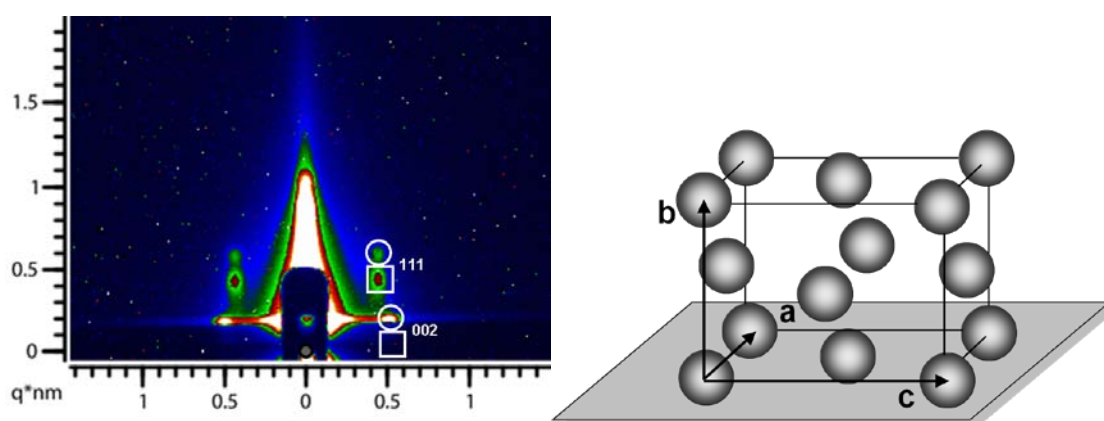


Figure 6.2: 2D-GISAXS pattern (left) of the extracted Por-PMO film according to the face-centred orthorhombic symmetry ($Fmmm$), with the (010) plane parallel to the substrate (right).

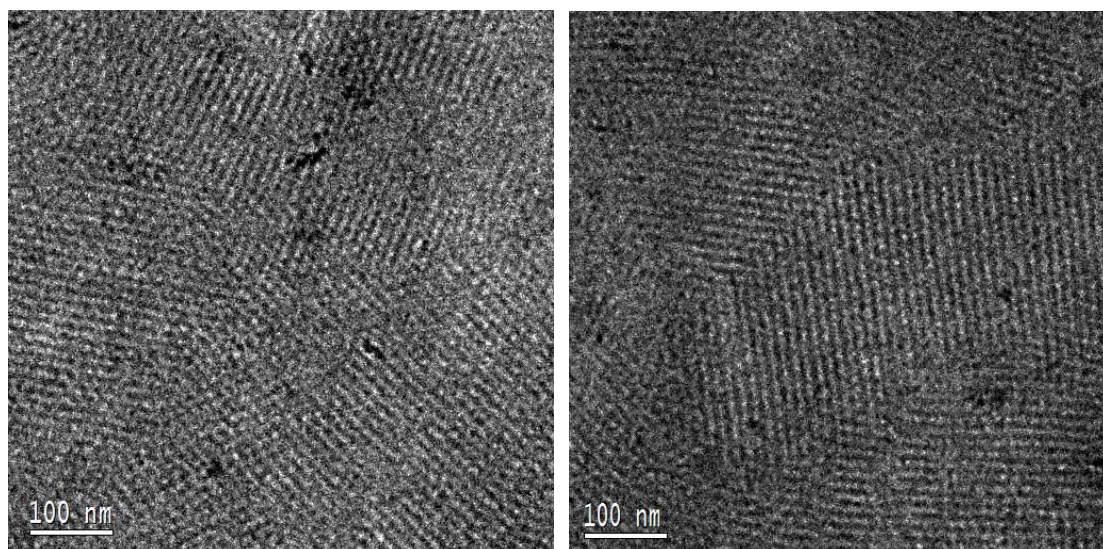


Figure 6.3: Plan-view TEM images of the extracted Por-PMO film. The presence of the ordered domains in the TEM images confirms the preservation of the mesostructure after removal of surfactant template.

Figure 6.3 shows transmission electron micrographs of the Por-PMO film after template removal. In plan-view images, the periodic mesostructure of the Por-PMO film with domain sizes in the range of hundreds of nanometers can be observed. The presence of the ordered domains in the TEM images confirms that the mesostructure is preserved after removal of surfactant template and that it is also stable against electron-beam damage during TEM characterization. The *d*-values determined from the TEM images and their Fourier Transforms are on average 13.3 nm, 9.6 nm and 7.8 nm, which fits well with the values expected for an *Fm $\bar{3}m$* structure with the *b*-axis along the film normal. The absolute values measured by TEM are slightly larger than observed by XRD, which may be attributed to sample preparation for TEM (ultrasonic treatment on the film scratched off from the glass slide).

6. Optoelectronically Active Periodic Mesoporous organosilica Film Containing Porphyrin Chromophores

To investigate the porosity of the extracted porphyrin-bridged PMO material, nitrogen sorption isotherms of the scratched-off films were recorded. Figure 6.4 shows the obtained isotherm with a typical type IV isotherm shape, which is commonly observed for mesoporous materials. The presence of the hysteresis loop suggests the existence of ink-bottle shaped pores. The resulting Por-PMO material has a Brunauer-Emmett-Teller (BET) surface area of $364 \text{ m}^2\text{g}^{-1}$ and a pore volume of $0.57 \text{ cm}^3\text{g}^{-1}$. The NLDFT pore-size distribution calculated from the adsorption branch indicates that the extracted Por-PMO material has mesopores with a diameter of about 15 nm (inset of Figure 6.4). The fairly broad pore size distribution is tentatively attributed to an incomplete template removal as well as the elliptically shaped pores resulting from the film shrinkage (35% shrinkage along the film normal was calculated from the 1D-XRD pattern).

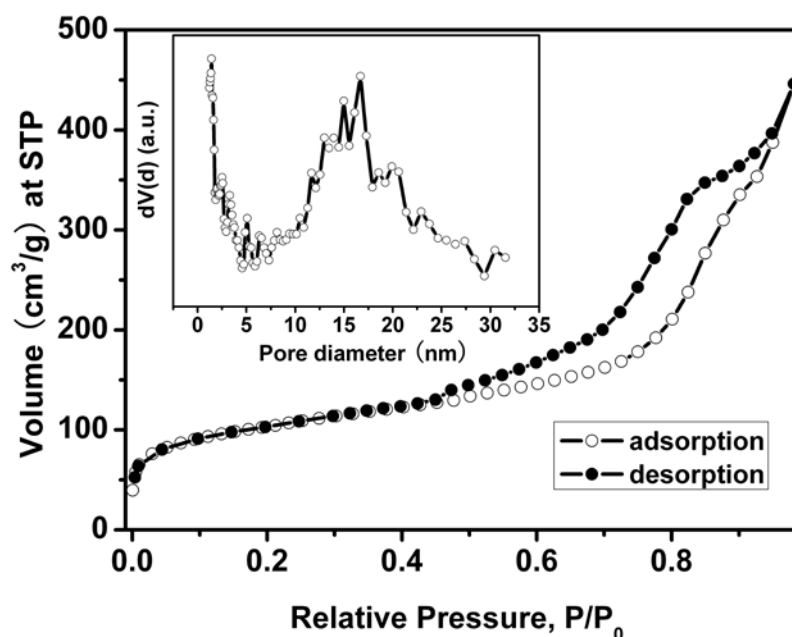


Figure 6.4: Nitrogen adsorption (○) and desorption (●) isotherms of the extracted Por-PMO material with an inset showing the pore size distribution calculated with the NLDFT model from the adsorption branch (○) using a SiO_2 kernel assuming cylindrical/spherical pore geometry for the sample.

6. Optoelectronically Active Periodic Mesoporous organosilica Film Containing Porphyrin Chromophores

The extracted Por-PMO material was also investigated by solid-state NMR spectroscopy in order to get detailed information about the chemical environment of both ^{13}C and ^{29}Si nuclei in the PMO material. In the ^{13}C -MAS NMR spectrum (Figure 6.5A), the detected chemical shifts in the range of 125 - 160 ppm are assigned to the carbon atoms in the aromatic ring of the porphyrin moiety.³⁵⁻³⁸ The signals at 7.8 ppm (SiCH_2), 23.2 ppm (SiCH_2CH_2), 42.1 ppm (CH_2NH) and 118.3 ppm ($\text{C}=\text{O}$) could be assigned to the carbon atoms in the propyl isocyanate moiety.³⁹⁻⁴³ The ^{13}C -NMR spectrum proves that the porphyrin organic bridges in the precursor are robust enough to survive the synthesis conditions. In the solid state ^{29}Si MAS-NMR spectrum (Figure 6.5B), chemical shifts of T^1 [$\text{CSi}(\text{OSi})(\text{OH})_2$], T^2 [$\text{CSi}(\text{OSi})_2(\text{OH})$] and T^3 [$\text{CSi}(\text{OSi})_3$] sites were observed at -46.5, -57.8 and -65.7 ppm, respectively.⁴⁴⁻⁴⁵ There were no signals observed in the range of -100 to -125 ppm which is representative of Q^n sites [$\text{Q}^n=\text{Si}(\text{OSi})_n(\text{OH})_{4-n}$], confirming that the Si-C bonds are stable and completely retained in the final mesoporous framework.⁴⁶⁻⁴⁸

6. Optoelectronically Active Periodic Mesoporous organosilica Film Containing Porphyrin Chromophores

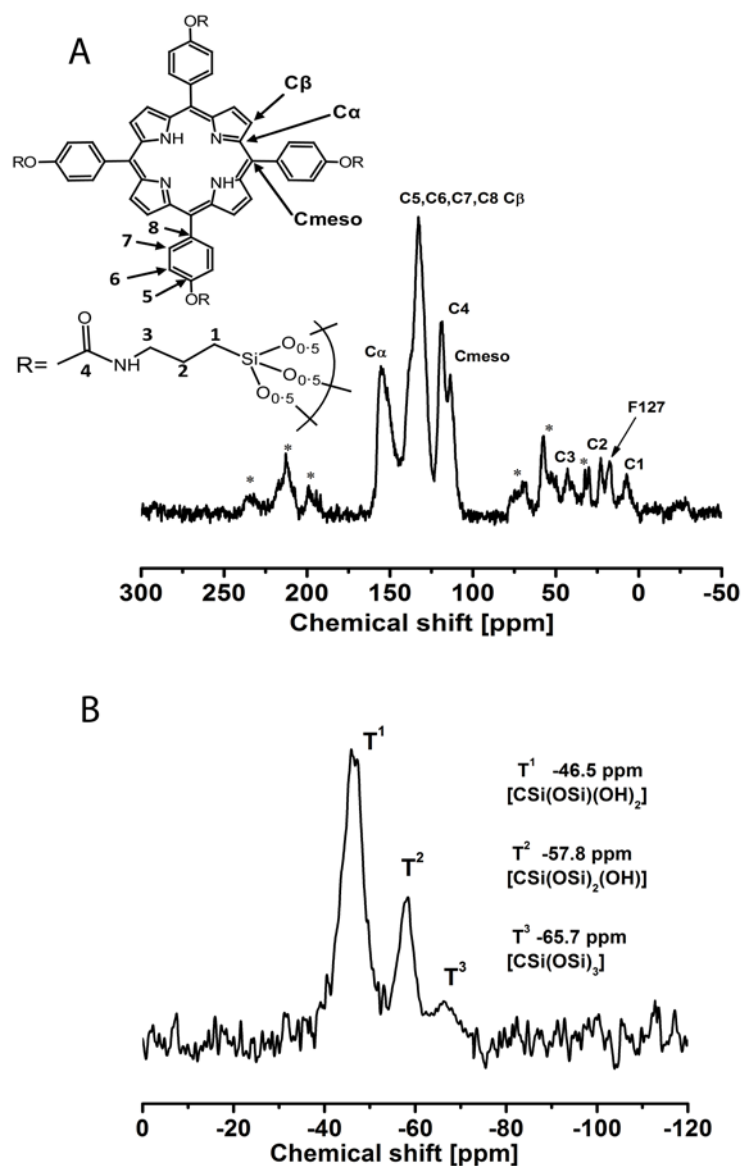


Figure 6.5: A) ^{13}C -MAS NMR and B) ^{29}Si -MAS NMR spectra of the extracted porphyrin-bridged PMO material with the corresponding assignments of the different resonances. Signals with asterisk * are the spinning side bands.

6.3.2. UV-Vis absorption properties

The optical properties of the Por-PMO film were evaluated with UV-Vis absorption

6. Optoelectronically Active Periodic Mesoporous organosilica Film Containing Porphyrin Chromophores

spectroscopy. The UV-Vis spectrum of a diluted solution containing porphyrin-bridged precursor molecules as well as that of the extracted Por-PMO film are shown in Figure 6.6. For the diluted precursor solution, the strong Soret band is observed at 416 nm. Additionally, four bands are seen at 514, 550, 590 and 651 nm, and are assigned to the Q-band signals, which is typical for non-aggregated, free-base porphyrin units.^{37-38, 49-50} Meanwhile, for the extracted Por-PMO film, the absorption bands between 380 nm and 700 nm have similar shape but are red-shifted compared to the spectrum of the precursor solution. Similar red-shifts have been observed in other systems with assembled porphyrin macrocycles, and are believed to result from densely packed molecular organization that allows electronic coupling and energy transfer among the porphyrin building blocks.⁵¹⁻⁵³

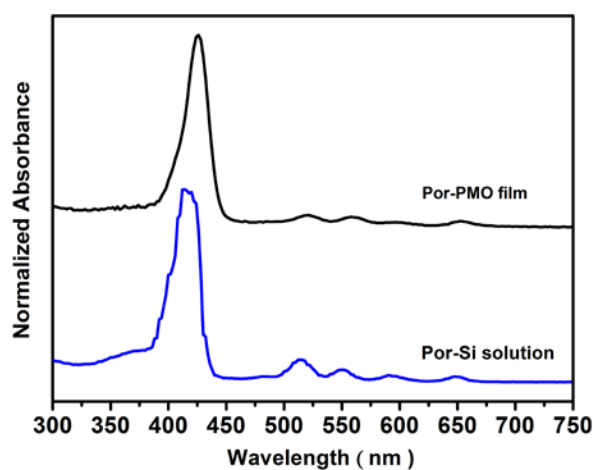
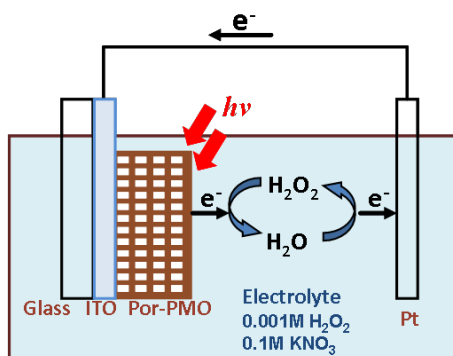


Figure 6.6: UV-Vis absorption spectra of the extracted Por-PMO film (black curve) and that of a diluted solution containing 10^{-5} M porphyrin organosilica precursor in THF (blue curve). For clarity, an offset is added to the black curve.

6.3.3 Optoelectronic properties

In order to investigate the photoactive and electronic properties of the Por-Si-PMO films we prepared samples on ITO-coated glass substrates.

For the measurements in an aqueous electrolyte containing 0.1 M KNO_3 and 1 mM H_2O_2 , the Por-PMO film was connected as working electrode and a Pt wire was the counter-electrode (Scheme 6.2). The time-resolved photocurrent response and the spectrally resolved response of such an extracted PMO film (120 nm thick) were investigated.



Scheme 6.2: Illustration of the set-up for photoelectrochemical experiments in electrolyte containing 0.1 M KNO_3 and 1 mM H_2O_2 .

Current transients were recorded at different intensities of simulated solar light (Figure 6.7A). A current pulse is generated upon illumination and quickly decays to a lower steady-state current. A pulse of similar amplitude with opposite sign is observed when switching off the light. These observed anodic and cathodic current spikes are well-known for films of organic semiconductors in electrolytes and could originate from charging and discharging of surface states.⁵⁴⁻⁵⁷ The sign of the photocurrent identifies

6. Optoelectronically Active Periodic Mesoporous organosilica Film Containing Porphyrin Chromophores

the Por-Si-PMO film as a p-type semiconductor, indicating that electron-hole pairs are generated upon illumination and the electrons are transferred to the electrolyte, whereas the holes are transported within the Por-Si-PMO film.

In addition to the time-resolved photocurrent we recorded the spectrally resolved photocurrent at short circuit (Figure 6.7B, dashed line). Above 500 nm, the spectrum of external quantum efficiency (EQE), which is the ratio of collected electrons to incident photons, closely resembles the absorbance spectrum of the Por-Si-PMO film. However, at the position of the strongest absorption the current output is unexpectedly low. Since the absorbance around 420 nm is far higher than at longer wavelengths, incident photons are absorbed mainly close to the film surface. Consequently, holes have to travel through the entire porphyrin network and might recombine with electrons from the electrolyte before they can be collected at the contact. In contrast, at longer wavelengths the light intensity does not vary dramatically through the depth of the film and thus the generation of electron-hole pairs is much more uniformly distributed over the entire film thickness, such that the current output seems to be more favorable in this case.

6. Optoelectronically Active Periodic Mesoporous organosilica Film Containing Porphyrin Chromophores

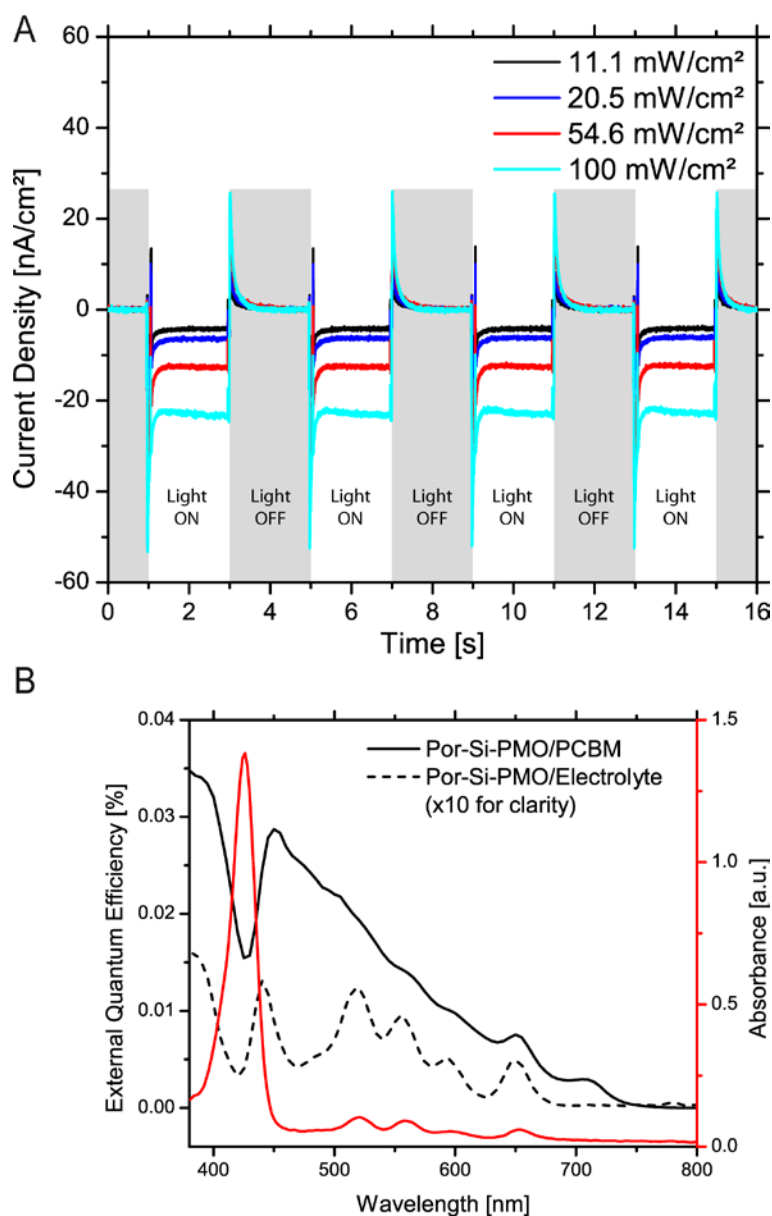
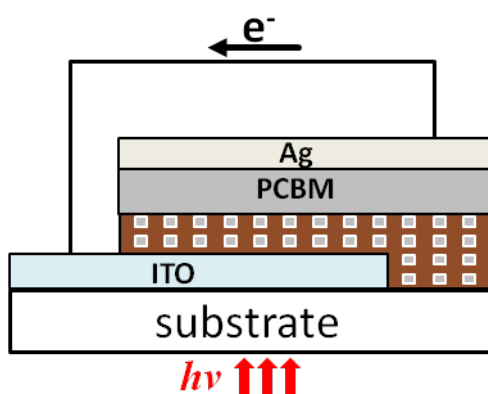


Figure 6.7: A) Time-resolved photocurrent response of the extracted Por-Si-PMO film deposited on ITO in an aqueous electrolyte containing 0.1 M KNO₃ and 1 mM H₂O₂ (active area is 1 cm²). The experiment was carried out using simulated AM1.5G solar light of different light intensity. B) External quantum efficiency of a Por-Si-PMO film in the electrolyte and of the Por-Si-PMO/PCBM solid-state device, and UV-Vis spectrum of a Por-Si-PMO film. The spectrum measured in the electrolyte was multiplied by 10 for clarity.

6. Optoelectronically Active Periodic Mesoporous organosilica Film Containing Porphyrin Chromophores

We also combined the p-type porphyrin-based PMO films with an electron acceptor to form a three-dimensional solid-state heterojunction by soaking the extracted mesoporous films in a solution of PCBM for infiltration of the electron-transporting species into the mesopores. Subsequent spin-coating with the PCBM solution results in an additional PCBM overlayer, which is required for avoiding contact between the Ag back electrode and the p-type material (configuration of the device illustrated in Scheme 6.3).



Scheme 6.3: Illustration of the configuration of the solid-state device with mesostructured PMO film. The porous layer on the surface of ITO represents the Por-PMO film.

The external quantum efficiency spectrum of the device follows the absorbance trend of the Por-Si-PMO film (Figure 6.7B, solid line). Compared to the measurements in an electrolyte the photocurrent response in the blue and UV part of the spectrum is much higher, which might be due to additional contribution from the PCBM. The observed photocurrent seems to be a superposition of excitons generated in the Por-Si-PMO followed by electron injection into the PCBM, and excitons generated upon light

absorption by the PCBM followed by hole injection into the Por-Si-PMO. As already observed for the liquid electrolyte sample, the photocurrent generated at the strong absorption peak of the porphyrin framework is in fact lower than at neighboring wavelengths. At around 420 nm, since the illumination is through the ITO substrate in this case, most excitons are created close to the contacts and the electrons in the PCBM have to diffuse a long way through the interpenetrating networks and might eventually recombine with holes in the PMO film before being collected by the Ag contact. Again, the more uniform charge generation throughout the entire film seems to be more favorable for current output.

6.4. Conclusion

In summary, a periodic mesoporous organosilica film material with optoelectronic activity based on a porphyrin moiety was successfully synthesized. The specially designed porphyrin-bridged ethoxysilyl precursor was polycondensed through an evaporation-induced self-assembly process to form a PMO film with Pluronic F127 acting as template. SAXS measurements and TEM experiments on the Por-PMO film showed that after thermal treatment and surfactant removal an orthorhombic mesoporous structure was formed on the surface of a flat substrate. Solid state NMR spectra confirmed the preservation of the porphyrin macrocycles after being incorporated in the condensed organosilica framework. The obtained Por-PMO material with pore size of 15 nm showed a surface area of $364 \text{ m}^2\text{g}^{-1}$ and a pore volume of $0.57 \text{ cm}^3\text{g}^{-1}$. The UV-Vis absorbance spectrum of the PMO film showed a wide absorption due to the porphyrin chromophores in the organosilica framework. The observed energy shifts of the porphyrin in the PMO film with respect to the precursor

molecules in solution point to strong electronic interactions of the porphyrin chromophores in the PMO framework. Finally, the investigation on the optoelectronic activity of the film showed a light-induced charge generation capability and a p-type semiconducting character of the PMO system. This study shows that novel periodic bulk heterojunctions can be designed on the basis of porphyrin-containing mesoporous organosilica materials. As the structural parameters such as pore size, pore volume and periodicity of these systems are known, we propose that such systems will be of interest as promising model systems for the study of bulk heterojunctions for photovoltaics.

6.5. References

1. F. Hoffmann and M. Fröba, *Chem. Soc. Rev.*, 2011, **40**, 608-620.
2. Y. Yamauchi and K. Kuroda, *Asian J. Chem.*, 2008, **3**, 664-676.
3. T. Asefa, M. J. MacLachlan, N. Coombs and G. A. Ozin, *Nature*, 1999, **402**, 867-871.
4. S. Inagaki, S. Guan, Y. Fukushima, T. Ohsuna and O. Terasaki, *J. Amer. Chem. Soc.*, 1999, **121**, 9611-9614.
5. B. J. Melde, B. T. Holland, C. F. Blanford and A. Stein, *Chem. Mater.*, 1999, **11**, 3302-3308.
6. J. Morell, M. Gungerich, G. Wolter, J. Jiao, M. Hunger, P. J. Klar and M. Froba, *J. Mater. Chem.*, 2006, **16**, 2809-2818.
7. A. Sayari and W. H. Wang, *J. Am. Chem. Soc.*, 2005, **127**, 12194-12195.

6. Optoelectronically Active Periodic Mesoporous organosilica Film Containing Porphyrin Chromophores

8. H. Takeda, Y. Goto, Y. Maegawa, T. Ohsuna, T. Tani, K. Matsumoto, T. Shimada and S. Inagaki, *Chem. Commun.*, 2009, 6032-6034.
9. C. Vercaemst, P. E. de Jongh, J. D. Meeldijk, B. Goderis, F. Verpoort and P. Van Der Voort, *Chem. Commun.*, 2009, 4052-4054.
10. N. Mizoshita, T. Tani and S. Inagaki, *Chem. Soc. Rev.*, 2011, **40**, 789-800.
11. M. P. Kapoor, Q. H. Yang and S. Inagaki, *J. Am. Chem. Soc.*, 2002, **124**, 15176-15177.
12. A. Sayari and W. Wang, *J. Am. Chem. Soc.*, 2005, **127**, 12194-12195.
13. M. Cornelius, F. Hoffmann and M. Fröba, *Chem. Mater.*, 2005, **17**, 6674-6678.
14. Q. H. Yang, J. Liu, L. Zhang and C. Li, *J. Mater. Chem.*, 2009, **19**, 1945-1955.
15. A. Kuschel and S. Polarz, *J. Am. Chem. Soc.*, 2010, **132**, 6558-6565.
16. E. Y. Jeong, M. B. Ansari and S. E. Park, *ACS Catal.*, 2011, **1**, 855-863.
17. M. Park, S. S. Park, M. Selvaraj, D. Y. Zhao and C. S. Ha, *Microporous Mesoporous Mat.*, 2009, **124**, 76-83.
18. C. Li, J. Liu, X. Shi, J. Yang and Q. Yang, *Journal of Physical Chemistry C*, 2007, **111**, 10948-10954.
19. S. Inagaki, O. Ohtani, Y. Goto, K. Okamoto, M. Ikai, K. Yamanaka, T. Tani and T. Okada, *Angew. Chem., Int. Ed.*, 2009, **48**, 4042-4046.

6. Optoelectronically Active Periodic Mesoporous organosilica Film Containing Porphyrin Chromophores

20. R. Hernandez, A. C. Franville, P. Minoofar, B. Dunn and J. I. Zink, *J. Am. Chem. Soc.*, 2001, **123**, 1248-1249.
21. P. N. Minoofar, R. Hernandez, S. Chia, B. Dunn, J. I. Zink and A. C. Franville, *J. Am. Chem. Soc.*, 2002, **124**, 14388-14396.
22. N. Mizoshita, Y. Goto, T. Tani and S. Inagaki, *Adv. Funct. Mater.*, 2008, **18**, 3699-3705.
23. N. Mizoshita, M. Ikai, T. Tani and S. Inagaki, *J. Am. Chem. Soc.*, 2009, **131**, 14225-14227.
24. N. Mizoshita, T. Tani and S. Inagaki, *Adv. Funct. Mater.*, 2011, **21**, 3291-3296.
25. C. J. Brinker, Y. F. Lu, A. Sellinger and H. Y. Fan, *Adv. Mater.*, 1999, **11**, 579-585.
26. H. Miyata and K. Kuroda, *Chem. Mater.*, 1999, **12**, 49-54.
27. E. Ortel, T. Reier, P. Strasser and R. Kraehnert, *Chem. Mater.*, 2011, **23**, 3201-3209.
28. J. Schuster, R. Köhn, A. Keilbach, M. Döblinger, H. Amenitsch and T. Bein, *Chem. Mater.*, 2009, **21**, 5754-5762.
29. L. Song, D. Feng, C. G. Campbell, D. Gu, A. M. Forster, K. G. Yager, N. Fredin, H.-J. Lee, R. L. Jones, D. Zhao and B. D. Vogt, *Journal of Materials Chemistry*, 2010, **20**, 1691-1701.

6. Optoelectronically Active Periodic Mesoporous organosilica Film Containing Porphyrin Chromophores

30. M. P. Tate, V. N. Urade, J. D. Kowalski, T.-c. Wei, B. D. Hamilton, B. W. Eggiman and H. W. Hillhouse, *J. Phys. Chem. B*, 2006, **110**, 9882-9892.
31. S. Tanaka, Y. Katayama, M. P. Tate, H. W. Hillhouse and Y. Miyake, *Journal of Materials Chemistry*, 2007, **17**, 3639-3645.
32. V. N. Urade and H. W. Hillhouse, *J. Phys. Chem. B*, 2005, **109**, 10538-10541.
33. P. Falcaro, D. Grosso, H. Amenitsch and P. Innocenzi, *J. Phys. Chem. B*, 2004, **108**, 10942-10948.
34. J. Schuster, R. Köhn, M. Döblinger, A. Keilbach, H. Amenitsch and T. Bein, *J. Am. Chem. Soc.*, 2012, doi: **10.1021/ja208941s**.
35. J. Y. Tung, J. H. Chen, F. L. Liao, S. L. Wang and L. P. Hwang, *Inorg. Chem.*, 1998, **37**, 6104-6108.
36. L. Frydman, A. C. Olivieri, L. E. Diaz, A. Valasinas and B. Frydman, *J. Amer. Chem. Soc.*, 1988, **110**, 5651-5661.
37. S. Wan, F. Gándara, A. Asano, H. Furukawa, A. Saeki, S. K. Dey, L. Liao, M. W. Ambrogio, Y. Y. Botros, X. Duan, S. Seki, J. F. Stoddart and O. M. Yaghi, *Chem. Mater.*, 2011, **23**, 4094-4097.
38. X. Feng, L. Chen, Y. Dong and D. Jiang, *Chem. Commun.*, 2011, **47**.
39. J. D. Bass and A. Katz, *Chem. Mater.*, 2003, **15**, 2757-2763.
40. B. Francis, D. B. Ambili Raj and M. L. P. Reddy, *Dalton Trans.*, 2010, **39**, 8084-8092.

6. Optoelectronically Active Periodic Mesoporous organosilica Film Containing Porphyrin Chromophores

41. B. Yan and D. J. Ma, *J. Solid State Chem.*, 2006, **179**, 2059-2066.
42. J. S. Lee and S. W. Ryu, *Macromolecules*, 1999, **32**, 2085-2087.
43. I. V. Mel'nik, O. V. Lyashenko, Y. L. Zub, A. A. Chuiko, D. Cauzzi and G. Predieri, *Russ. J. Gen. Chem.*, 2004, **74**, 1658-1664.
44. B. Radi, R. M. Wellard and G. A. George, *Macromolecules*, 2010, **43**, 9957-9963.
45. M. Takafuji, N. Azuma, K. Miyamoto, S. Maeda and H. Ihara, *Langmuir*, 2009, **25**, 8428-8433.
46. M. A. Wahab and C. B. He, *Langmuir*, 2009, **25**, 832-838.
47. A. Keilbach, M. Döblinger, R. Köhn, H. Amenitsch and T. Bein, *Chem. Eur. J.*, 2009, **15**, 6645-6650.
48. Y. Li, A. Keilbach, N. Mizoshita, S. Inagaki and T. Bein, *J. Mater. Chem.*, 2011, **21**, 17338-17344.
49. M. A. García-Sánchez and A. Campero, *J. Non-Cryst. Solids*, 2001, **296**, 50-56.
50. M. A. García-Sánchez and A. Campero, *J. Non-Cryst. Solids*, 2004, **333**, 226-230.
51. N. C. Maiti, S. Mazumdar and N. Periasamy, *J. Phys. Chem. B*, 1998, **102**, 1528-1538.
52. V. De la Luz, M. A. García-Sánchez and A. Campero, *J. Non-Cryst. Solids*, 2007, **353**, 2143-2149.

6. Optoelectronically Active Periodic Mesoporous organosilica Film Containing Porphyrin Chromophores

53. H. Peng and Y. Lu, *Adv. Mater.*, 2008, **20**, 797-800.
54. T. Oekermann, D. Schlettwein and N. I. Jaeger, *J. Electroanal. Chem.*, 1999, **462**, 222-234.
55. R. J. C. Brown and A. R. Kucernak, *J. Solid State Electrochem.*, 2005, **9**, 459-468.
56. T. Oekermann, D. Schlettwein and N. I. Jaeger, *J. Phys. Chem. B*, 2001, **105**, 9524-9532.
57. D. Schlettwein, E. Karmann, T. Oekermann and H. Yanagi, *Electrochim. Acta*, 2000, **45**, 4697-4704.



7. Conclusions and Outlook

This thesis focused on synthesizing novel periodic mesoporous organosilica (PMO) materials with different chromophores in their frameworks. A modified evaporation-induced self-assembly (EISA) process was employed to produce PMO materials either in the tubular channels of anodic alumina membranes (AAM) or on the surface of flat substrates.

Choosing the porous AAM as host system for PMO materials was based on the favorable interactions of silica species with AAM channel walls found in inorganic silica/AAM systems. In the course of this thesis, the first PMO material confined within the channels of AAM was synthesized with 4, 4'-bis(triethoxysilyl)biphenyl (BTEBP) as the organosilica precursor. By using the ionic surfactant cetyltrimethylammonium bromide (CTAB) as the structure-directing agent (SDA), the resulting PMO showed a phase mixture of the 2D-hexagonal columnar and a lamellar mesostructure. When using the nonionic surfactant F127 as SDA, a 2D-hexagonal circular mesophase was obtained in the AAM channels. Additionally, a cubic *Im-3m* phase was formed with the same surfactant F127 after the addition of lithium chloride to the precursor solution. Both the circular and cubic confined biphenylene-bridged PMOs were stable against calcination temperatures of up to 250 °C. Besides, all the biphenyl PMO/AAM composites showed fluorescence in the UV light region due to the presence of biphenyl chromophores in the stable organosilica frameworks.

The other PMO material within the channels of AAM was synthesized with 1,3,5-tris(4-triethoxysilylstyryl)benzene (a three-armed oligo(phenylenevinylene))

compound, denoted as 3a-OPV) as precursor. Depending on different structure directing agents, different mesophases were observed. Pluronic F127-templated 3a-OPV-PMO showed a 2D-hexagonal circular phase formed in the confined environment of the AAM channels. When using Pluronic F108 (which can form micelles with higher curvature than F127), a body centered cubic (*Im-3m*) mesophase was formed within the AAM channels. It is noteworthy that the resulting circular and cubic 3a-OPV-PMO/AAM composites were both structurally stable against thermal treatments at temperatures of up to 200 °C and also rather stable in the electron beam of an electron microscope. Fluorescence spectra showed that the confined 3a-OPV-PMO materials still preserved fluorescent emission, and that their emission in the visible light region was red-shifted with respect to the precursor molecules in solution, which indicates that there are strong electronic interactions between the intact phenylenevinylene chromophores in the condensed 3a-OPV-PMO pore walls.

Given the charge-conducting ability of many π -conjugated systems, we reasoned that incorporating such conjugated organic units in alkoxy-silyl precursors might lead to novel PMO materials with novel optical and optoelectronic properties. Accordingly, two novel poly-trialkoxysilyl precursors, one with a phthalocyanine chromophore and the other with a porphyrin macrocycle as bridging-units, were designed and used to synthesize the corresponding PMO film materials on flat glass substrates. Compared to small precursor molecules, it is often far more challenging to obtain ordered mesostructures from bulky organic precursors, as this type of precursor shows low solubility and high hydrolysis rates leading to almost instant precipitation under common synthesis conditions. Sometimes a certain amount of pure silica precursor such as tetraethyl orthosilicate (TEOS) is needed to assist the bulky organic precursor in forming an ordered structure through interactions with the block copolymer aggregates.

This turned out to be the case for the synthesis of the PMO containing phthalocyanine chromophores (denoted as Pc-Si-PMO). With triblock co-polymer F108 as template and 50 wt% TEOS as co-precursor, highly ordered mesoporous films were formed on flat substrates by using the spin-coating method. The removal of template was realized by supercritical CO₂ extraction. With a view toward its porosity as well as the periodicity and orientation of the mesostructure, the extracted Pc-Si-PMO was thoroughly characterized by nitrogen sorption measurements, 1D and 2D small angle X-ray diffraction techniques and transmission electron microscopy (TEM). The extracted PMO features an orthorhombic porous structure with pore diameter of 17 nm and surface area of 379 m² g⁻¹. The phthalocyanine molecules are still intact after being incorporated in the condensed silica walls, which was confirmed by energy dispersive X-ray spectroscopy (EDX), electron energy loss spectroscopy (EELS) and nuclear magnetic resonance (NMR) spectroscopy. Furthermore, upon inclusion of electron-accepting species such as [6, 6]-phenyl-C₆₁-butyric acid methyl ester (PCBM), the anticipated light-induced charge generation and hole-transporting capabilities were indeed observed for these Pc-Si-PMO films.

Finally, the synthesis of novel PMO films containing porphyrin macrocycles was achieved by using 100 wt% of a newly designed porphyrin-bridged organosilane precursor without addition of any inorganic silica precursor. Through the spin-coating technique, F127-templated Por-PMO film material was formed on flat glass substrates. After removal of F127 by solvent extraction, the resulting Por-PMO film showed an orthorhombic mesostructure with surface area of 364 m² g⁻¹ and a pore diameter of 15 nm. The UV-Vis absorbance spectrum of the PMO film showed a broad absorption due to the porphyrin chromophores in the organosilica frameworks. The optoelectronic activity of the Por-PMO film material was investigated in an electrolyte and also in a

solid device containing interpenetrating PCBM electron acceptor, showing light-induced charge generation performance and hole-conducting ability.

This thesis was guided towards the functionality and utility of periodic mesoporous organosilica materials. Our experiments were conducted with the aim to diversify the mesophase of a particular PMO via confinement and to rationally design novel functional PMOs. In our work, the studies related to the AAM host systems show that combining the PMO material with porous AAM system could lead to different mesophase behavior and phase stability and thus open a way to designing novel hierarchical nanosystems based on the PMO materials. Furthermore, the achievement of successfully synthesizing novel PMO films with large π -conjugated chromophores shows that it is possible to obtain PMO films by using precursors with rather large organic bridges, whose synthesis and self-assembly has always been a significant challenge. Additionally, these novel PMO films show indeed the anticipated optoelectronic activities, *i.e.*, light-induced charge generation and hole-conducting capability. The knowledge gained in this work is hoped to lead the way towards designing and synthesizing novel PMO materials with unique properties that might, on the one hand, serve as well-defined model systems for bulk heterojunctions in photovoltaics, and on the other hand show promise for future applications in photodetectors, photocatalysis, displays and photovoltaics based on their light-absorbing, light-emitting and charge-transporting abilities studied in the course of this thesis.

8. Appendix

A-1. Synthetic Procedures for 2,3,9,10,16,17,23,24-Octa

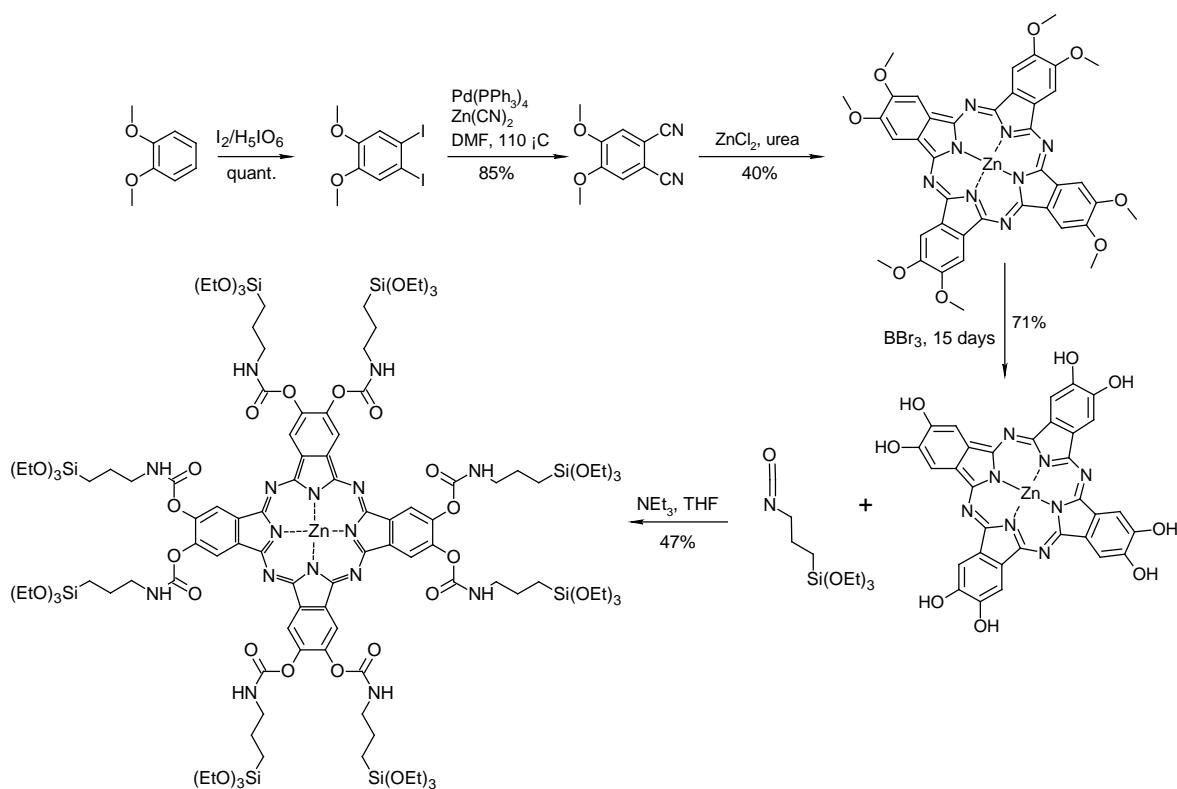
[(3-triethoxysilylpropylaminocarbonyloxy) phthalocyaninato zinc (II)]

Synthesis was done by Florian Löbermann from the Trauner group in the organic chemistry division of LMU.

General Experimental Details. Unless otherwise noted, all reagents were purchased from commercial suppliers and were used without further purification. Unless otherwise noted, all reaction mixtures were magnetically stirred in oven-dried glassware under a blanket of argon. External bath temperatures were used to record all reaction mixture temperatures. Analytical thin layer chromatography (TLC) was carried out on Merck silica gel 60 F₂₅₄ TLC plates. TLC visualization was accomplished using 254 nm UV light or charring solutions of KMnO₄ and ceric ammonium molybdate. All organic extracts were washed with brine, dried over sodium sulfate and filtered; solvents were then removed with a rotary evaporator at aspirator pressure. Flash chromatography was performed on Dynamic Adsorbents Silica Gel (40-63 μm particle size) using a forced flow of eluant at 1.3–1.5 bar pressure. Yields refer to chromatographically and spectroscopically (¹H NMR and ¹³C NMR) homogenous material. ¹H NMR spectra were recorded on Bruker ARX 200, AC 300, WH 400, or AMX 600 instruments. Chemical shifts are reported in ppm with the solvent resonance employed as the internal standard (CDCl₃ at 7.26 and 77.0 ppm; DMSO at 2.50 and 39.5 ppm). The following abbreviations are used to explain the multiplicities: s = singlet, d = doublet, t = triplet, q = quartet, m =

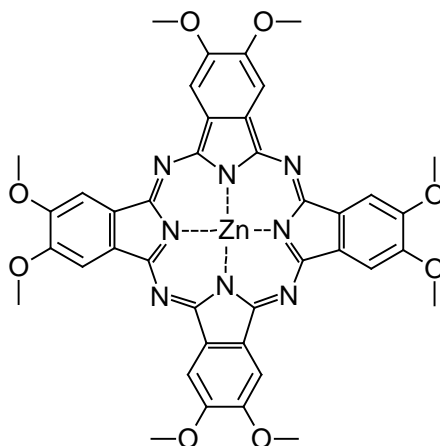
8. Appendix

multiplet, br = broad. IR spectra were recorded 4000–400 cm^{-1} on a Perkin Elmer Spectrometer BY FT-IR-System with a Smith Dura sample IR II ATR-unit. Samples were measured as neat materials (neat). The absorption bands are reported in wave numbers (cm^{-1}). Mass spectra were recorded on a Varian MAT CH 7A for electron impact ionization (EI) and high resolution mass spectra (HRMS) on a Varian MAT 711 spectrometer.



Scheme A-1.1: Synthetic route of the octa-substituted phthalocyanine-bridged organosilane precursor.

The ethoxysilyl precursor containing phthalocyanine macrocycle was synthesized according to the synthetic route shown in Scheme A-1.1.

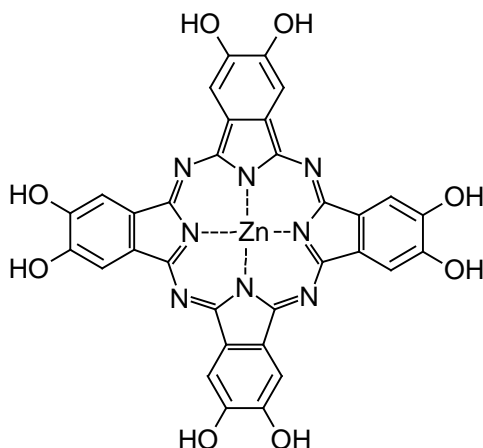


Scheme A-1.2: Chemical structure of zinc-octamethoxyphthalocyanine

Zinc-octamethoxyphthalocyanine. To a solution of zinc(II)chloride (0.274 g, 2.0 mmol, 0.25 *eq.*), 4,5-dimethoxyphthalonitrile (1.49 g, 7.9 mmol, 1.0 *eq.*) and urea (0.474 g, 7.9 mmol, 1.0 *eq.*) in ethylene glycol (24 mL) was added a spatula tip of ammonium molybdate. The mixture was heated in a sealed tube to 170 °C under stirring over night. The dark green reaction mixture was diluted with water (50 mL) and centrifuged to obtain a dark green, waxy solid. The precipitate was washed with acetone and dried on air over night. The dark powder was now washed with DMSO, followed by acetone to yield 1.41 g (87%) of zinc-octamethoxyphthalocyanine as a dark green solid.

Analysis Data:

IR (neat): ν (cm^{-1}) = 3364 (br), 3006 (w), 2936 (w), 2218 (w), 1600 (m), 1494 (s), 1476 (s), 1393 (s), 1276 (s), 1205 (s), 1099 (m), 1052 (s), 876 (m), 847 (m), 741 (m); ^1H NMR (200 MHz, $\text{DMSO-}d_6$): δ = 7.29 (s, 8H), 3.88 (s, 24H); MS (EI) calcd. for $\text{C}_{40}\text{H}_{32}\text{N}_8\text{O}_8\text{Zn}$ (M^+): 816.1635; found: 816.1622.

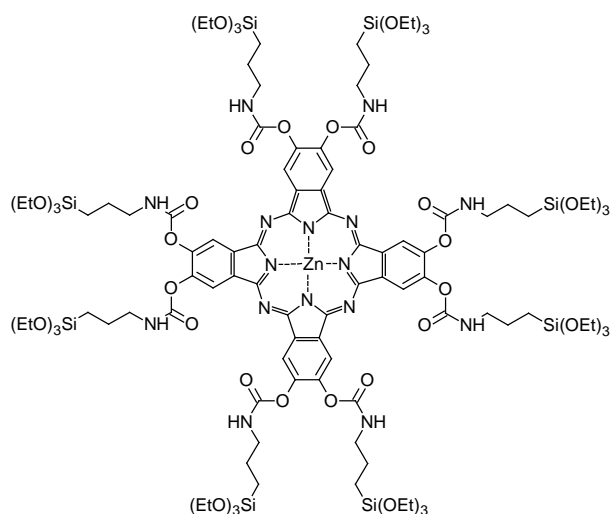


Scheme A-1.3: Chemical structure of zinc-octahydroxyphthalocyanine.

Zinc-octahydroxyphthalocyanine. To a suspension of zinc-octamethoxyphthalocyanine (818 mg, 1.0 mmol, 1.0 *eq.*) in dry CH_2Cl_2 (20 mL) was added a 1.0 M solution of boron tribromide in CH_2Cl_2 (40 mL, 40 mmol, 40 *eq.*) dropwise at 0°C . The reaction mixture was stirred at rt for 5 days and subsequently treated with MeOH (200 mL) at 0°C . All volatiles were removed *in vacuo* and the resulting dark solid was suspended in MeOH (100 mL) and centrifuged. The precipitate was filtered off, washed with MeOH and dried *in vacuo* to yield 530 mg (75%) of title compound zinc-octahydroxyphthalocyanine.

Analysis data:

IR (neat): ν (cm^{-1}) = 3196 (br), 2361 (s), 2342 (s), 1647 (m), 1603 (m), 1476 (s), 1380 (br), 1288 (s), 1170 (w), 1087 (m), 1033 (m), 827 (w);



Scheme A-1.4: Chemical structure of the phthalocyanine-containing ethoxysilyl precursor.

Phthalocyanine-containing ethoxysilyl precursor. To a suspension of zinc-octahydroxyphthalocyanine (100mg, 0.14 mmol, 1 *eq.*) in dry THF (10 mL) was added TEA (724 mg, 7.15 mmol, 50 *eq.*), followed by 3-isocyanatopropyl-triethoxysilane (566 mg, 2.29 mmol, 16 *eq.*). The reaction mixture was stirred at rt over night and all volatiles were removed *in vacuo*. The resulting oily residue was taken up in dry toluene and precipitated with hexanes. The suspension was centrifuged and the precipitate was filtered off, dissolved in toluene and precipitated again. After drying 180 mg (47%) of title compound were obtained as a green-blue solid.

Analysis data:

IR (neat): ν (cm⁻¹) = 3322 (br), 2973 (m), 2928 (w), 2881 (w), 1714 (vs), 1536 (s) 1453 (m), 1404 (m), 1391 (m), 1244 (s), 1165 (m), 1073 (vs), 938 (vs); ¹H NMR (400 MHz,

8. Appendix

DMSO- d_6): $\delta = 9.20$ (s, 8H), 8.19 (d, 8H, $J = 4.8$), 3.82 (q, 48H, $J = 7.0$), 7.29 (s, 8H),
3.88 (s, 24H)

A-2. Analysis of the extracted Pc-Si-PMO film by energy dispersive X-ray spectroscopy (EDXS) and electron energy loss spectroscopy (EELS).

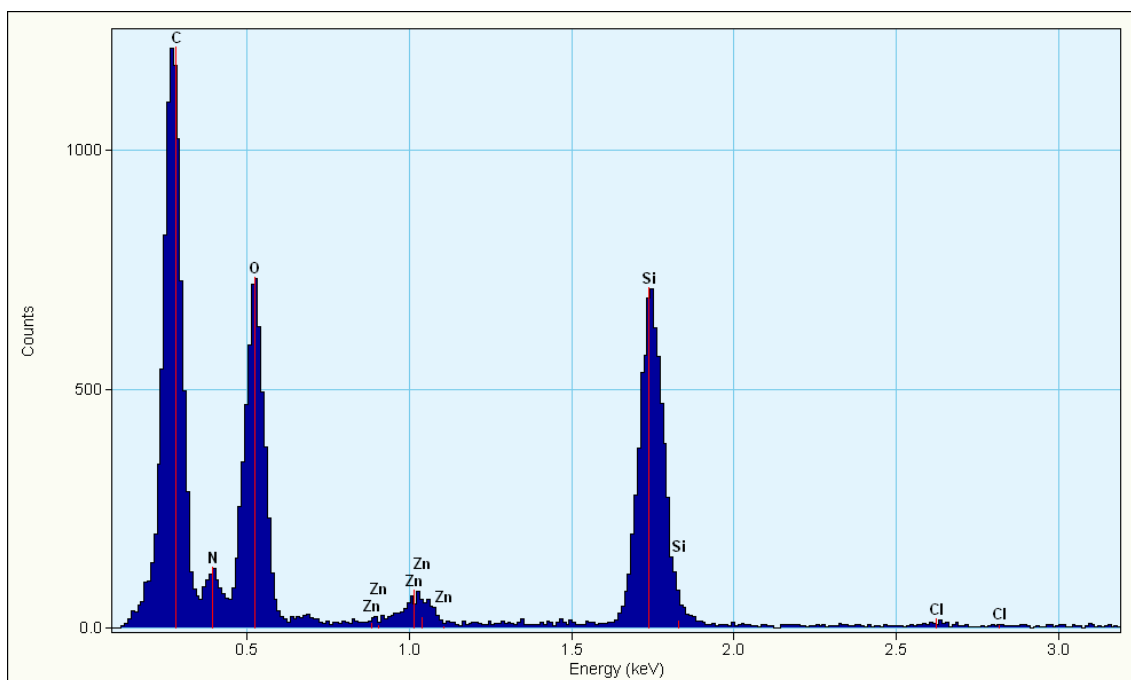


Figure A-2.1: Low energy part of a typical EDX spectrum from a CO₂ extracted film showing the presence of the expected elements.

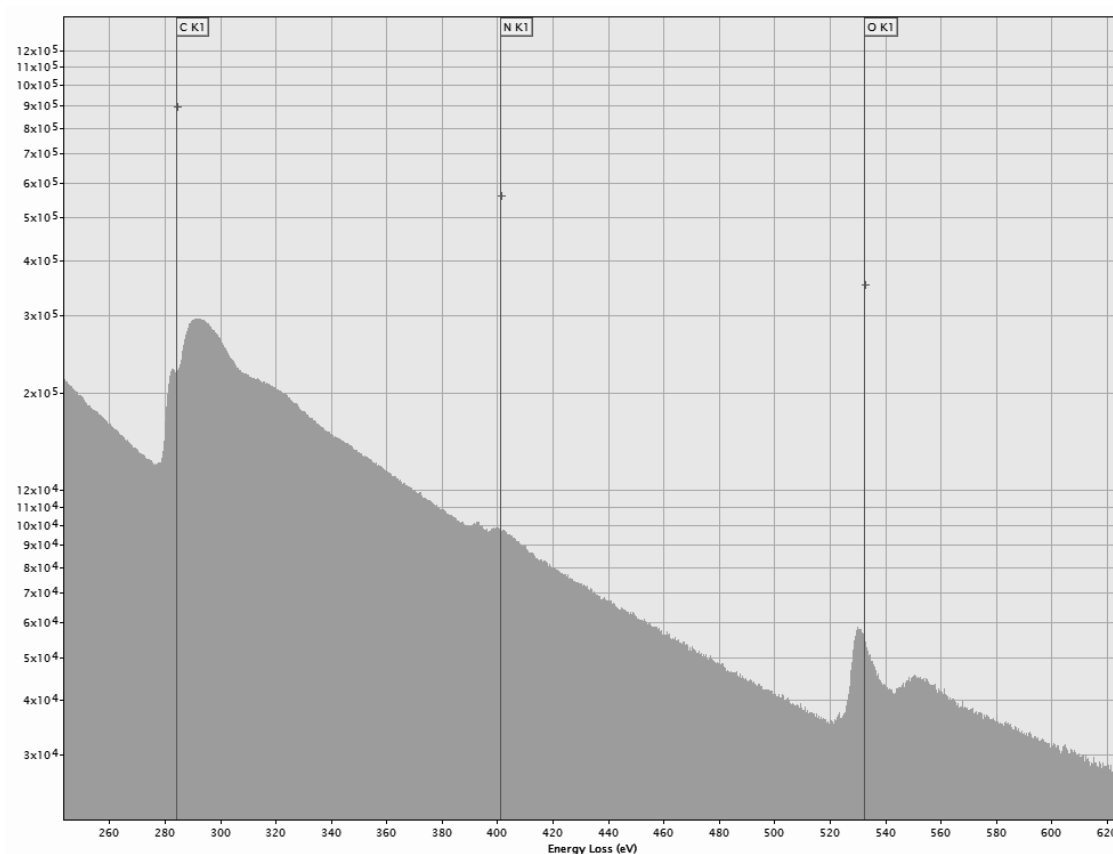
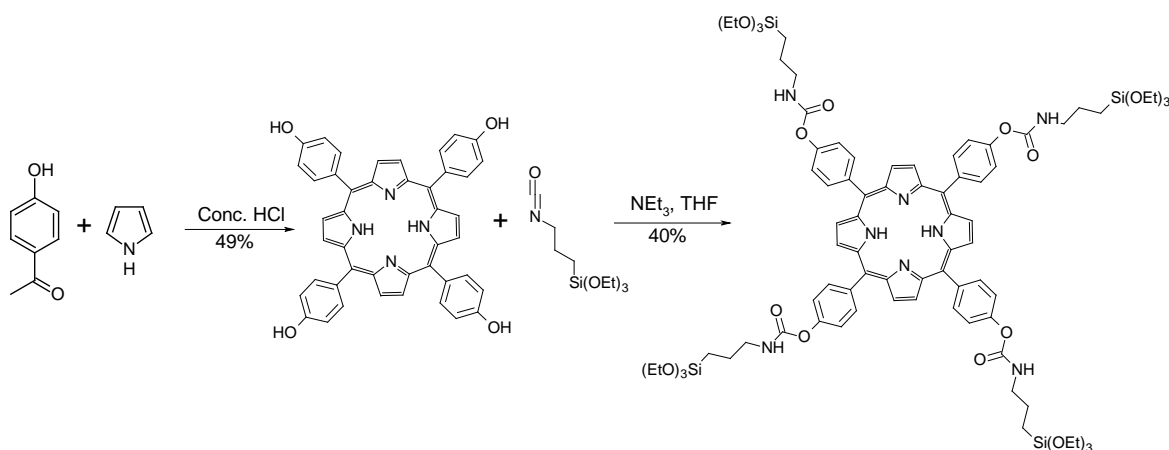


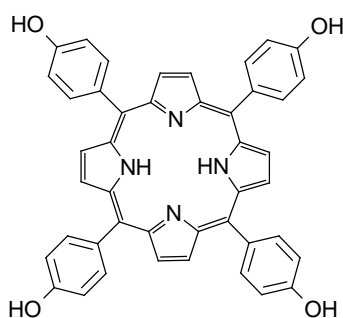
Figure A-2.2: Typical EEL spectrum of a CO₂ extracted film. Apart from nitrogen and oxygen K edges, the carbon K edge and the Si L edge can be recognized. The latter edges were not used for quantification because the silicon L edge is close to the plasmon region which makes a proper background subtraction difficult. Carbon can be easily quantified. However, the amount of carbon can be affected by contamination due to long exposure times.

A-3. Synthetic procedures of the porphyrin-containing ethoxysilyl precursor

Synthesis was done by Florian Löbermann from the Trauner group in the organic chemistry division of LMU.



Scheme A-3.1: Synthetic route for the porphyrin-bridged ethoxysilyl precursor.



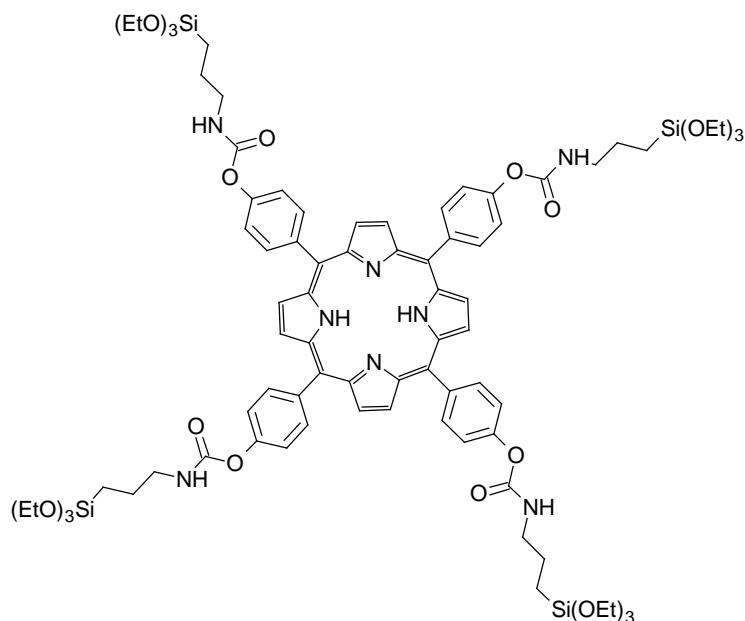
Scheme A-3.2: Chemical structure of *meso*-tetra(*p*-hydroxy)phenyl porphyrin.

Meso-tetra(*p*-hydroxy)phenyl porphyrin. 4-Hydroxybenzaldehyde (3.6 g, 30 mmol,

1.0 *eq.*) was dissolved in refluxing propionic acid (150 mL). Upon addition of pyrrole (C_4H_4NH) (2.0 g, 30 mmol, 1.0 *eq.*) the reaction mixture was refluxed for further 30 min. The solution was subsequently slowly cooled to 0 °C for 15 min. The resulting precipitate was washed excessively with $CHCl_3$ (200 mL) and then dissolved in acetone (100 mL) and $CHCl_3$ (50 mL), washed with saturated sodium bicarbonate solution (2×50 mL), brine (3×50 mL), dried, filtered and concentrated. The crude product was purified by repetitive silica gel chromatography (1% MeOH in $CHCl_3$) to afford 2.5 g (49%) of *meso*-tetra(*p*-hydroxy)phenyl porphyrin as a purple solid.

Analysis data:

IR (neat): ν (cm^{-1}) = 3313 (br), 1700 (m), 1607 (s), 1509 (s), 1350 (s), 1213 (vs), 1171 (vs), 966 (s), 794 (vs), 728 (s); 1H NMR (300 MHz, DMSO-*d*6): δ = 9.94 (s, 4H), 8.87 (s, 8H), 8.00 (d, 8H, J = 8.5), 7.21 (dd, 8H, J = 1.2, 8.5), -2.88(s, 2H); ^{13}C NMR (100 MHz, DMSO-*d*6): δ = 157.8, 157.7, 136.0, 120.4, 116.1, 114.4; MS (EI) calcd. for $C_{44}H_{30}N_4O_4$ (M^+): 687.2267; found: 687.2271.



Scheme A-3.3: Chemical structure of the porphyrin-containing ethoxysilyl precursor.

Porphyrin-containing ethoxysilyl precursor. A dry Schlenk-tube was charged with *Meso*-tetra(*p*-hydroxy)phenyl porphyrin (204 mg, 0.30 mmol, 1 *eq.*) in dry THF (15 mL). To the solution was added 3-isocyanatopropyltriethoxysilane (445 mg, 1.8 mmol, 6 *eq.*) and TEA (9.11 mg, 0.09 mmol, 0.3 *eq.*) at *rt* and under argon atmosphere. The reaction mixture was hereafter heated to 80 °C for 4 h. After concentration *in vacuo*, filtration and washing with EtOAc (50 mL), all volatiles were removed. The resulting oily residue was taken up in little EtOAc and precipitated with hexanes. The precipitate was collected after centrifugation and the procedure was repeated five times. The resulting solid was dried under high vacuum to obtain 200 mg (40%) of title compound as purple solid.

Analysis data:

IR (neat): ν (cm⁻¹) = 3315 (br), 2971 (w), 2926 (vw), 2884 (vw), 1714 (vs), 1608 (s), 1586 (w), 1498 (s), 1470 (w), 1349 (s), 1205 (vs), 1166 (s), 1069 (vs), 965 (w); ¹H NMR

8. Appendix

(400 MHz, CDCl₃): δ = 8.88 (s, 8H), 8.18 (d, 8H, J = 8.4), 7.53 (d, 8H, J = 8.4), 5.60 (t, 4H, J = 5.9), 3.91 (dt, 24H, J = 6.2, 7.0), 3.42 (dd, 8H, J = 6.6, 13.0), 1.88-1.78 (m, 8H), 1.30 (td, 36H, J = 1.6, 7.0), 0.82-0.76 (m, 8H), -2.83 (s, 2H); ¹³C NMR (100 MHz, CDCl₃): δ = 154.7, 151.1, 138.9, 135.7, 135.2, 119.8, 119.3, 113.7, 58.6, 43.7, 23.2, 18.3, 7.8; MS (ESI) calcd. for C₈₄H₁₁₅N₈O₂₀Si₄ [M+H]⁺: 1667.7305; found: 1667.7306.

9. Curriculum Vitae

Personal information

Name: Yan, Li
Gender: Female
Date of birth: 07. July 1983
Place of birth: Dezhou, Shandong, China
Citizenship: Chinese

Education

09/2001 – 07/2005: Bachelor study in department of Chemistry and Chemical Engineering,
Shandong University
01.07.2005: Bachelor of Engineering, Chemical Engineering
09/2005 - 07/2008: Master study in department of Chemistry and Chemical Engineering,
Shandong University
01.07.2008: Master of Science, Chemistry
10/2008 - present: Ph.D study in AK Bein at Department of Chemistry, LMU

Awards and scholarship

09/2002: “First-class Scholarship for Excellent Student”, Shandong University (awarded
to top 5 per 100 students)
09/2003: “Second-class Scholarship for Excellent Student”, Shandong University
(awarded to top 10 per 100 students)
09/2004: “Second-class Scholarship for Excellent Student”, Shandong University
(awarded to top 10 per 100 students)
12/2006: “Scholarship for excellent student in social practice”, Shandong University
09/2008: “Scholarship for PhD student studying abroad”, China Scholarship Council

Language skill

Mandarin (Mother language); English (Fluent); German (Basic)



10. Publications and Presentations

Publications

Y. Li, A. Keilbach, M. Kienle, Y. Goto, S. Inagaki, P. Knochel, T. Bein, “Hierarchically Structured Biphenylene-Bridged Periodic Mesoporous Organosilica”, *Journal of Materials Chemistry*, 2011,21(43),17338.

Y. Li, A. Keilbach, N. Mizoshita, S. Inagaki, T. Bein, “Formation of Hexagonal and Cubic Fluorescent Periodic Mesoporous Organosilicas in the Channels of Anodic Alumina Membranes”, *in preparation*.

Y. Li, F. Löbermann, F. Auras, M. Döblinger, J. Schuster, L. Peter, D. Trauner, T. Bein, “A Periodic Mesoporous Organosilica with Phthalocyanine Macrocycles Exhibiting Optoelectronic Properties”, *in preparation*.

Y. Li, F. Löbermann, F. Auras, M. Döblinger, J. Schuster, L. Peter, D. Trauner, T. Bein, “Optoelectronically Active Periodic Mesoporous organosilica film containing porphyrin chromophores”, *in preparation*.

Presentations

Y. Li, A. Keilbach, S. Inagaki, T. Bein, “Hierarchically Structured Periodic Mesoporous Organosilica”; 23rd. Germany Zeolite-Conference, Munich, 02.-04.03.2011.

10. Publications and Presentations

Y. Li, A. Keilbach, Y. Goto, S. Inagaki, M. Kienle, P. Knochel, T. Bein, “Optically active periodic mesoporous organosilica in confined environments”; CeNS Workshop 2010 "Nanosciences - Merging Disciplines", Venice (Italy), 20.-24.09.2010.

Keilbach, J. Schuster, Y. Li, M. Döblinger, T. Bein, “Periodic mesoporous organosilicas and carbons in confined spaces”; 16th International Zeolite Conference, Sorrento (Italy), 04.-09.07.2010.

Y. Li, A. Keilbach, S. Inagaki, T. Bein, “Optically active biphenylene bridged periodic mesoporous organosilica in confined environments”; 22nd. Germany Zeolite-Conference, Munich, 03.-05.03.2010.